Applied Catalysis B: Environment and Energy 344 (2024) 123605

Contents lists available at ScienceDirect

Applied Catalysis B: Environmental

journal homepage: www.elsevier.com/locate/apcatb

Photocatalytic degradation by TiO_2-conjugated/coordination polymer heterojunction: Preparation, mechanisms, and prospects

Heng Zhou [a,1], Hao Wang [a,1], Caiyan Yue [a], Lijuan He [a], Hui Li [b], Heng Zhang [a,*], Song Yang [a,*], Tianyi Ma [b,*]

[a] National Key Laboratory of Green Pesticide, State-Local Joint Laboratory for Comprehensive Utilization of Biomass, Center for Research & Development of Fine Chemicals, Guizhou University, Guiyang, Guizhou 550025, China
[b] School of Science, RMIT University, Melbourne, VIC 3000, Australia

ARTICLE INFO

Keywords:
TiO_2-polymer heterojunction photocatalyst
MOF
C_3N_4
Pollutant degradation
Degradation pathways

ABSTRACT

Photocatalytic technology having the advantages of low-cost, environmental friendliness, is important in removing organic pollutants. To enhance the catalytic efficacy of well-established TiO_2 photocatalyst, TiO_2-conjugated/coordination polymer heterojunction photocatalysts have been rapidly developed in the area of environmental remediation. However, a comprehensive summary and description of these advancements are lacking. To fill this gap, the research progress of TiO_2-conjugated/coordination polymer heterojunction photocatalysts for organic pollutants degradation is reviewed. Firstly, classifications, working principles, and photodegradation pathways of TiO_2-based heterostructures are introduced. Subsequently, the synthesis strategies, photocatalytic performance, and mechanisms of TiO_2-conjugated/coordination polymer photocatalysts are comprehensively summarized. The effects of operational parameters on photodegradation are discussed. Lastly, promising prospects of TiO_2-based heterojunction photocatalysts systems and urgent issues to be solved are foreseen. It is hoped that this review sets the trajectory for providing references in preparation and catalytic capacities of TiO_2-based heterojunction photocatalysts, providing new ideas for resourceful wastewater remediation.

1. Introduction

Nowadays, owing to the high rate of global economic development, and rapid progress of industrialization and urbanization, a series of environmental problems have inevitably occurred. Among them, the water body has been severely polluted due to the industrial wastewater discharged at will and the intervention of human activities [1,2]. Numerous industries such as pharmaceuticals, textiles, printing with dyeing, and pesticides all discharge large amounts of wastewater into our ecosystems. Pollutants generally include organic pollutants (dyes, pesticides, antibiotics, fertilizers, and pharmaceutical ingredients), inorganic pollutants, and nutrients. However, organic pollutants are the leading cause of environmental pollution because they can stay in our living environment. Therefore, efficient purification of organic pollutants in water has attracted continuous global attention [3,4].

Several traditional methods have been used for the treatment of wastewater, for example, adsorption, membrane filtration, and coagulation, while these are time-consuming, limited efficiency, and induce

Abbreviations: MOFs, metal-organic frameworks; AOPs, advanced oxidation processes; MNPs, metal nanoparticles; VB, valence band; CB, conduction band; HOMO, highest occupied molecular orbital; LUMO, lowest unoccupied molecular orbital; LMCT, ligand-metal charge transfer; 0D, zero dimentional; 1D, one dimentional; 2D, two dimentional; 3D, three dimentional; h^+, holes; e^-, electrons; e^-−h^+, electron−hole pair; •OH, hydroxyl radicals; $\bullet O_2^-$, superoxide radicals; g−C_3N_4, graphite-phase carbon nitride; NHE, normal hydrogen electrode; PL, photoluminescence; UiO, University of Oslo; MIL, Materials of Institut Lavoisier; ZIF, Zeolite imidazole framework; ASS, all−solid−state; DZS, direct Z-scheme; NPs, nanoparticles; SSA, specific surface area; TEM, transmission electron microscope; SEM, scanning electron microscope; UV, Ultra-violet; DRS, diffuse reflective spectra; XRD, X-ray diffraction; ESR, electron spin resonance; EIS, electrochemical impedance spectroscopy; GO, graphene oxide; RGO, reduced graphene oxide; TC, tetracycline; MB, methylene blue; RhB, rhodamine B; MO, methyl orange; Rh6G, rhodamine 6 G; CR, Congo red; BPA, bisphenol A; ENR, enrofloxacin; TTZ, tartrazine; CIP, ciprofloxacin.

* Corresponding authors.
E-mail addresses: hzhang23@gzu.edu.cn (H. Zhang), syang@gzu.edu.cn (S. Yang), tianyi.ma@rmit.edu.au (T. Ma).
[1] contributed equally to this work.

https://doi.org/10.1016/j.apcatb.2023.123605
Received 28 September 2023; Received in revised form 25 November 2023; Accepted 9 December 2023
Available online 18 December 2023
0926-3373/© 2023 The Author(s). Published by Elsevier B.V. This is an open access article under the CC BY license (http://creativecommons.org/licenses/by/4.0/).

secondary pollution and incomplete removal [5–7]. The exploitation of more efficient wastewater treatment technologies for the removal of organic pollutants is currently a highly discussed and researched field. AOPs have the advantages of complete mineralization of pollutants, environment-friendly products, and mild reaction conditions. AOPs in sewage treatment include but are not limited to Fenton/Fenton-like reactions, electrocatalysis, and photocatalysis [8]. Among them, photocatalysis technology employs semiconductor materials and derivatives by absorbing solar energy to conduct oxidation and reduction treatment of organic pollutants in wastewater will result in non-toxic and harmless substances, achieving the effective green degradation of pollutants [9]. Among the photocatalytic materials, TiO_2, ZnO, CdS, MnO_2, g−C_3N_4, and other semiconductor photocatalysts have been widely studied and applied [10–12]. TiO_2 has been recognized as one of the idealized photocatalytic materials due to its good oxidation performance, excellent photochemical stability, low production cost, non-toxicity, and harmlessness [13]. The pioneering study of TiO_2 can be traced back to the 1968 s. However, their further development has lagged for a long time, mainly because of the formidable chemical synthesis of high-quality TiO_2-based photocatalyst. The significant growth in

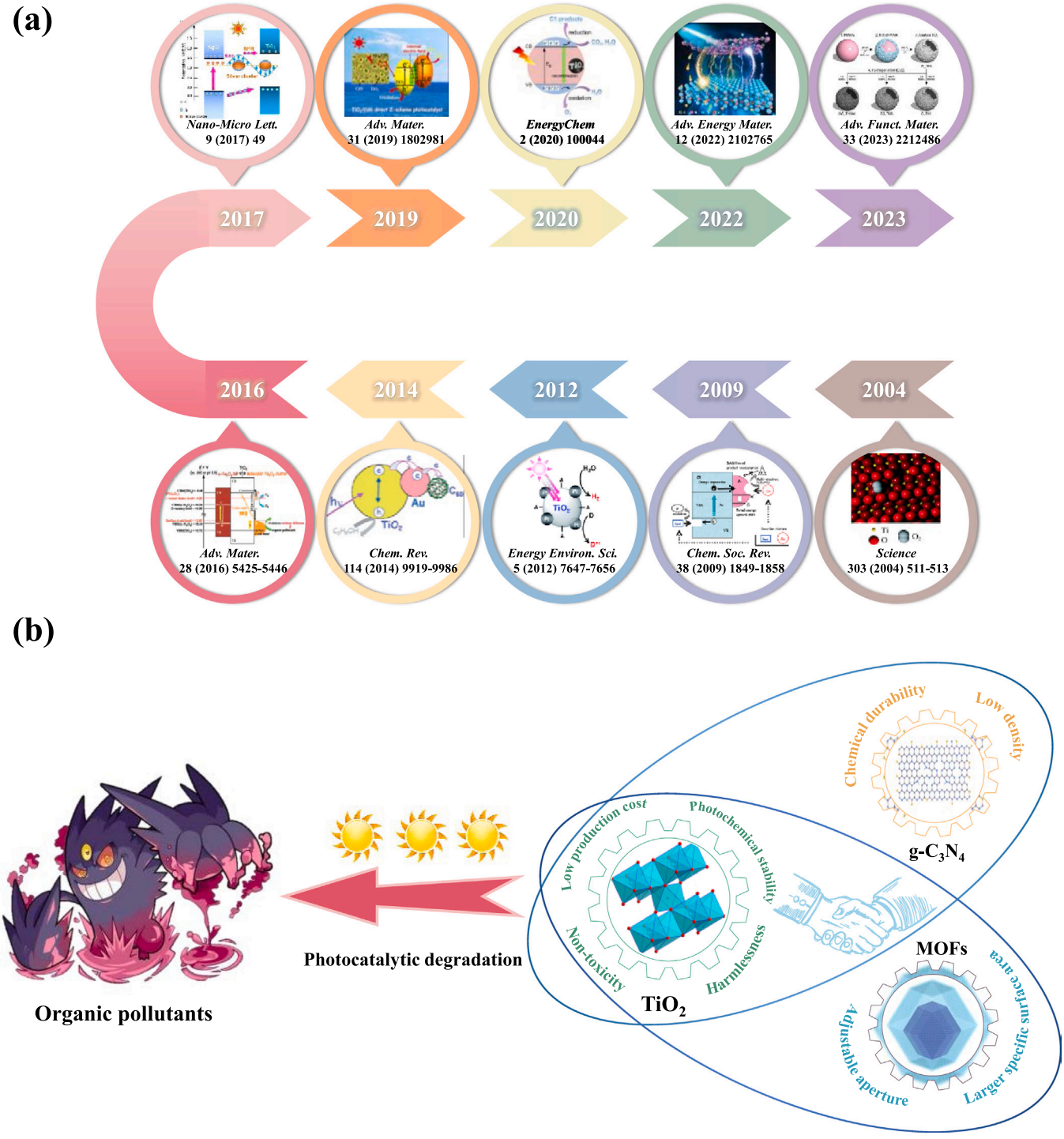

Fig. 1. (a) The timeline of TiO_2-based photocatalytic materials. The adopted sub-graphs came from references of [17–26]. (b) Schematic diagram of the correlation network of TiO_2, g-C_3N_4, and MOFs in the field of photocatalytic degradation of organic pollutants.

research activities on TiO_2-based heterojunction photocatalysts in recent years has been mainly attributed to the advances in synthesis techniques and the development of new semiconductor photocatalysts. Fig. 1a illustrates the historical trends in TiO_2 research. TiO_2 has a large band-gap of about 3.2 eV, which absorbs ultraviolet light about less than 387 nm in wavelength (radiation energy only share 7% of the total energy of solar light), however, visible light account for approximately 43% of solar energy that cannot be absorbed and utilized by TiO_2, restricting its photocatalytic application in visible light absorption scope [14]. Aiming to improve the photocatalytic properties of TiO_2, methods including doping of metals, non-metallic elements, surface noble metal deposition, encapsulation of carbon nanotubes, dye sensitization, etc. have been employed [15,16]. Nonetheless, these methods can not completely overcome the above-mentioned drawbacks.

The method of constructing a heterojunction structure can effectively solve the defects of a single TiO_2 material [27]. In general, a heterojunction photocatalyst is formed by coupling two semiconductors about relative band positions, complementary properties, and Fermi energy level differences [28]. Just as it should be, it can promote opposite-direction transfer of photoinduced e^- and h^+, which can effectively reduce e^-—h^+ compounding, improve effective making use of e^- and h^+, and enhance redox capacity [29]. Hence, the introduction of polymer semiconductors to make up heterojunctions is a high-efficiency means to enhance the visible photocatalytic degradation properties of TiO_2.

Conjugated polymers have attracted increasing attention in recent years as a promising alternative to traditional inorganic semiconductors due to their low cost, high porosity, and high chemical stability [30,31]. Currently, semiconductor materials for building heterojunction-modified TiO_2 include polythiophene conjugated polymers, polyaniline conjugated polymers, covalent organic frameworks, g−C_3N_4, and others [32–34]. In particular, g−C_3N_4 attracted broad consideration as being a stable and inexpensive non-metallic conjugated polymer semiconductor material. Atoms of C and N in g−C_3N_4 are hybridized in sp^2 to form a highly delocalized π-conjugate, and the unique two-dimensional structure of the triazine linked by tertiary amines gives it high thermal stability, chemical durability, low density, and other characteristics. In addition, the band gap of g−C_3N_4 is relatively narrow (approximately 2.6 eV), which expands its response range to visible light to 450 nm [35]. However, the shortcomings of g−C_3N_4, for instance, small surface area, low quantum utilization, easy compounding of photoinduced e^-—h^+, and weak oxidizing power reduce its photocatalytic efficiency [36]. The well-matched g−C_3N_4 and TiO_2 energy bands and constructing heterojunctions of both are considered excellent ways to improve photocatalytic power. There is a sufficient energy level difference between CB and VB, and irreversible space charge separation is pretty easy, which inhibits photogenerated e^- and h^+ recombination [37]. The interesting coupling expands the light-absorbing scope and increases surface-based active sites of catalyst, which significantly improves the photocatalytic degradation efficiency [29]. Based on these advantages, research on TiO_2/g−C_3N_4 −based heterojunction system for removing organic contaminants have been flourishing.

Due to the wide variety of coordination polymers, controllable structure, good thermal stability, large specific surface area, and permanent pores, they have been widely used in photocatalysis [38,39]. Among these coordination polymers, "MOFs", which are known as the star material, and have been more widely studied in the photocatalytic field [40]. MOFs are a novel type of inorganic-organic hybrid porous coordination polymers consisting of metal ions or metal clusters and different ligand organic, which own the advantages of the aperture can be adjusted freely, homogeneous metal active sites, larger SSA, etc. [41]. Notably, organic ligands usually contain double bonds or conjugated structures, which can form conjugated systems, which enable MOFs to have faster electronic conductivity and excellent optical properties and help accelerate the catalytic reaction process [42]. Additionally, they enable the addition of semiconductor components to create heterojunctions to increase quantum efficiency, showing promise in a photocatalytic application [43]. The photocatalytic process of general depiction by MOFs can be completely comparable to those of classical semiconductor catalysts such as TiO_2 and g−C_3N_4. The occupied molecular orbital (HOMO) of organic ligand lone electron pair and the unoccupied molecular orbital (LUMO) of metal ion empty orbital correspond to VB and CB in inorganic semiconductors, respectively, and e^- are excited from HOMO to LUMO, giving rise to e^-—h^+ [44]. However, the different electronic conformations of organic ligands and metal ions result in photo-induced e^-—h^+ rapid recombination with a high band gap value, which reduces their photocatalytic activity. With the semiconductor-like properties of MOFs, it is interesting to construct composite materials with other semiconductor materials such as TiO_2 to improve photocatalytic activity. MOFs/TiO_2 composites have the following advantages in photocatalytic degradation: (1) MOFs as photosensitizers can more efficient utilization of light energy; (2) Photoexcited electrons are easily transferred from the organic ligand to the metal ion; (3) TiO_2 is main catalyst, and MOFs play the role of cocatalyst; (4) The framework of MOFs can effectively prevent the agglomeration of TiO_2. Up to now, TiO_2/MOFs−based heterojunction systems formed by combining MOFs with TiO_2 of different morphology have been widely studied for high-efficiency photocatalysts to degrade contaminants [45,46]. Specifically, Fig. 1b depicted a cross-correlation network of TiO_2, g−C_3N_4, and MOFs in the photodegradation direction.

For the past few years, relevant scholars have devoted themselves to reviewing the research progress of TiO_2 −based heterojunction photocatalytic removal of organic contaminants from different perspectives. Such as Kanakaraju et al. overviewed TiO_2/ZnS−based photocatalysts research progress for organic contaminant removal [47]. Rajput et al. summarized TiO_2/SnO_2 heterojunction photocatalysts for removing dyes and organic contaminants [48]. The basic application of TiO_2/MOF composites was reviewed by Wang et al. [44]. Recently, Acharya and his coworkers discussed the heterogeneous structure of TGCN and the progress of research in environmental remediation [37]. Although some reviews on TiO_2 −based heterojunction materials have been published, however, the systematic review of TiO_2-conjugated/coordination polymer heterojunctions in the field of photocatalytic degradation of pollutants has not been reported. To fill this gap, different preparation strategies, catalytic properties, and mechanisms of TiO_2-conjugated/coordination polymer heterojunction photocatalytic systems are systematically reviewed in this paper. Table 1 illustrates a comparative analysis between this review paper and comparable articles within the field. Over the past decade, the research on novel TiO_2 −based composite photocatalysts has made considerable advancement.

This review presents the first systematic analysis of published research on TiO_2-conjugated/coordination polymer heterojunction photocatalysts used to degrade organic contaminants. The methods of preparation, photocatalytic degradation performance, and degradation mechanisms are described in detail. The effects of operating parameters (pH, catalyst dosage, initial pollutant concentration, light source, coexisting inorganic ions, and coexisting organic) on the photodegradation of organic pollutants are also reviewed. Finally, the advantages, limitations, and emerging challenges of the two photocatalytic systems are effectively evaluated, and the promising application prospects are foreseen. To more clearly present the research content, Fig. 2 summarizes the core framework of this review, presented sequentially from top to bottom.

2. Advanced oxidation process of water treatment

The AOPs are a string of chemical reactions that can effectively eliminate organic contaminants through the in-situ generation of non-selective, highly oxidizing active radicals (e.g., •OH and $•O_2^-$). It is worth noting that conventional ozonation and Fenton oxidation processes have the potential to yield undesired inorganic substances. Similarly, electrochemical oxidation is marred by drawbacks such as

Table 1
A comparison of the present work with previous reviews on TiO_2-based photocatalysts for environmental applications.

Ref.	Description of TiO_2-based conjugated/coordination polymer heterojunction	Synthesize methods for producing TiO_2-based heterojunction photocatalyst	Detailed description of photocatalytic degradation pathway	Operating parameters for degradation of organic pollutants	Detailed description of photodegradation mechanism of TiO_2-based heterojunction
[37]	×	✓	×	×	×
[49]	×	×	×	×	✓
[29]	×	×	×	×	✓
[44]	×	×	×	×	✓
[47]	×	✓	×	✓	×
[48]	×	✓	×	✓	✓
This work	✓	✓	✓	✓	✓

high cost and anode corrosion. However, photodegradation has emerged as a highly favored alternative due to its utilization of regenerative solar power, cost-effectiveness, mild reaction conditions, and remarkable efficacy in transforming organic pollutants into environmentally friendly products [50]. Fig. 3 visually demonstrates the significant advantages of photocatalytic processes, compared to other APOs.

2.1. Photocatalytic degradation mechanism

A very effective catalytic process for converting solar energy into chemical energy is called photocatalysis. In the environmental remediation field, the photocatalysis process is dedicated to the removal of organic contaminants in wastewater [51]. Fig. 4 is a typical photocatalytic process of TiO_2, consisting of several indispensable steps. (1) Excitation: when the band gap width is smaller than the incident light energy, e^- in VB absorbs light energy and transitions to CB, while VB leaves photogenerated h^+; (2) Separation and migration: Resulting e^- and h^+ are separated and migrated to surface or interface with the semiconductor under condition of electrical field or diffusion. The redox reaction occurs between e^- and h^+ and substance adsorbed on the exterior of catalysts, producing various active substances. They can further oxidize organic contaminants into H_2O, CO_2, etc.; (3) Recombination: On the catalyst surface, photogenerated e^- and h^+ unite once more.

Below is a summary of reaction mechanisms utilized in photocatalytic processes: (Eq. (1) – (8)).

(1) Photoexcitation:

$$TiO_2 + hv \rightarrow e^-_{CB} + h^+_{VB} \quad (1)$$

(2) electron-hole recombination:

$$e^-_{CB} + h^+_{VB} \rightarrow Energy \quad (2)$$

(3) Production of superoxide anion radical:

$$e^-_{CB} + O_2 \rightarrow \bullet O_2^- \quad (3)$$

(4) Two ways of generating hydroxyl radicals:

$$h^+_{VB} + H_2O \rightarrow \bullet OH + H^+ \quad (4)$$

$$\bullet O_2^- + H^+ \rightarrow HOO\bullet \quad (5)$$

$$2\ \bullet OOH \rightarrow O_2 + H_2O_2 \quad (6)$$

$$H_2O_2 + hv \rightarrow 2\bullet OH \quad (7)$$

(5) Degradation processes:

$$\text{Organic pollutants} + \bullet O_2^-, h^+, \bullet OH \rightarrow CO_2 + H_2O \quad (8)$$

However, the photogenerated carriers in the degradation process of single semiconductor photocatalysts are readily recombined, reduced photocatalytic efficiency, need for ultraviolet light irradiation, and short catalytic life, which seriously hinder its practical application.

2.2. TiO_2-based heterojunction

Heterojunction was defined as a microenvironment formed between semiconductor materials with different band structures [28,52,53]. To overcome the limitations of TiO_2 in the degradation process, TiO_2 can be coupled with other semiconductors to form heterojunction, inhibiting the compounding of light-induced e^-–h^+. Among many semiconductor materials, g−C_3N_4 was considered to be one of the suitable materials to construct heterojunctions with TiO_2 [54]. Tao et al. [55]. successfully

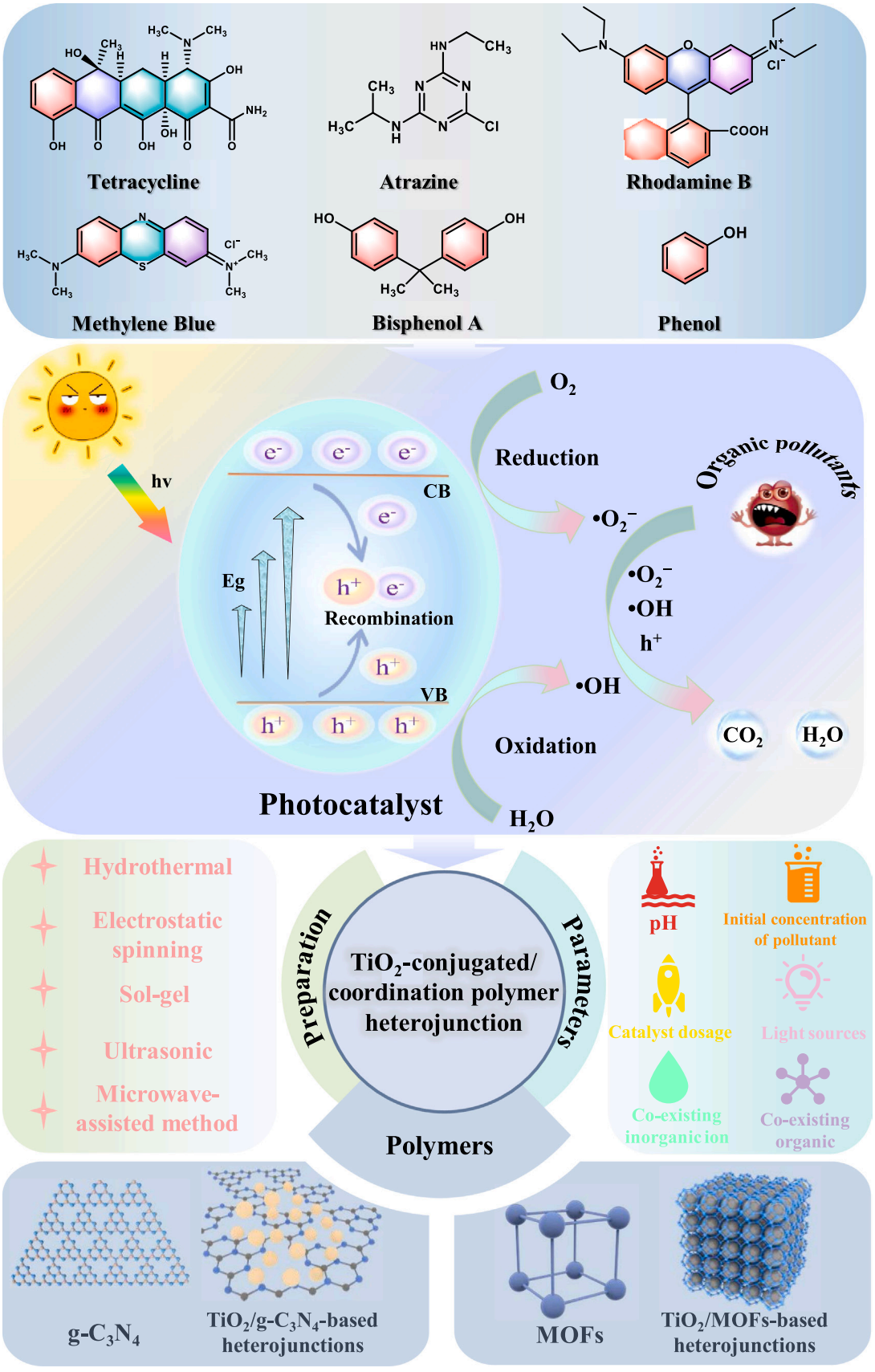

Fig. 2. Core framework diagram of the study on TiO_2-based conjugated/coordinated heterojunction photocatalysts.

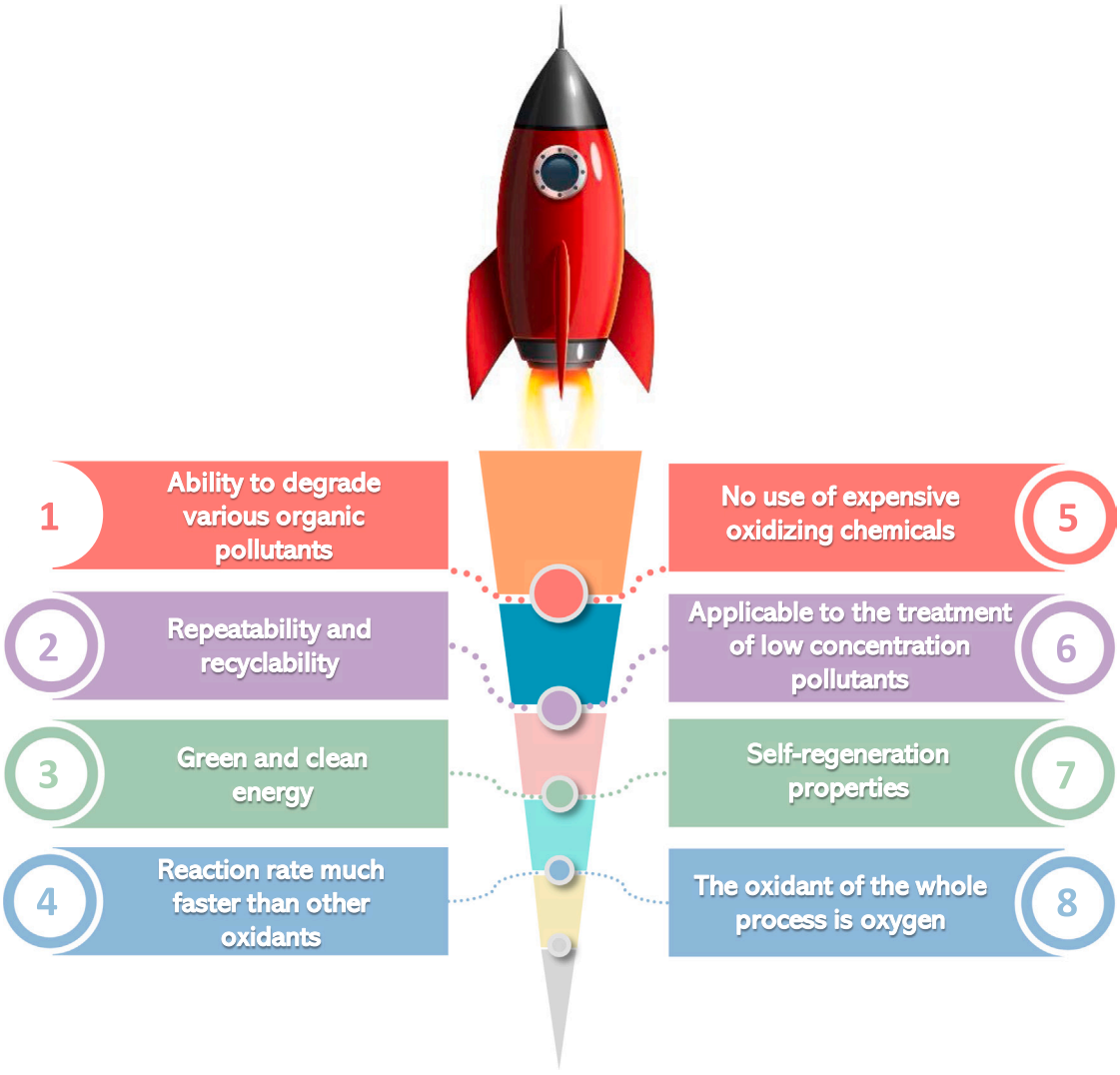

Fig. 3. The main advantages of photocatalytic process.

prepared TiO_2/g−C_3N_4 heterojunction by an atomic deposition method, when exposed to simulated sunlight, demonstrated strong catalytic activity. Because heterojunction structure greatly improved the isolation efficiency of light-induced carriers. Besides, MOF materials have semiconductor-like behavior and can be combined with TiO_2 to form TiO_2/MOFs heterojunction photocatalysts. When a heterojunction was formed, an internal electric field generated in the interface between TiO_2, and MOFs provided a driving force for directional separation and light-induced e^-−h^+ migration, hence increasing photocatalytic effectiveness [56]. However, the degradation process of contaminants by non-heterojunction TiO_2/MOFs was merely MOFs as adsorbent and TiO_2 as photo activator to increase the contact between pollutants and photocatalysts surface, which did not improve photodegradation performance significantly [57]. Therefore, the non-heterojunction TiO_2/MOFs composites will not be described in this paper.

With the continuous development of photocatalytic technology in recent years, the original concept of heterojunction can no longer meet our needs for in-depth study of photocatalytic mechanism. First, a basic understanding of the classification of heterojunctions was established: the Fermi energy levels and energy band structures of the interacting components determine the behavior of carriers at heterojunctions and affect the multiple pathways of carrier migration. It was worth noting that heterojunctions can be defined from different perspectives so that there was some overlap between different types of heterojunctions rather than a simple parallelism. For this reason, heterojunctions were categorized according to their component properties, energy band structures and carrier motion mechanisms [52,58,59].

(1) Component properties: These included Schottky junctions (semiconductor-metal (S-M)), semiconductor-carbon group (S-C) heterojunctions, n-n junctions, p-n junctions, and p-p junctions (semiconductor-semiconductor (S-S)).
(2) Energy band structure: divided into I-type (embedded structure), type II (intertwined structure, including traditional II-type and direct Z-scheme), and III-type (separated structure).
(3) Carrier migration mechanism: including conventional II-type, direct Z-scheme, and S-scheme.

Up to now, the widely studied heterojunction structures were, (1) p-n junctions; (2) Schottky junctions; (3) I-type heterojunctions; (4) II-type heterojunctions; (5) Z-scheme heterojunctions; (6) S-scheme heterojunctions. Fig. 5 briefly analyzes the carrier separation mechanism of these six heterojunction structures.

The p-n junction suppressed photogenerated carriers recombination [60]. In Fig. 5a, an internal electric field was produced by interfaces when two semiconductors came into contact. Under the action of the electric field, e^- and h^+ accumulated on n-type and p-type semiconductors, respectively. Separation of photogenerated carriers in space

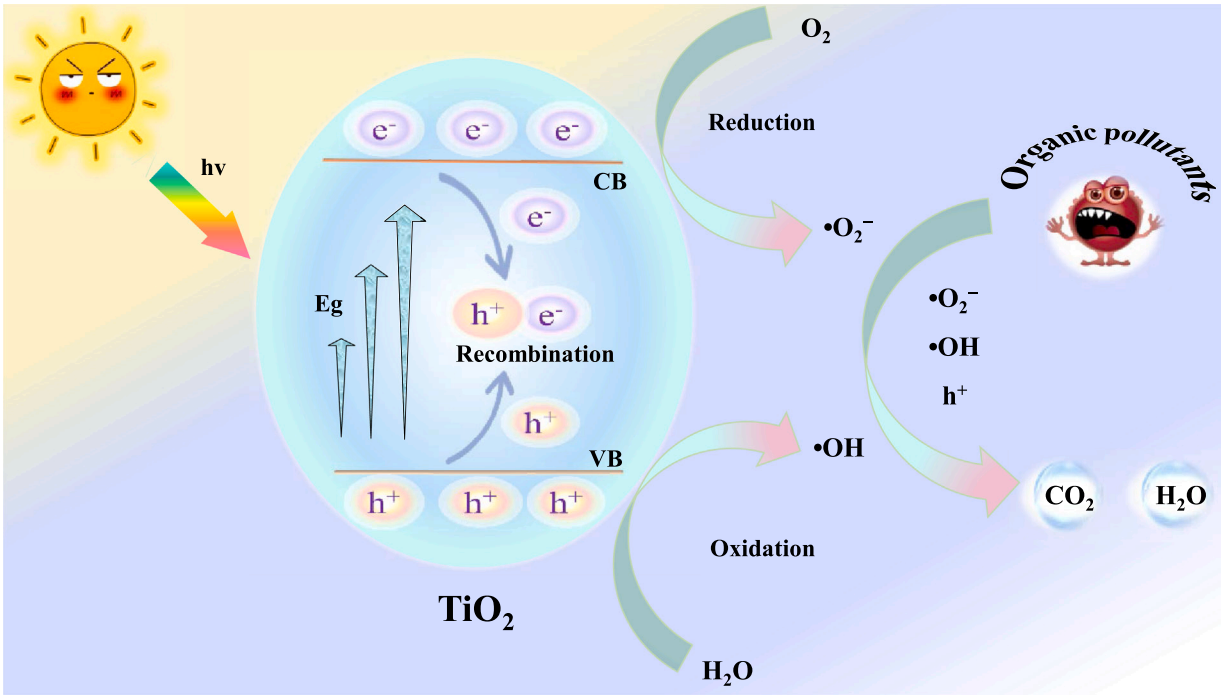

Fig. 4. Diagram of TiO_2 degradation by photocatalysis.

was realized, which considerably reduced the recombination probability of photogenerated carriers; the Schottky junction (Fig. 5b), composed of metal and metal-like materials, could generate the Schottky barrier, accelerated the migration of carriers from semiconductor into metal, and effectively avoided recombination of photogenerated carriers [61]. According to the position of the band, there were three types of conventional heterojunction: I-type, II-type, and III-type. The III-type heterojunction had an interlaced band location. Given the report rarity of this heterojunction structure, it will not be covered in this review; The I-type heterojunction (Fig. 5c) belonged to the embedded structure. Semiconductor A had a higher CB, whereas the VB of semiconductor A was lower, which led to the migration of e^- and h^+ to the VB and CB of semiconductor B, respectively. The inhibition effect of the photogenic carriers combination was not very ideal, and the carrier recombination rate was still high [62]; The II-type heterojunction (Fig. 5d) belonged to the interlaced structure. The potential gap between semiconductors generated an electric field, resulting e^- enrichment on CB of semiconductor B, h^+ enrichment on VB of semiconductor A, which significantly enhanced photocatalytic activity and encouraged separating photogenerated carriers [63]; Z-scheme heterojunction (Fig. 5e) belonged to the interwoven structure. When the energy band structure of the two semiconductor materials was well matched and well contacted, e^- on the CB of semiconductor B had directly or indirectly combined with h^+ on semiconductor B VB, it considerably encouraged the photoinduced carrier separation and reserved mighty oxidation of catalyst [64]; S-scheme heterojunction (Fig. 5f). It was a good upgrade solution for Z-scheme heterojunctions. The motion mechanism of photogenerated carriers was the same as that of the Z-scheme, but the S-scheme heterojunction was innovatively divided into oxidizing photocatalyst (OP) and reducing photocatalyst (RP) according to semiconductor energy band composition photocatalytic materials. Photoinduced e^- and h^+ retained in the CB of RP, and the VB of OP, respectively, while inefficient photoinduced carriers were reorganized [65].

In TiO_2/g−C_3N_4 −based heterojunction photocatalysts, II-type, Z-scheme, and S-scheme heterojunctions have been research hotspots in the field of photodegradation in recent years. The next chapter will introduce their application in pollutant degradation in detail.

2.3. Photocatalytic degradation pathways of common organic pollutants

In this subsection, we provide a summary of common organic pollutants in an aqueous environment, exempli gratia antibiotics, dyes, pesticides, and phenolics, and provided a reasonable explanation of their degradation pathways.

2.3.1. Antibiotics

As the pharmaceutical industry was rapidly developing, the demand for antibiotics was increasing for humans and animals because they could cure many diseases promptly. However, it was not fully absorbed by humans and animals, resulting in the discharge of ample antibiotic residues in water environments and causing environmental pollution [66]. Tetracyclines, quinolones, and sulfonamides were the most used antibiotics, so it was very meaningful to study their degradation pathways.

Li et al. [67]. successfully prepared TiO_2/g−C_3N_4 photocatalyst and achieved high photodegradation efficiency for TC. The intermediates in the TC photocatalytic process were accessed by HPLC-MS, and possible degradation routes could be inferred from the *m/z* values of the intermediates. A typical photodegradation pathway of TC is shown in Fig. 6. First, TC attacked with $\bullet O_2^-$, which resulted in an intermediate product for aldehyde and carbonyl addition. Then P11 continued to be attacked by $\bullet O_2^-$, and an intermediate product was obtained by hydroxyl and methyl group stripping. Further cleavage and hydroxylation of the ring gave products with *m/z* values of 164, 149, 136, and 90, respectively. Furthermore, in the second pathway, the TC molecule was first attacked through h^+ to form a major demethylation product (P2-P5). The intermediates continued to be attacked by reactive radicals (h^+ and •OH) and were converted to small organic molecules after deamidation, addition, ring opening, and oxidation reactions.

In addition, the degradation of sulfonamide antibiotics was primarily attributed to the cleavage of sulfonamide groups, the detachment of amino groups on the benzene ring, and the breaking of C═N and N-O bonds [68]. Zhang et al. [34]. prepared mesoporous TiO_2/g−C_3N_4

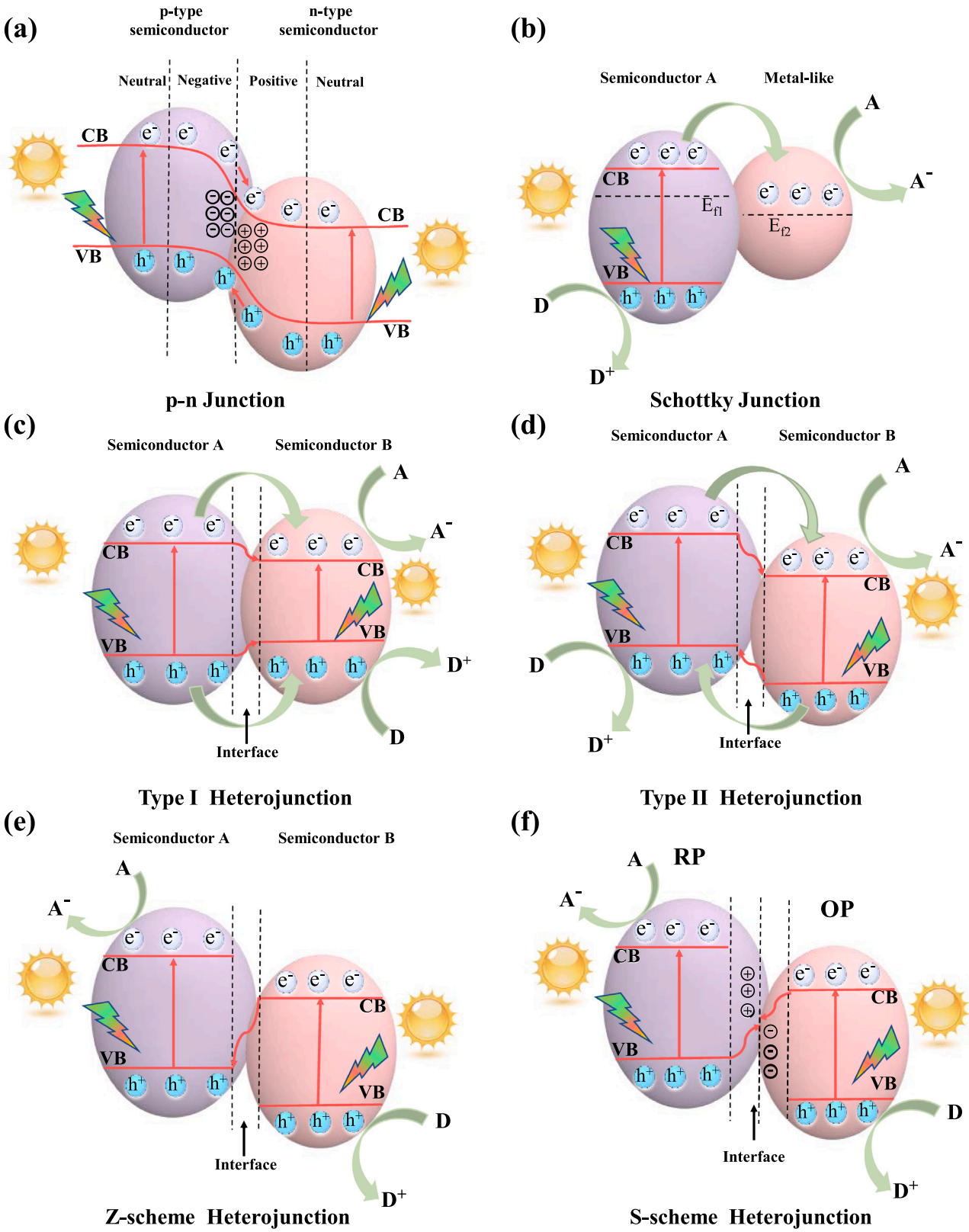

Fig. 5. Band structures of various heterojunctions:(a) p-n junction, (b) Schottky junction, (c) Type I heterojunction, (d) Type II heterojunction, (e) Z-scheme heterojunction, (f) S-scheme heterojunction. The letters A, D, and Ef stand for the electron acceptor, electron donor, and fermi level, respectively.

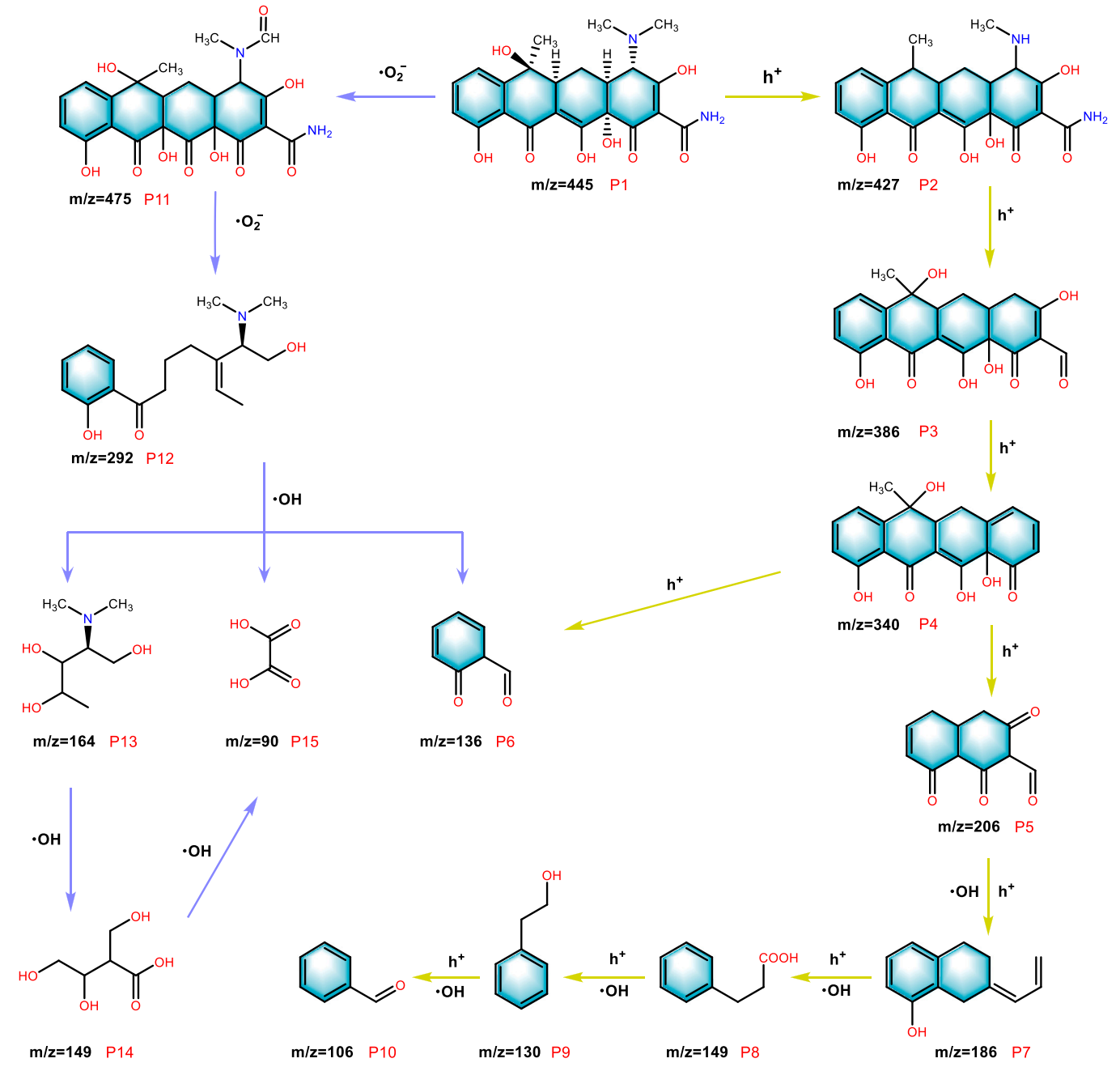

Fig. 6. Degradation pathways of TC. Copyright 2021, Elsevier. Adapted with permission from [67].

composites, and studied the photodegradation pathway of ENR. During an $\bullet O_2^-$ attack, ENR lost the piperazine part and subsequently amino group was oxidized to amide or underwent hydroxylation and decarboxylation reactions, and the end product was mineralized to CO_2 and H_2O small molecules.

2.3.2. *Dyes*

Contaminants with dyes in industrial wastewater were of great concern because of their high visibility, toxicity, and difficulty in degradation [69]. Thus, removing dyes from wastewater was essential to preventing water contamination. Common dye pollutants in wastewater were RhB, MB, MO, CR, etc.

The photodegradation mechanism of RhB was N demethylation and chromophore cleavage [2]. Iqbal et al. [70]. synthesized TiO_2/-Fe_2O_3/g−C_3N_4 for degradation of RhB, in addition, investigated the photodegradation pathway. Fig. 7a depicts the typical photodegradation pathway of RhB. MB was another toxic cationic dye, whose typical photodegradation pathway was shown in Fig. 7b, mainly through demethylation, hydrogenation, and sulfur-chloride bond cleavage [71]. Zhang and his partners have conducted in-depth learns on photodegradation pathways about the dye MO, mainly benzene ring hydroxylation, C−N bond cleavage and azo bond breaking, further oxidation, and ring opening to degrade the dye to smaller intermediates and environmentally friendly molecules [72].

2.3.3. *Phenolic pollutants*

The environmental problems posed by phenolic compounds were of increasing concern to the international community. For example, industrial activities such as the manufacture of phenolic resins, pesticide synthesis, and textiles discharged toxic phenolic pollutants into lakes

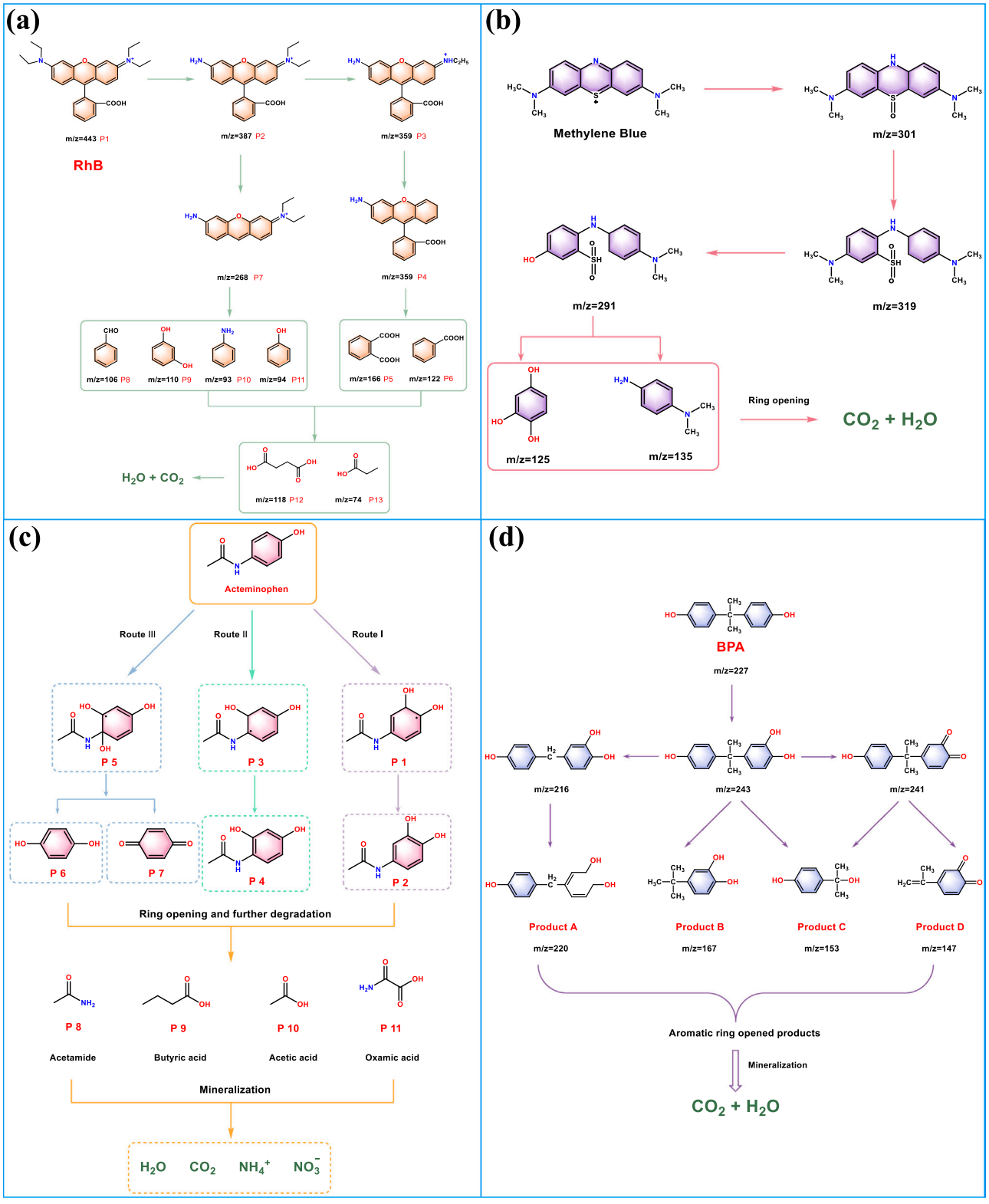

Fig. 7. Degradation pathways of (a) RhB, (b) MB, (c) Acetaminophen, and (d) BPA.
a) Adapted with permission from [73]. Copyright 2023, Elsevier. (b) Adapted with permission from [71]. Copyright 2022, Elsevier.(c) Adapted with permission from [74]. Copyright 2022, Elsevier. (d) Adapted with permission from [75] Copyright 2020, Elsevier.

and seas [76].

The acetaminophen (ACM) and BPA were common phenolic contaminants in water bodies. Only part of ACM was metabolized in the body and the rest was excreted, thus causing water pollution [36]. The photodegradation pathways of these two typical phenolic pollutants are described carefully below. In Fig. 7c, the hydroxyl group detachment process was most likely to blame for the breakdown of ACM, so •OH attacked the three active sites of ACM to form three main degradation pathways, all undergo a series of hydroxylation reactions, oxidation, and ring-opening reactions to form less toxic small molecule intermediates,

which were eventually further mineralized to H_2O and CO_2 [74].

BPA causes hormonal imbalance in the human body and can cause genital cancer even at low concentrations [77]. Fig. 7d presented the typical photodegradation pathway of BPA [75]. Initially, BPA was attacked by •OH to form mono-hydroxylated BPA, which continued oxidative decomposition to form demethylated intermediate B, further oxidation, and ring opening to form product A. The reactive radicals continued to attack to obtain products C and D. Finally, all intermediates underwent cyclic cleavage and mineralization to CO_2 and H_2O [78].

2.3.4. Pesticides

The rapid development of modern agricultural technology has led to lots of pesticide residues being left in the soil and water environment from excessive use. The low biodegradability and toxicity of pesticides made them a major source of water pollution [79]. In this context, photocatalytic degradation of pesticides was of great significance, so further research on the pathways of photodegradation of pesticides was imminent. Two organophosphorus pesticides that are most frequently employed in agricultural processes are chlorpyrifos and dichlorvos. Therefore, the study of chlorpyrifos removal pathways was guidance for the development of photodegradation catalysts for organophosphorus pesticides. First, reacted with •OH, after oxidation and hydroxylation, then further dehydroxylation and dechlorination, and lastly, the mineralization of all intermediates produced tiny molecules like H_2O, CO_2, PO_4^{3-}, NO_3^-, etc. [80].

It is worth mentioning that atrazine (ATZ) is a very efficient herbicide that has been widely used worldwide. Due to its highly stable chemical properties and immunity to microorganisms, it was widely retained in agricultural wastewater, posing an enormous intimidation to both the health of people and the environment. Even though many countries have banned the use of atrazine, its presence can still be detected in water bodies to date [81]. The study of atrazine photocatalytic degradation pathways can guide one to design more efficient pesticide removal processes. Fig. 8 shows the photodegradation pathway of a typical ATZ [82]. The active substances were $^1O_2$ and •OH, which undergo demethylation, oxidation, substitution, and ring-opening reactions and were lastly mineralized into H_2O, CO_2, and NH_3 small molecules.

2.3.5. Toxicological evaluation of photodegradation processes

It is well known that most organic pollutants and the intermediates produced by their photodegradation processes are toxic and represent an immediate danger to human life and ecological balance. The advantages of the oxidation process can be evaluated not only by the decomposition of the target contaminants but also by the degree of toxicity of the product intermediates [83]. The risks associated with potential toxicity of degradation products and their biodegradation analysis are thus highly important. To gain a better understanding of how toxicity shifts as a result of photodegradation, a toxicity estimation software tool (T.E.S.T) based on quantitative structure-activity relationship (QSAR), prediction can be used to quickly assess the toxicity of the products. Toxicological data are commonly used to evaluate target contaminants and intermediates, including the fathead minnow LC50 (96 h), Daphnia magna LC50 (48 h), bioaccumulation factor, developmental toxicity, and mutagenicity. Gan et al. used oxygen-doped g-C_3N_4 modified g-C_3N_4/TiO_2 hybrid heterogeneous structure to degrade gatifloxacin (GTA), demonstrating outstanding degradation performance [84]. They employed the T.E.S.T tool for toxicity assessment analysis. The results showed that the degradation process significantly reduced the acute toxicity of GAT solution; developmental toxicity may be due to carbamylation, and aminomethanesulfinic acid can reduce developmental toxicity; almost all the bioaccumulation factor of the intermediates were reduced. In conclusion, the photocatalytic degradation process can significantly reduce the toxicity of GAT wastewater. Most

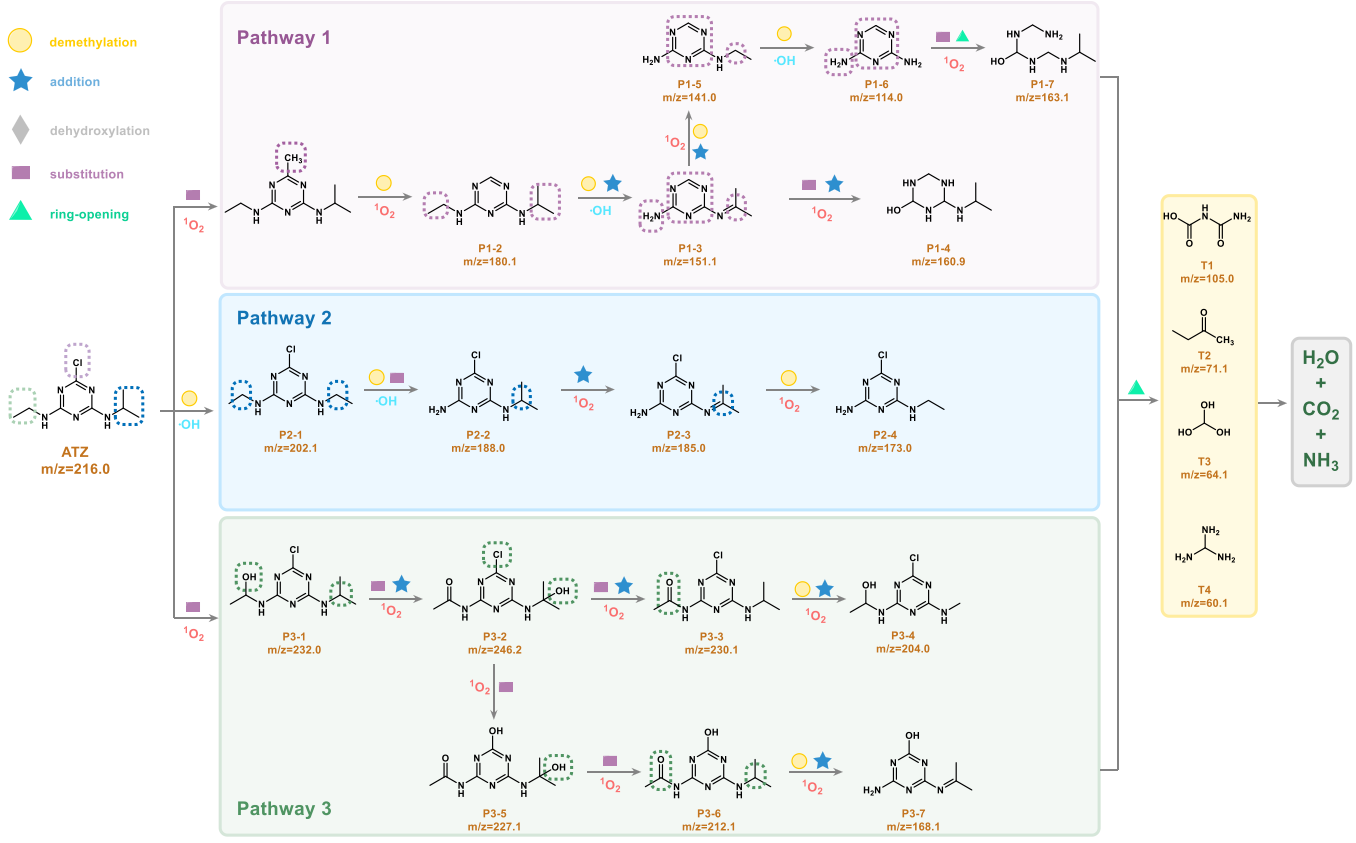

Fig. 8. Degradation pathways of ATZ.
Adapted with permission from [82] Copyright 2020, Elsevier.

degradation intermediates had low toxicity, indicating photocatalysis can achieve the removal of the target pollutants and reduce their toxicity. With respect to most reactions, the deeper the reaction progresses, the less toxic the degradation products tend to be [85].

3. TiO_2/g−C_3N_4 −based heterojunction photocatalysts

Researchers have observed that the utilization of two semiconductors to generate a heterojunction structure significantly augments the photocatalytic properties of catalysts. Various methods can be employed to synthesize TiO_2 −based heterojunctions, such as hydrothermal, solvothermal, electrostatic spinning, sol-gel, and ultrasonic- and microwave-assisted approaches. The synthesis process is visually depicted in Fig. 9. Furthermore, it is widely recognized that the formation of a suitable heterojunction between g−C_3N_4 and TiO_2 promotes effective spatial separation of photogenerated e^-−h^+ and greatly enhances photocatalytic activity. Depending on distinct mechanisms of carrier separation in different hybrid heterostructures resulting from the coupling of TiO_2 and g−C_3N_4, TiO_2/g−C_3N_4-based heterojunction photocatalysts can be categorized into three types: type II heterojunction, Z-scheme heterojunction, and S-scheme heterojunction. This chapter provides a comprehensive introduction to the preparation methods of common heterojunction photocatalysts, and a detailed discussion and description of the latest research progress on the degradation of organic pollutants by these three heterojunction systems.

3.1. Fabrication of TiO_2 −based heterojunctions

3.1.1. Hydrothermal/solvothermal

Last few years, hydrothermal and solvothermal have played very important roles in the preparation of nanocomposites. Hydrothermal synthesis describes non-homogeneous processes. A water solution (solvent solution) containing precursors was heated to above boiling in a closed stainless-steel autoclave, leading to the creation of a high-pressure environment, where nanomaterials can be successfully made in one step under synergistic implication of elevated temperature and high pressure. The hydrothermal/solvothermal method had moderate reaction temperature, high crystallinity, and stability of the products. Ease of operation and environmental friendliness of synthesis procedure were also among the reasons for its widespread use [86,87]. Furthermore, the method allowed for easier control of the precipitation phase, resulting in better control of the size and shape of material. However, the reaction lasted for a long time, and the difficulty in achieving identical size remained a real problem for the hydrothermal/solvothermal method.

3.1.2. Electrospinning method

Electrostatic spinning technology was commonly used to produce micro and nanofibers. It was an effective technique for the preparation of continuous nanoscale fibers, which was a process of charging and spraying the solution at high pressure through a spinneret. This method was influenced by potential, viscosity, pressure, and flow rate, with viscosity being the most important indicator. Advantages included simplicity and ease of operation, high efficiency, relative economy, and many parameters that can be set (width of fibers, composition). Disadvantages included the usage of organic solutions, yield is low, and general stability of the fibers [88].

3.1.3. Sol-gel

Sol-gel was a wet chemical method, which was one of the simple methods used to prepare nanocomposites. It specifically included several steps of hydrolysis, condensation, gelation, aging, drying, and

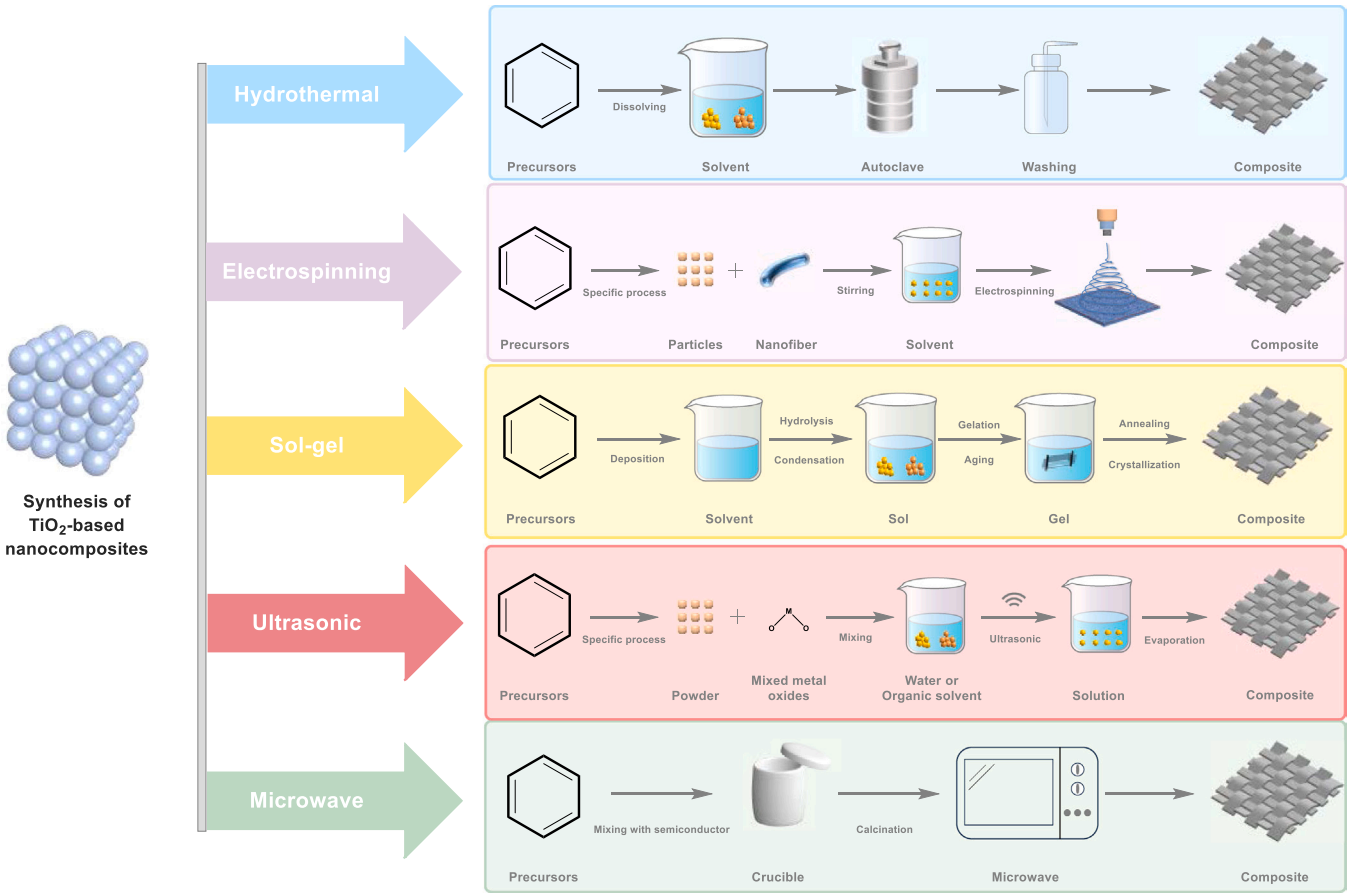

Fig. 9. Synthesis methods of TiO_2 −based heterojunctions.

calcination, among which hydrolysis and thermal condensation reactions were the most important. The most significant advantage was that it can provide a significant amount of surface area and solid surface, and is a low-cost, low-temperature, highly controllable, easy-to-operate, and high-purity product synthesis process [89]. The disadvantages were also obvious: the organic solution used was harmful, the reaction time was too long, and residual carbon and hydroxyl groups were present [90].

3.1.4. Ultrasonic and microwave-assisted methods

Radiation with specific wavelengths, such as ultrasound and microwave, often affects the reaction-catalyzing capacity of prepared materials. The conventional method of synthesis of nanomaterials was ultrasound-assisted treatment during the chemical reaction so that metal oxides could be uniformly distributed on the face of another semiconductor, and finally, evaporation through the corresponding solvent to obtain the desired material [91]. The microwave method was usually applied in the preparation of nanomaterials that require heat treatment, which can substantially enhance the contact between semiconductors, reduce the interfacial energy between them, and bring them to the same phase plane as soon as possible [92]. The advantages of both methods were: both are efficient, eco-friendly, green, fast, and simple approaches to preparing nanocomposites; nanostructures of different shapes and sizes can be prepared; the disadvantages were: that the prepared composites exhibit weak chemical bonds between them, the charge transfer was relatively weakened, the crystallization time was shorter, and the new energy consumption was added [93].

3.2. Type II $TiO_2/g-C_3N_4$ –based heterojunction photocatalyst

Owing to the separation between e^-–h^+ in space in type II heterojunction structure, the photocatalytic performance was enhanced, but the relatively poor oxidation-reduction ability of type II photocatalyst restricted its application [94]. However, it has been attempted to create a very effective $TiO_2/g-C_3N_4$ type II heterojunction composite photocatalyst based on defective complementary characteristics of $g-C_3N_4$ with TiO_2, which can facilitate carrier separation and improve photocatalytic activity [49]. For instance, Zhang et al. [34]. produced $TiO_2/g-C_3N_4$ by thermal polymerization of TiO_2 with carbamide precursors. XPS confirmed the presence of O–Ti–N bonds in $TiO_2/g-C_3N_4$, leading to electron delocalization and the formation of heterojunctions between energy bands. The photocatalytic performance was much greater than $g-C_3N_4$ because the presence of the O–Ti–N bond improved the conjugation system, which facilitated the transport of electrons, and optimized the band gap that was better for using visible light.

Similarly, Zhang et al. [95]. synthesized $TiO_2/g-C_3N_4$ using hydrothermal. Fig. 10a-b indicated $TiO_2/g-C_3N_4$ NPs had uniform

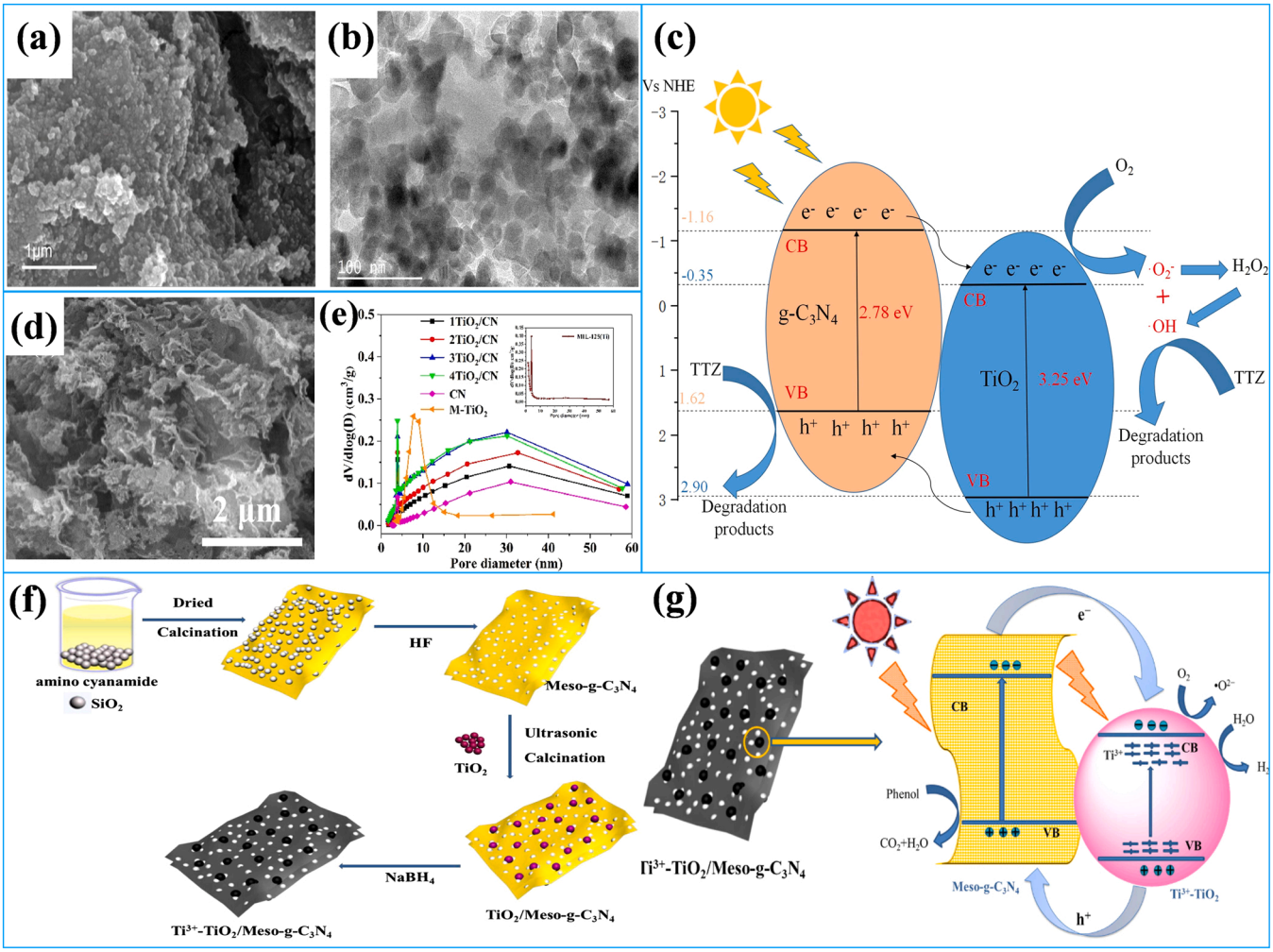

Fig. 10. SEM (a) and TEM (b) image of 18% $TiO_2/g-C_3N_4$. (c) Photocatalytic mechanism of $TiO_2/g-C_3N_4$. (d) SEM image of $4TiO_2/CN$. (e) Pore size distribution plots of $4TiO_2/CN$. (f) Formation procedure of $Ti^{3+}-TiO_2/Meso-g-C_3N_4$. (g) Transfer path mechanism of photoinduced carriers in $Ti^{3+}-TiO_2/Meso-g-C_3N_4$. (a-b) Reproduced with permission from Ref. [95]. Copyright 2021, Elsevier. (c) Reproduced with permission from Ref. [96]. Copyright 2022, Elsevier. (d-e) Reproduced with permission from Ref. [97]. Copyright 2021, Elsevier. (f-g) Reproduced with permission from Ref [98]. Copyright 2017, Elsevier.

morphology, and TiO_2 was distributed on g−C_3N_4 thin section. Experimental results of PBX degradation showed that the degradation rate reached 97.1% under simulated light irradiation for 100 min. Cao et al. [96]. prepared TiO_2/g−C_3N_4 heterojunction using the hydrothermal method, which dispersed a large amount of TiO_2 nanosheets on a light coating of g−C_3N_4, which facilitated photoinduced e^-−h^+ movement and improved utilization of optical energy. Under the irradiation of simulated sunlight, the rate of degradation of TTZ was as high as 93% within 1 h. Radical capture experiments showed that $\bullet O_2^-$ played dominant plays in the process of removal, indicating that the composites were consistent with carrier transfer in a typical type II heterojunction (Fig. 10c). Under simulated solar irradiation, TiO_2 CB potential was much more negative than $O_2/\bullet O_2^-$ was much more negative, so e^- in TiO_2 CB was easily trapped by O_2 to generate $\bullet O_2^-$. The VB potential was lower than redox potential for g−C_3N_4 of $\bullet OH/H_2O$, so h^+ left in VB cannot react with H_2O. To improve photocatalytic performance, people had modified the morphology of the two semiconductor materials themselves, nanoparticles and nanosheets of semiconductor materials as precursors to prepare heterojunction have become commonplace. The overall degradation effect was still unsatisfactory due to the weak redox ability of type II heterojunctions.

MOFs materials as a template for precursors to be derived from organic frameworks by calcination to nano metal oxides, using MOFs materials topology an important application. Recently, Xiao et al. [97]. synthesized defect-rich TiO_2/g−C_3N_4 by in-situ pyrolysis. TiO_2/g−C_3N_4 heterojunction improved by this method had a narrow band-gap (2.27 eV) and enhanced absorption capacity of light. SEM images of 4TiO_2/CN exhibited a very different morphology to dense g−C_3N_4, showing a wavy, more loose morphology (Fig. 10d). And, Fig. 10e displayed MIL− 125(Ti) pore structure. The authors concluded the combination of MIL− 125(Ti) and thermal condensation of melamine facilitated the improvement of the pore catalyst structure, thus synergistically promoting the photocatalytic performance.

In contrast, Tan et al. [98]. prepared Ti^{3+}−TiO_2/Meso−g−C_3N_4 nano-heterojunction by calcination-ultrasonic assisted method combined with in-situ solid-state chemical reduction method by melamine as a precursor and SiO_2 being template (Fig. 10f). XPS analysis demonstrated oxygen vacancies and Ti^{3+} presence, which inhibited compounding of e^- and h^+, increasing photocatalytic activity and phenol degradation efficiency by 93.1% within 10 min Fig. 10g shows the possible degradation mechanism. According to the result the CB position of g−C_3N_4 is higher than Ti^{3+}-TiO_2, e^- will transfer to Ti^{3+}−TiO_2, while photo-induced h^+ will transition to Meso−g−C_3N_4, which accelerated carriers' separation rate and inhibits e^-−h^+ recombination rate. Wu et al. [99]. constructed TiO_2 @C/O-doped g−C_3N_4 heterojunction using an in-situ growth method, exposing more active sites than conventional TiO_2/g−C_3N_4 heterojunctions to ramp up photocatalytic activity, with twice the photodegradation efficiency of g−C_3N_4 for MB. Similarly, the modification methods of TiO_2 or g−C_3N_4 included non-metallic element doping, self-doping, MOFs template sacrificial method, etc. This led to advantages such as oxygen vacancy generation, more active sites, and better adsorption properties. Notably, Sheng et al. [100]. applied one-step calcination to prepare 3D g−C_3N_4/TiO_2 heterojunction. The composites obtained showed satisfactory degradation efficiency in both static and dynamic systems, mainly because of the complementary nature of adsorption enrichment. Furthermore, 3D g−C_3N_4/TiO_2 composites can continuously degrade pollutants without separation and have high stability. However, there was little literature on the photodegradation of 3D composites in static and dynamic pollutant systems, which had a high reference value. Nanoparticles synthesized from plant source extracts are known to be green, low toxicity and environmentally friendly, which is a good strategy in line with green chemistry. Faryad et al. prepared boron doped g-C_3N_4/TiO_2 nanocomposite photocatalysts by wet co-precipitation method using Spinacia oleracea leaves as a boron source [101]. The addition of boron substantially increased the light absorption range as well as the catalytic activity of the composites. The catalytic performance of the composite B-g-C_3N_4/TiO_2-8% with optimal co-catalyst ratio was tested and found to be much better than that of other synthesized pristine catalysts and composites. The doping of appropriate B elements can enhance the visible light response principle. Table S1 summarizes the research progress of type II TiO_2/g−C_3N_4 −based heterojunction composite photocatalysts.

Summary: Type-II heterojunctions, consisting of two semiconductors with interlocked energy band positions, have been extensively studied for their efficient charge separation and simple structure. TiO_2/g−C_3N_4 −based heterojunction photocatalysts are prepared using lots of methods e.g., hydrothermal, calcination, electrostatic spinning, and sol-gel techniques. This section elaborates on the advantages and disadvantages of typical type II TiO_2/g−C_3N_4 −based heterojunction photocatalysts, serving as a guideline for researchers to develop more efficient type II TiO_2 −based heterojunctions. Despite efforts to create novel type II TiO_2/g−C_3N_4 −based heterojunction photocatalysts, improved e^-−h^+ separation achieved in type II heterojunctions is insufficient to overcome the rapid recombination rate of e^-−h^+ complexes in semiconductors, and inherent weak oxidation ability continues to hinder their progress. However, researchers have recently employed a new heterojunction structure called Z-scheme heterojunction to overcome these limitations [102].

3.3. *Z-scheme TiO_2/g−C_3N_4 −based heterojunction photocatalyst*

Similar energy band configuration exists in type II and Z-scheme heterojunction, they have very different carrier migration paths (Fig. 5d-e). Z-scheme heterojunction better completed the two "tasks" that people often consider to increase photocatalytic activity, the catalyst band-gap is reduced to broaden spectral response range; CB moves to the negative band, and VB moves to the positive band to promote the photocatalytic redox process [103]. According to the presence or absence of a solid medium, Z-scheme heterojunctions can be classified as ASS Z-scheme heterojunctions and DZS heterojunctions (no medium). In this chapter, we categorically summarize the research progress of ASS Z-scheme TiO_2/g−C_3N_4 −based heterojunction photocatalysts and DZS TiO_2/g−C_3N_4 −based heterojunction photocatalysts.

3.3.1. *ASS Z-scheme TiO_2/g−C_3N_4 −based heterojunction photocatalyst*

The ASS Z-scheme heterojunction photocatalysts were composed of two different semiconductor materials and solid materials such as precious metal particles and carbon-based materials as electron media, which had the advantage of promoting carrier separation and retaining a high redox capacity. Interestingly, precious metals readily accepted e^- carried in the CB of semiconductor materials, so precious metal particles as electron mediators can act as a sparse guide and substantially reduce compounding rate of photogenerated e^-−h^+.

Typically, Wei et al. [104]. synthesized Au/g−C_3N_4/TiO_2 heterojunction modified with Au NPs. The Au NPs loaded on g−C_3N_4 formed charge separations effectively charge separation, so Au/g−C_3N_4/TiO_2 incarnated terrific properties with organic pollutants degradation. Au/g−C_3N_4/TiO_2 heterojunction had the highest electric field intensity (Fig. 11a). Fig. 11b showed the PL spectrum, with AuC-T exhibiting good interfacial charge separation. Nyquist plot's narrower semicircle radius (Fig. 11c) illustrated the reduction of interfacial charge transfer resistance and improvement of carrier separation. Compared with TiO_2, hybridization of g−C_3N_4 made it have better light absorption ability, and the hybrid structure showed a strong plasma-induced electric field in the metal-carrier interface. Above phenomena suggested that interactions at the metal carrier interface can improve plasma-induced hot electron density, and accelerate transmission of e^- between surfaces, resulting enhancement of photocatalytic performance [105]. The schematic diagram of AuC-T photocatalytic degradation pathway is shown in Fig. 11d. The modification of Au NPs altered the charge transfer behavior in a way that was different from common type II g−C_3N_4/TiO_2 heterojunction. With Au contacted with g−C_3N_4 and TiO_2 acting as an

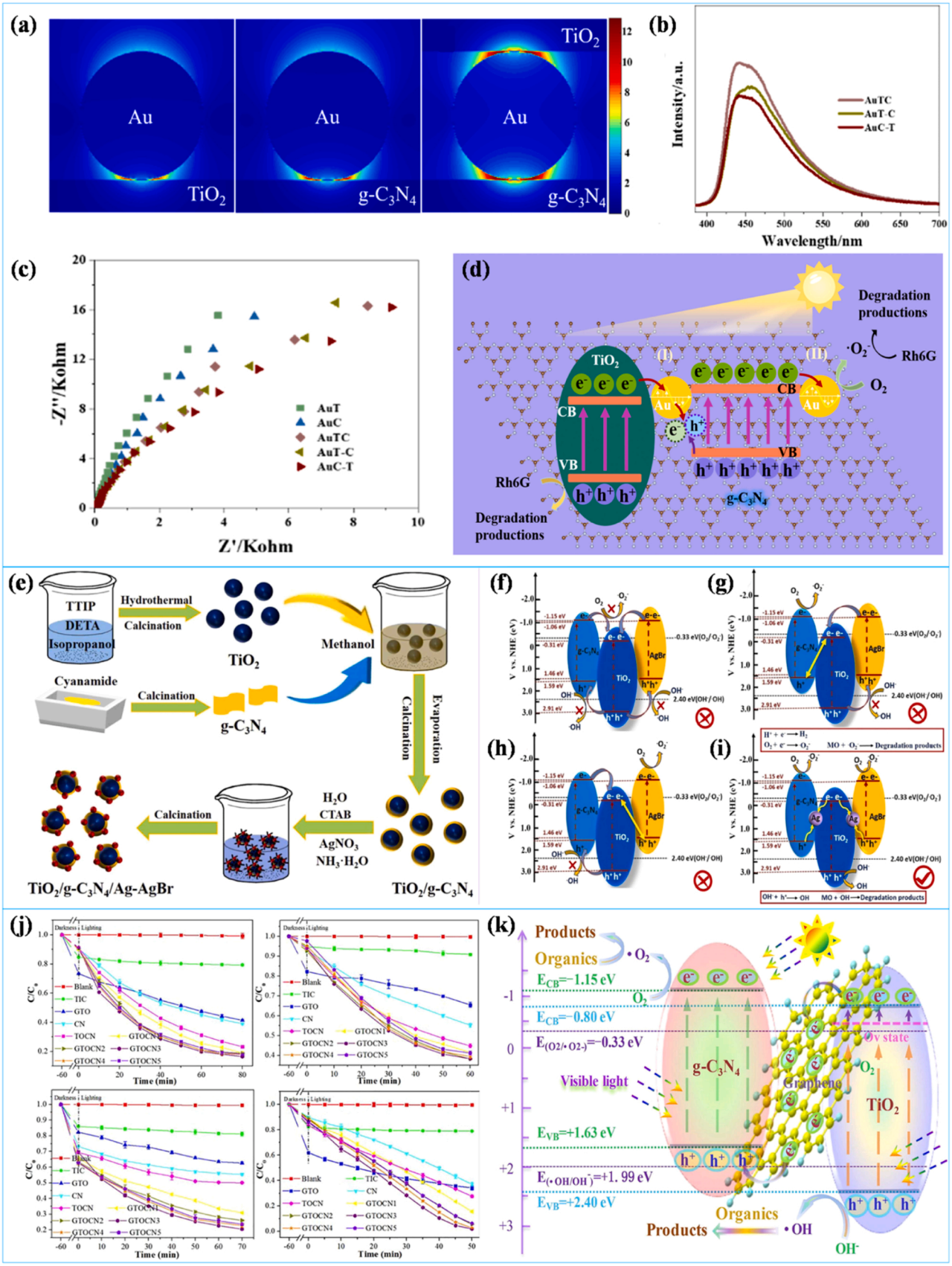

Fig. 11. (a) Distribution of the electric field across all samples. (b) PL spectra and (c) Nyquist plots of all samples. (d) Diagram of charge movement. (e) The manufacturing process of TCNAAB. (f-i) Schematic diagram of charge movement by TCNAAB-50. (j) Degradation performance of TC, CIP, BPA, and RhB. (k) Mechanism of photodegradation process of GTOCN3.

(a-d) Reproduced with permission from Ref. [104]. Copyright 2022, Elsevier. (e-i) Reproduced with permission from Ref. [106]. Copyright 2022, Elsevier.(j-k) Reproduced with permission from Ref [107]. Copyright 2020, Elsevier.

electron mediator, e^- trapped from TiO_2 VB bound to h^+ on $g-C_3N_4$ VB, and the Z-scheme mechanism emerged. Simultaneously, e^- on $g-C_3N_4$ CB migrated to another Au nanoparticle. Results suggested dual synergistic effect of gold as an electron mediator and co-catalyst can facilitate the separation of carriers.

Likewise, Rabé et al. [108]. prepared $g-C_3N_4/Fe^0(1\%)/TiO_2$ photocatalyst using chemical reduction. Photocatalytic degradation of RhB, TC, and BH resulted in 98%, 92%, and 90% degradation within 90 min respectively. It was worth mentioning that Guo et al. [106]. constructed a novel $TiO_2/g-C_3N_4/Ag-AgBr$ dual-Z multilayer composite photocatalyst using Ag as the charge transfer medium. The synthesis process is shown in Fig. 11e. TCNAAB-50 showed terrific photocatalytic activity against MO. The authors proposed a new double Z-scheme silver-bridge heterojunction, and conceivable charge transfer mechanism and photocatalytic reaction are shown in Fig. 11f-i. In this case, Fig. 11f showed a double type II charge transfer pathway, where the O_2 on TiO_2 cannot generate $\bullet O_2^-$ when it reacted with e^- and OH^- cannot react with h^+ in AgBr and $g-C_3N_4$ to form •OH, which was opposed to the conclusions reached by experiments. In Fig. 11g, $TiO_2/g-C_3N_4$ and $TiO_2/AgBr$ belonged to the type II combination, showing h^+ in VB of AgBr cannot oxidize OH^- to •OH, residual e^- in CB of $g-C_3N_4$ reduced O_2 to $\bullet O_2^-$. Similarly, residual e^- in AgBr reduced O_2 to $\bullet O_2^-$, as seen in Fig. 11h, while h^+ on VB of g-C_3N_4 was unable to oxidize OH^- to •OH. Therefore, type II and Z-scheme with dual charge movement paths can produce $\bullet O_2^-$ but not •OH. As a result, a double Z-scheme route could be used for the charge movement operation (Fig. 11i). Ag can act as a charge transfer medium for double Z-scheme heterojunction, and e^- on TiO_2 CB can transfer to Ag, and Ag can transport h^+ from VB of AgBr and $g-C_3N_4$ and combined with e^-. This resulted in the reaction of O_2 to form $\bullet O_2^-$. In summary, the active substances $\bullet O_2^-$ and •OH can degrade MO, which was in agreement with the holding result of an experiment. The proposed double Z-scheme charge movement mechanism provided an idea for efficient catalyst preparation for the design of a multi-carrier transport channel. Besides MNPs, new carbon materials often served as electronic media to construct Z-scheme photocatalysts[109,110]. For example, $g-C_3N_4$ $-RGO-TiO_2$ heterojunction was used as an ASS Z-scheme photocatalyst for MB photocatalytic degradation [110]. Author revealed multiple roles of RGO act as a solid electron mediator, adsorbent, photosensitizer, and electron acceptor through different experimental methods, which provided a design concept for the creation of ASS Z-scheme carbon-based materials as electron media.

On this basis, it had been found that graphene had larger SSA and topping conductivity. Wu et al. [107]. adopted MXene Ti_3C_2 as ingredients to prepare Z-scheme graphene layer-anchored $TiO_2/g-C_3N_4$ photocatalyst (GTOCN) with high catalytic activity using a one-step calcination. GTOCN morphology characterization analysis proved successful preparation of composites. As shown in Fig. 11j, TIC, GTO, CN, and GTOCN's photocatalytic efficiency samples were compared by persistent organic contaminants such as TC, CIP, BPA, and RhB. It can be observed removal rate of these organics in presence of TIC is less than 20%, which is due to adsorption and weak photosensitive degradation. TOCN degraded 76.7%, 55.2%, 50.0%, and 72.4% of the four pollutants, respectively. CN and GTOCN degradation efficiency is better compared to GTO. Among them, The removal rate of GTOCN3 was the highest, and rates at which TC, CIP, BPA, and RhB degrade were 83.5%, 61.7%, 79.5%, and 98.0%, respectively. Based on results of the experiments in which active substances were tested, the order of contribution of three active substances to the photodegradation process was $\bullet O_2^- > h^+ >$ •OH. Finally, the authors analyzed the possible degradation mechanisms as shown in Fig. 11k. From the light generation process of heterojunction carriers, the absorption of photons by $g-C_3N_4$ excites e^- to CB, while an equal amount of h^+ is generated on the VB. Because oxygen vacancies induced TiO_2 to form a localized state below CB, TiO_2 can also be activated to form $e^- - h^+$. Graphene increased the photo sorption capacity of TiO_2, accelerated the excitation of light to $e^- - h^+$, and acted as a co-catalyst [111]. Assuming that the carriers at the interface follow the path of motion of type II, reciprocal transfer of e^- from $g-C_3N_4$ CB and h^+ from TiO_2 VB, resulting in e^- buildup in TiO_2 CB and h^+ in $g-C_3N_4$ VB. Therefore, standard redox potential of $\bullet OH/OH^-$ (+1.99 eV vs. NHE) was higher than the VB potential of $g-C_3N_4$ (1.63 eV), so •OH radicals could not be produced, which was inconsistent with ESR and free radical quenching assay. So, interface transfer and separation of light-induced $e^- - h^+$ were more suitable for the Z-scheme heterojunction model than the II-type heterojunction. The e^- of TiO_2 was rapidly captured by graphene and immediately transferred to $g-C_3N_4$ to complex with the h^+. Therefore, e^- and h^+ separation effectiveness was much improved compared with original $g-C_3N_4$ and TiO_2, e^- enriched on $g-C_3N_4$ reacts with O_2 adsorbed on the material's surface to create $\bullet O_2^-$, then h^+ enriched on TiO_2 contacted with OH^- to form •OH, both of which were used to degrade organic pollutants. Similarly, Moradi et al. [36]. prepared efficient ASS Z-scheme TiO_2/graphene/$g-C_3N_4$ (TGCN) heterojunction. Graphene was inserted between TiO_2 and $g-C_3N_4$, forming low-resistance ohmic, and carrier migration can be promoted by ohmic contact. ACM could be degraded within 2 h under simulated sunlight radiation conditions. The higher photocatalytic activity was owing to graphene-promoted separation carriers, which resulted in promoting interfacial charge migration and accelerating the formation rate of •OH and $\bullet O_2^-$ radicals. Interestingly, Xue and his colleagues prepared a $g-C_3N_4$ (Ag)/Gr/TiO_2 photocatalyst using a classic hydrothermal. $g-C_3N_4$(Ag)/Gr/TiO_2 degraded RhB almost completely within 2 h [112]. A series of experiments have proved that Gr between $g-C_3N_4$ and TiO_2, as electron "intermediary", makes photogenerated carriers easier to compound, while silver clusters, as the e^- reserve layer, the catalytic performance was further improved by the acceleration of the reduction process of photogenerated e^-. It is of concern that conventional photocatalysts are inefficient in treating low doses of antibiotics in wastewater, so there is an urgent need to develop a technology for the selective degradation of antibiotics. Liu et al. prepared a novel molecularly imprinted $Fe_3O_4/g-C_3N_4/TiO_2$ catalyst (MI-UCT) using hydrothermal and molecularly imprinted techniques [113]. The catalyst, with $Fe_3O_4/g-C_3N_4/TiO_2$ (FCT) as the substrate and chlorotetracycline (CTC) as the templating agent, possessed specific recognition and highly efficient photocatalytic properties. The adsorption of CTC by MI-FCT was about 24.54 $mg \cdot g^{-1}$ with a removal rate of 91.87%, which successfully proved the catalyst's role in the specific removal of CTC. Table S2 shows the research progress of ASS Z-scheme $TiO_2/g-C_3N_4$ −based heterojunction photocatalysts in the direction of pollutant degradation in the past five years.

Although the ASS Z-scheme heterojunction structure owns excellent photocatalytic performance, it is difficult to be applied in practical production due to the cost of common electronic media. These electronic media will inevitably affect the environment; the synthesis conditions are harsh, and the optimal spatial presence of solid media between two catalytic materials is difficult to determine[94]. To overcome the above difficulties, DZS heterojunctions without electron dielectrics are starting to receive a lot of attention.

3.3.2. *DZS $TiO_2/g-C_3N_4$ −based heterojunction photocatalyst*

Within the last five years, for photo-degradation of organic contaminants, numerous studies on DZS $TiO_2/g-C_3N_4$ −based photocatalyst composites have been described. Because it did not require the use of expensive electronic media, it greatly reduced the production cost of DZS heterojunction. In addition, it retained the fast e^- and h^+ separation effectiveness and a powerful redox capacity and overcame the

shortcomings of the ASS Z-scheme system [28,114]. To summarize, the research of DZS TiO_2/g−C_3N_4 −based photocatalysts had a very promising future in the field of photocatalysis.

Based on this theory, Vijayan et al. [115]. used simple wet impregnation way to prepare g−CN−TiO_2 heterostructure composites. DZS heterojunction successfully avoided rapid compounding of light-induced e^- and h^+, and improved the efficiency of photocatalysis. With the in-depth research, the spatial morphology of TiO_2 or g−C_3N_4 was modified to become nanosheets, nanorods, nanoparticles, and other nanomaterials for coupling to form Z-scheme heterojunction to further enhance their photocatalytic performance.

As a classical example, Zhang et al. [116]. prepared (2D/0D) g−C_3N_4/TiO_2 through putting melamine and TiO_2 NPs by a co-annealing process. In Fig. 12a, when the mass ratio of the two was greater than 0.5, g−C3N4 had no peak. When mass ratio of the two was 0.2, two crystal plane peaks of g−C_3N_4 appeared on the photocatalyst, which demonstrated creation of TiO_2/g−C_3N_4. The SSA and pore size distribution of g−C_3N_4/TiO_2 photocatalyst were studied (Fig. 12b-c). The isotherm of g−C_3N_4/TiO_2 belongs to type IV, indicating that it is a mesoporous material. The g−C_3N_4/TiO_2 had more mesopores, which led to greater SSA. Increased adsorption capacity and additional active sites may offer improved catalytic activity. From Fig. 12d, within 2 h, TC was degraded by TiO_2, g−C_3N_4, and g−C_3N_4/TiO_2 at the rates of 95%, 90%, and 99%, respectively. The g−C_3N_4/TiO_2 had high photocatalytic activity perhaps owing to matched energy band structure between g−C_3N_4 and TiO_2, which formed a non-homogeneous structure promoted the charge transfer within catalyst, and exhibited a powerful redox ability. The quick separation of photogenerated carriers can be facilitated by this photocatalytic system. The degradation process was a reaction of e^- with dissolved oxygen to arise $\bullet O_2^-$, h^+ combined with water to generate •OH, and the action of reactive free radicals degraded TC to CO_2 and H_2O at the end.

With the in-depth study, the use of metal and non-metal doping can help to promote carrier isolation and improve photocatalytic activity [117]. Li et al. [118]. synthesized C−TiO_2 containing oxygen vacancies by in situ doping, and then constructed g−C_3N_4 @C−TiO_2 by chemical vapor deposition. Meanwhile, authors explored g−C_3N_4 @C-TiO_2 (Fig. 12e-h), photocatalytic degradation efficiency increased first and then decreased. The increase in photocatalytic performance may be because g−C_3N_4 was tightly bound to the surface of C−TiO_2 through

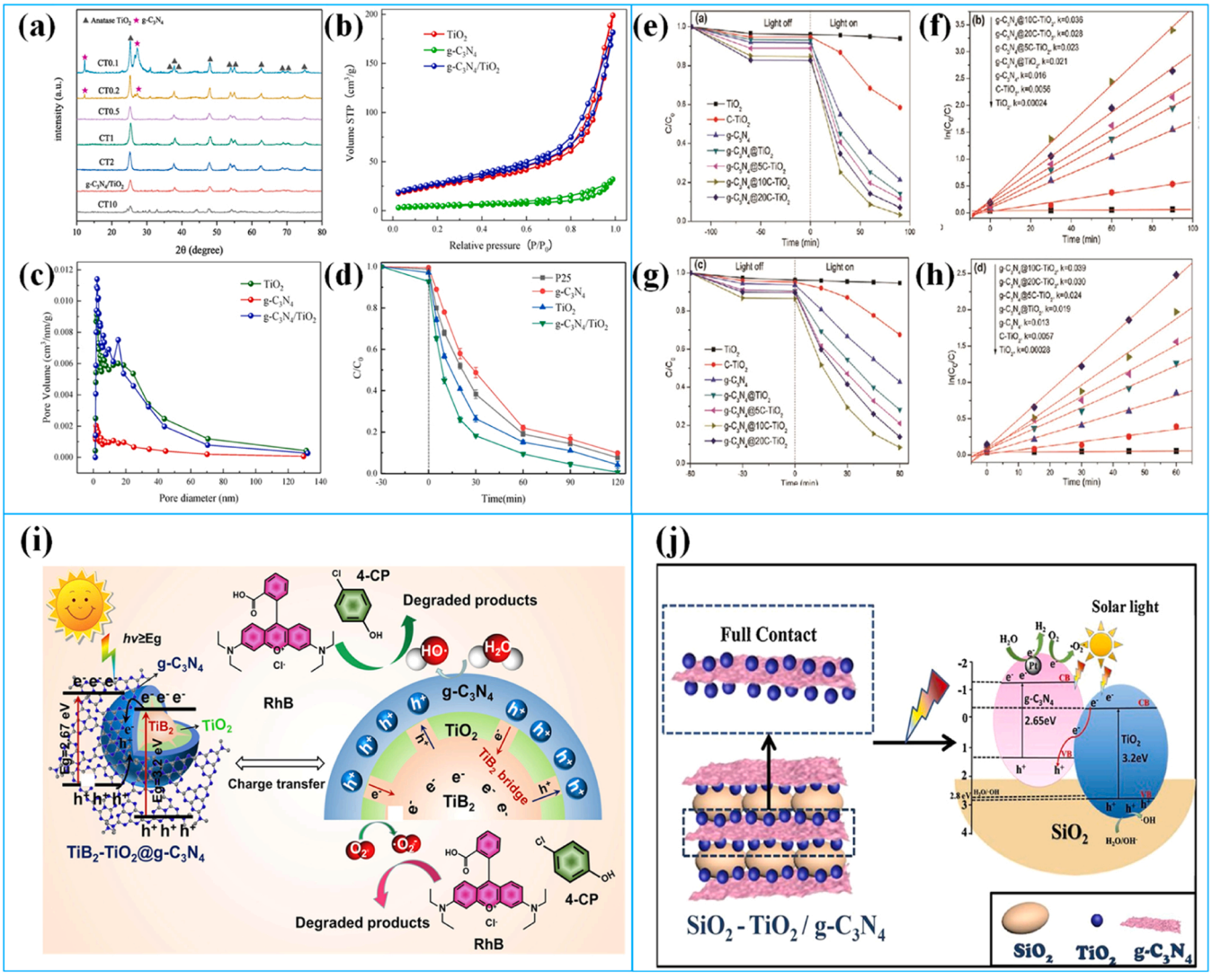

Fig. 12. (a) XRD pattern of g−C_3N_4/TiO_2. (b) N_2 adsorption-desorption isotherms, (c) Pore size distribution curves, (d) Photodegradation TC of by all samples. Time-course variation of C/C_0 (e) and $\ln(C_0/C)$ (f) curves for RhB degradation. Time-course variation of C/C_0 (g) and $\ln(C_0/C)$ (h) curves for phenol degradation. (i) Schematic diagram of charge separation and transfer of TiB_2 −TiO_2 @g−C_3N_4. (j) Schematic representation of charge migration of SiO_2 −TiO_2/CN.
(a-d) Reproduced with permission from Ref. [116]. Copyright 2020, Elsevier.(e-h) Reproduced with permission from Ref. [118]. Copyright 2019, Elsevier. (i) Reproduced with permission from Ref. [119]. Copyright 2022, Elsevier.(j) Reproduced with permission from Ref [120]. Copyright 2020, Elsevier.

π-conjugated and hydrogen bonds, introducing new non-local impurity energy levels and surface states, which can more effectively separate and transfer photogenerated carriers. Similarly, Yu et al. [119]. successfully prepared core-shell TiB_2 −TiO_2 @g−C_3N_4 heterojunction utilizing a single-step calcination process. Meanwhile, g−C_3N_4 wrapped around TiB_2 −TiO_2 nuclei formed a DZS heterojunction, which led to rapid separation and transport of charge carriers and greatly improved photo-catalyzed degradation capacity (Fig. 12i). Experimental results showed TiB_2 −TiO_2 @g−C_3N_4 had higher photodegradation performance for RhB and 4-chlorophenol compared with pure g-C_3N_4. In summary, the elemental doping modified TiO_2 optical properties or g−C_3N_4, which further enhanced the photocatalytic performance of synthesized TiO_2/g−C_3N_4 DZS heterojunction.

Notably, the addition of other materials to TiO_2/g−C_3N_4 to construct ternary TiO_2/g−C_3N_4/X heterojunction materials was also a hot topic of research. Because of its special ternary structure, the path of carrier transport became longer, resulting in significant inhibition of photogenerated e^-−h^+ recombination process. Sun et al. [120]. prepared SiO_2 −TiO_2/CN photocatalyst using sol-gel. The removal rate of RhB by composites reached 98% after 180 min of illumination, indicating that SiO_2, TiO_2, and CN had synergistic effect on performance improvement. The possible degradation mechanism is shown in Fig. 12j. Due to the existence of SiO_2 support, TiO_2 and CN formed an efficient Z-scheme heterostructure through a tight interface. Amorphous SiO_2 had a high surface activity and a lot of active functional groups, so more TiO_2 surfaces contact and combined with CN, which was beneficial to the effective photocarrier migration of TiO_2 and CN in an internal electric field. Similarly, Rajendran et al. [121]. successfully prepared a new kind of ternary g−C_3N_4 coupled TiO_2 and α − Fe_2O_3 magnetic nanocomposites (g−C_3N_4/TiO_2/α − Fe_2O_3) by hydrothermal. Owing to an interfacial synergy between TiO_2, g−C_3N_4, and α − Fe_2O_3, e^- and h^+ migration can be accelerated. Recently, Gan et al. successfully coupled oxygen-doped g-C_3N_4 with g-C_3N_4/TiO_2 heterojunction via a self-assembly strategy to prepare novel oxygen-doped g-C_3N_4-modified g-C_3N_4/TiO_2 double Z-scheme heterojunction (OCN@CNT-2) [84]. The degradation rate of gatifloxacin (GAT) by OCN@CNT-2 was 91.7% within 2 h. The tight adhesion of OCN to the surface arrays of g-C_3N_4 and TiO_2 increased the carrier transfer paths and efficiently separated e^-−h^+. The formation of a double Z-scheme mechanism improved the catalytic performance, while the effect of the generated internal electric field enhanced the absorption edge and improved the visible light responsiveness. Despite complexity of ternary heterojunction preparation process, its ability to improve photocatalytic performance has led a large number of researchers to develop new ternary heterojunction photocatalysts for organic contaminants degradation. Table S3 gives the research progress of DZS TiO_2/g−C_3N_4 −based heterojunction photocatalysts in the direction of pollutant degradation in recent years.

Summary: Z-scheme heterojunctions, a type of energy-band interleaved heterojunctions, endow improved redox reactions due to the position of CB and VB, and are named after the migration path of photogenerated carriers resembling the letter "Z". This section provides a detailed description of the degradation performance and mechanism of typical Z-scheme TiO_2/g−C_3N_4 −based heterojunction photocatalysts. It also offers guiding recommendations for creating ternary TiO_2 −based photocatalysts and for improving the photocatalytic power from a preparation process perspective. Z-scheme and typical type II heterojunctions both have kinetic and thermodynamic restrictions, which reduce the oxidant power of photocatalysts [65,122]. Fu et al. presented a novel heterojunction, S-scheme, as a replacement for the straight Z-scheme. Further investigation revealed that the S-scheme eliminates the drawbacks of the straight Z-scheme while maintaining the same carrier motion mechanism [122]. Consequently, the new S-scheme heterojunction photocatalyst is gaining significant attention from researchers.

3.4. S-scheme TiO_2/g−C_3N_4 −based heterojunction photocatalyst

With addition and refinement of the S-scheme heterojunction photocatalytic mechanism by Yu et al., the development of new high-efficiency S-scheme heterojunction photocatalysts has received increasing attention [52]. Interestingly, carrier mobile in S-scheme heterojunction resembled a “step” (Fig. 5f). S-scheme heterojunction can be used to improve the efficiency of photocarrier separation by an internal electric field and energy band bending, and redox ability of system is still preserved.

Recently, the corresponding metal oxide NPs prepared through calcining MOFs as sacrificial templates had unique characteristics, not only retaining the basic structure of the skeleton and pores well but also effectively avoiding the agglomeration of metal oxides so that the NPs can be fully dispersed [123]. Yang et al. [124]. constructed S-scheme TiO_2/g−C_3N_4 photocatalyst by assembling TiO_2 NPs calcined from NH_2 −MIL− 125(Ti) with g−C_3N_4 nanosheets with interface engineering strategy (Fig. 13a). Fig. 13b displayed HOT was embedded into the porous g−C_3N_4 nanosheet structure, formed a tight heterojunction. To further understand microstructure, Fig. 13c revealed the (101) faces of distance between lattices of anatase TiO_2 was 0.35 nm, which indicated photocatalysts are prepared by spontaneous aggregation between charges. In summary, the uniform distribution of HOT on UPCN formed a tightly connected interface, which provided more channels for the rapid migration of carriers and further improved photocatalytic performance. HOT/UPCN0.4 had the highest COD removal rate of 50.4% for actual LBW. An in-depth study of photo-degradation mechanism of HOT/UPCN0.4 is necessary. The free radical quenching experimental results indicated •OH had the greatest degradation effect on the actual LBW, while h^+ had the least effect, and the ESR analysis results further proved presence of •OH and $•O_2^-$. The possible removal process is shown in Fig. 13d. Assuming that the complexes operate according to the type II heterojunction mechanism, •OH and $•O_2^-$ radicals cannot be generated, which is inconsistent with the above experimental findings, so the type II heterogeneous junction mechanism is not justified here. The authors therefore provided a more logical S-scheme heterojunction explanation for its mechanism, where HOT belonged with oxidized semiconductors and UPCN was included with reduced semiconductors [122]. Because of the potent interaction between HOT and UPCN Fermi energy levels of the two materials gradually balanced during the charge’s migration over the contact surface, finally generating a large IEF [125]. IEF speeded up the separation and extraction of photo-induced e^-−h^+, accumulated more h^+ and e^- on the catalyst surface, and produced •OH and $•O_2^-$ in the waste water solution.

Intriguingly, doping generated a local net charge that led to a charge imbalance in g−C_3N_4 and thus promoted carrier migration. On this theory, Wang et al. [126]. developed g−C_3N_4(SCN)/TiO_2 S-scheme photocatalysts prepared by electrostatic spinning and calcination methods. The stability of the composites was verified by photo-degradation cycling tests using SCNT6 samples. The outcomes demonstrated that after 5 cycles, the photocatalytic activity of composites did not decrease, indicating their excellent chemical stability. Fig. 13e showed the photocatalytic mechanism of SCN/TiO_2 S-scheme heterojunction, where e^- were migrated to SCN to TiO_2 through SCN/TiO_2 composite for interface when simulated sunlight irradiation, and IEF, band edge bending, and Coulomb interactions work together to speed up the heterojunction’s compounding of relatively worthless e^- and h^+ so that remaining e^- and h^+ had high redox ability properties. Recently, Dong et al. [127]. designed and prepared N-TiO_{2-x}/g−C_3N_4 (NTCN) photocatalyst by hydrothermal-calcination method. N and Ti^{3+}/Ov co-doping reduced TiO_2band-gap and firmly encapsulated the surface of N-TiO_{2-x} was covered in g−C_3N_4 nanosheets, creating a tight heterojunction. Under visible light irradiation, after 70 min, approximately 93% of 2,4-DNPH was photo-catalytically degraded. In addition to the doping of non-metallic elements, the modification of precursors can also be carried out. Coupling other semiconductor materials to form ternary

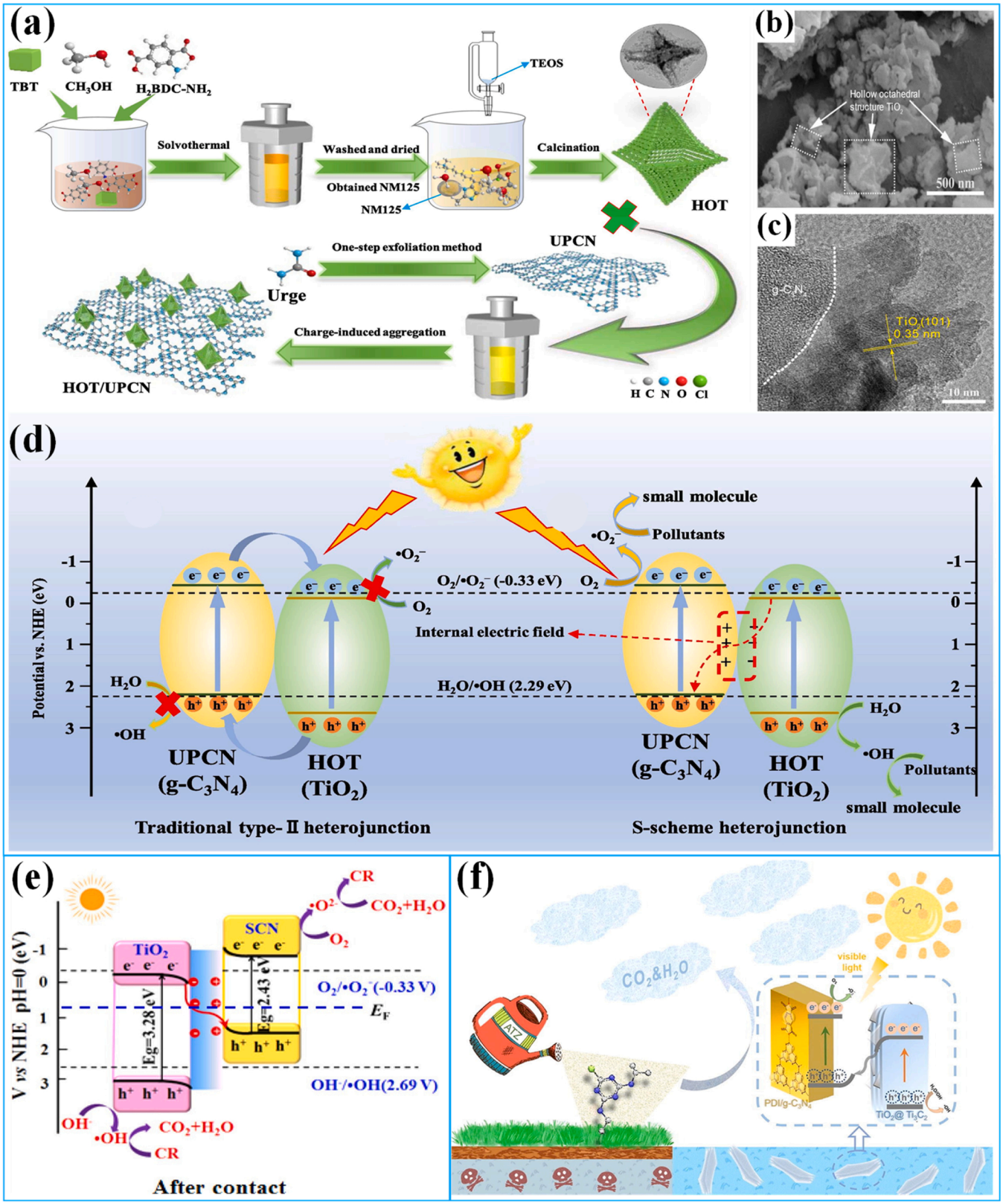

Fig. 13. (a) Demonstration diagram of HOT/UPCN preparation. (b) SEM image of HOT/UPCN0.4. (c) HOT/UPCN0.4 HRTEM picture. (d) Diagram of the contaminant removal mechanism. (e) SCN/TiO_2 photocatalytic mechanism. (f) Schematic diagram of ATZ degradation by PDI/g−C_3N_4/TiO_2 @Ti_3C_2.
a-d) Reproduced with permission from Ref. [124]. Copyright 2023, Elsevier. (e) Reproduced with permission from Ref. [126]. (f) Reproduced with permission from Ref Copyright 2021, Elsevier [82]. Copyright 2022, Elsevier.

heterojunction materials can also improve photocatalytic performance. A prime example, Tang and his team constructed a new π-π stacked PDI/g−C_3N_4/TiO_2 @Ti_3C_2 photocatalyst that promotes ATZ photocatalytic degradation by activating peroxide-sulfate [82]. Photoelectron delocalization was brought on by π-π interaction in PDI/g−C_3N_4, which promoted migration of photo-electrons, while closed contact and interleaved energy band structure between PDI/g−C_3N_4 and TiO_2 @Ti_3C_2 led to S-scheme heterojunction, which reduced complexation of carriers. The synergistic effect of the two resulted in 75% ATZ removal within 1 h, and a schematic diagram of the whole degradation process was shown in Fig. 13f. Finally, Table S4 gives the research progress of S-scheme TiO_2/g−C_3N_4 −based heterojunction photocatalysts in direction of pollutant degradation in recent years.

Summary: The performance of heterojunctions in photocatalysis is greatly influenced by the matching of electric field effects and energy band structures of the photocatalysts. Various methods, such as radical scavenging, electron gain and loss calculations using XPS, and effective mass calculations using DFT, are commonly used to verify the type of heterojunctions by studying active radicals and carrier generation and transfer.

In S-scheme heterojunctions, electron transfer occurs in a "step" fashion, which facilitates faster electron migration. Weaker redox e^- and h^+ are consumed and transferred during this process, while stronger redox e^- and h^+ are maintained, thereby enhancing the photocatalyst's redox capability[65,126]. This section briefly introduces several typical S-scheme TiO_2/g−C_3N_4-based heterojunction photocatalysts that leverage an oxygen vacancy strategy to increase active sites and enhance catalytic performance. However, despite the extensive research on S-scheme TiO_2/g−C_3N_4 −based heterojunction photocatalysts, there are still some challenges. These challenges include a more complex preparation process, higher production costs, inadequate long-term stability, and room for improvement in terms of photocatalytic efficiency. In addition, the photocatalytic mechanism of S-scheme heterojunction systems still lacks a comprehensive explanation and requires further investigation.

Overall, the advantages of TiO_2/conjugated polymer heterojunctions over classical TiO_2/metal oxide heterojunctions are summarized below.

1. Improved photocatalytic activity: TiO_2/conjugated polymer heterojunctions have a larger specific surface area and light absorption capacity, thus absorbing light energy more efficiently and improving photocatalytic activity.
2. Improved spectral response: TiO_2/conjugated polymer heterojunctions typically absorb light energy in both the visible and ultraviolet regions, and are therefore able to utilize a wider range of wavelengths for photocatalytic reactions, whereas conventional metal oxide/TiO_2 heterojunctions often require further design modifications for visible light response.
3. Improved photostability: TiO_2/conjugated polymer heterojunction has better photostability due to the presence of conjugated structure, which can maintain efficient photocatalytic activity for a long time.
4. Better adjustability: The photoelectric and catalytic properties of TiO_2/conjugated polymer heterojunctions can be adjusted through the synthesis process and material design, so they have greater flexibility and customizability and can be used to design suitable photocatalysts according to the specific needs of applications.

4. TiO_2/MOFs−based heterojunction photocatalysts

MOFs can be coupled with TiO_2 to form heterogeneous knot structures, leading to significant enhancements in quantum utilization and charge mobility [44,128]. It was noteworthy, however, that the construction of heterojunction structures was currently limited to a number of classical MOFs materials. In light of this, this section provides an overview of reported TiO_2/MOFs-based heterojunction photocatalysts and categorizes them into UiO series, MIL series, and ZIF series based on the different MOFs materials utilized. The preparation methods, photocatalytic properties, and photocatalytic mechanisms of these photocatalysts are discussed in detail.

4.1. TiO_2/UiO series

UiO− 66 has received extensive attention owing to its good chemically stable, extraordinary SSA. It was ultra-high chemically stable, which was caused by Zr−O bond interaction and Zr (IV) with a high coordination number. However, this material had a wide HOMO-LUMO gap and was relatively inefficient when illuminated by visible light [129]. The modification of UiO− 66 structures to give a visible light response was promising.

Safaralizadeh and colleagues synthesized C_3N_4 −TE@TiO_2/UiO− 66 (CNTU) using the superficial solvothermal technique [130]. Due to the ultrathin nanosheet structure of C_3N_4 −TE, after being combined with UiO− 66, 35CNTU had SSA (670 $m^2\ g^{-1}$). Although SSA of 35CNTU was still lower than that of UiO− 66, it was much larger than that of C_3N_4 −TE and 35CNT, indicating that 35CNTU can provide massive photons capture active sites, and simplified transport process of photogenerated carriers, enhancing the degradation effectiveness [131]. The best 35CNT@ 35%U66 had a TC degradation rate of 96% under simulated sunlight irradiation. Contrasted with binary material, double Z-scheme heterojunction material exhibited higher photocatalytic efficiency (Fig. 14a). In addition, the author proposed and explained two photocatalytic mechanisms of 35CNTU ternary composite heterojunction for TC in Fig. 14b. In a traditional heterojunction system, the reduction ability of e^- on TiO_2 CB and h^+ oxidation power on UiO− 66 and C_3N_4 −TE VB were weaker than the potential of $O_2/\bullet O_2^-$ and $H_2O/\bullet OH$, respectively. That was, $\bullet OH$ and $\bullet O_2^-$ cannot be generated in light reaction, which was contradictory to experimental results. Therefore, traditional degradation mechanism was ineffective for 35CNTU photo-degradable TC. Interestingly, the photocatalytic degradation process of TC was successfully explained by a double Z-scheme photocatalytic system, and light-induced e^- on TiO_2 CB was migrated to VB of UIO− 66 and C_3N_4 −TE, and coupling with h^+. Because CB of C_3N_4 −TE and U66 had a more negative potential than $O_2/\bullet O_2^-$, photogenerated e^- staid in C_3N_4 −TE CB and UiO− 66 to retain strong reducibility. Therefore, e^- reacted with O_2 to form $\bullet O_2^-$, resulting in significant degradation of TC, and enriched h^+ on TiO_2 VB can react with H_2O adsorbed on the surface to generate $\bullet OH$. The active radicals completely degraded TC into small molecules. In short, following experience can be obtained from this work. Firstly, a binary channel is created for charge transport in the double Z-scheme, which significantly increases the separation of e^-−h^+, and reduces their recombination rate. Secondly, the introduction of UiO− 66 increases surface area material, causes band bending, and enhances charge separation ability.

With extensive research on the popular MOF (UiO−66), it has been found band-gap energy of MOF will be affected through modification of the connector and transferred to the visible light region [132]. Thus, UiO− 66 −NH_2 had unique porosity and Zr−O of high activity, which made it extensively used in photocatalysis, gas adsorption/separation, and other fields [133]. Recently, Wang and his colleagues proposed an easy two-step solvothermal to assemble Sr@TiO_2 with UiO− 66 −NH_2 in various ratios to construct Sr@TiO_2/UiO− 66 −NH_2 [74]. The whole preparation process is shown in Fig. 14c, Sr@TiO_2/UiO− 66 −NH_2 was prepared by doing $SrTiO_3$ synthesized by solvothermal as a precursor, and afterward, surface-produced UiO− 66 −NH_2. Fig. 14d showed that $SrTiO_3$ had an irregular layered structure, which was in sharp contrast to polyhedral morphology of UiO− 66 −NH_2 (Fig. 14e). Fig. 14f-g showed a more detailed surface covered by spherical particles of Sr@TiO_2/UiO− 66 −NH_2-2. Fig. 14h was the EDS spectrum, and Zr, O, and N were the main elements of MOF. The above analysis proved the successful preparation of Sr@TiO_2/UiO− 66 −NH_2. Authors compared their UV–vis DRS spectra (Fig. 14i-j) to investigate visible-light absorption ability of synthesized materials and showed that all

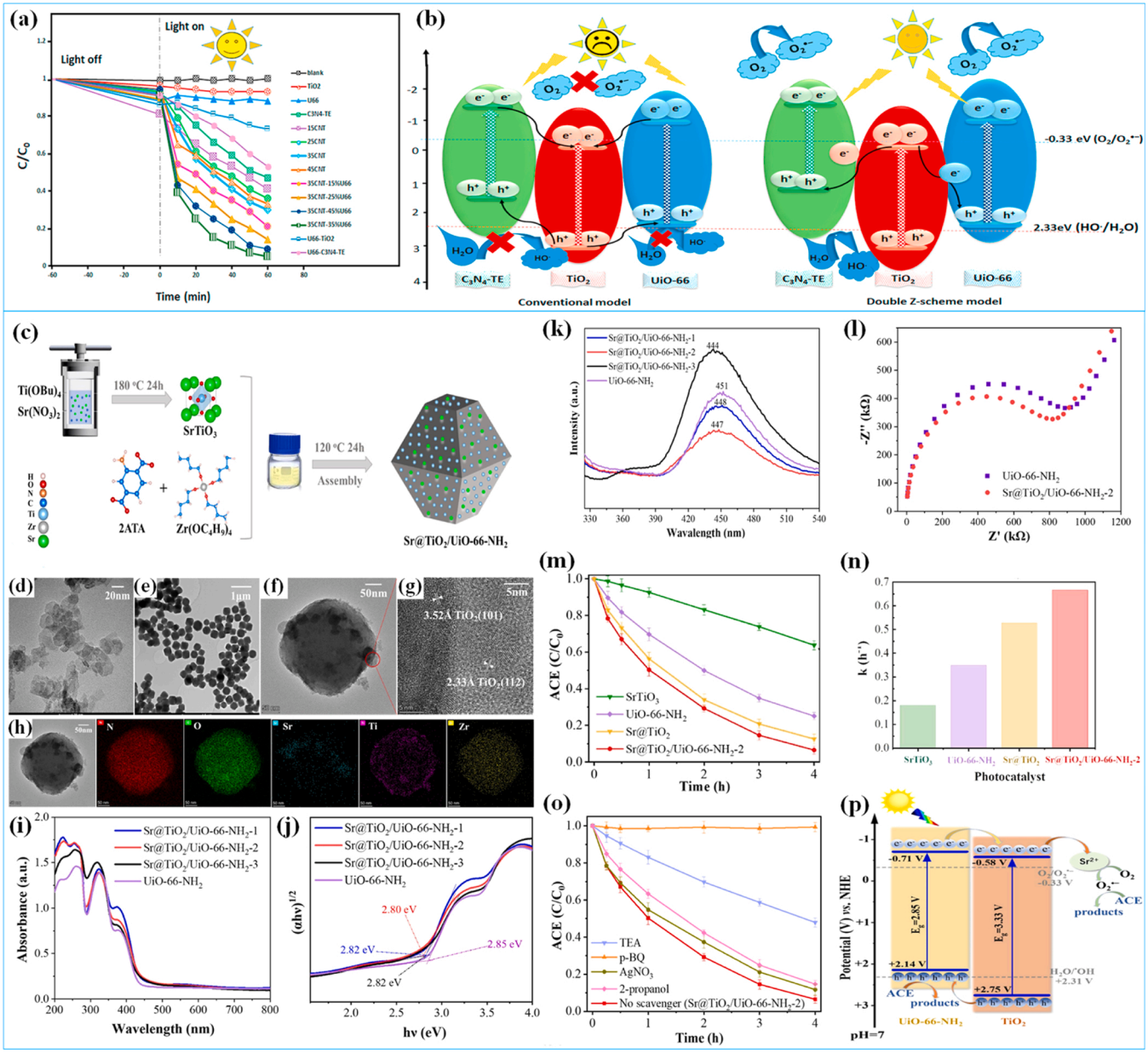

Fig. 14. (a) Catalytic performance of samples. (b) Mechanism of TC photocatalytic removal. (c) Sr@TiO_2/UiO− 66 −NH_2 preparation procedure demonstration. TEM images of (d) $SrTiO_3$, (e) UiO− 66 −NH_2, and (f) Sr@TiO_2/UiO− 66 −NH_2-2. (g) HRTEM image and (h) EDS mapping of Sr@TiO_2/UiO− 66 −NH_2-2. (i) UV–vis DRS spectra. (j) Tauc plots of $(\alpha h\nu)^{1/2}$ vs. photon energy. (k) PL spectrum of all samples. (l) EIS Nyquist plots. (m) Illustration of ACE degradation performance. (n) Pseudo first-order rate constants. (o) Free radical capture experiment. (p) Charge migration pathways in Sr@TiO_2/UiO− 66 −NH_2-2 degraded ACE.
(a-b) Reproduced with permission from Ref. [130]. Copyright 2021, Elsevier. (b) (c-p) Reproduced with permission from Ref [74]. Copyright 2022, Elsevier.

heterojunctions were similar to UiO− 66 −NH_2 spectra. The authors also characterized samples' electrochemistry behavior using PL spectroscopy (Fig. 14k) and EIS (Fig. 14l). Small radius Nyquist curves represented low resistance when e^- and h^+ can move quickly and thus migrated photogenerated carriers more efficiently. It was shown that Sr@TiO_2/UiO− 66 −NH_2-2 had high catalytic activity. It was a good means to evaluate catalytic activity of materials by degradation efficiency. From Fig. 14m, Sr@TiO_2/UiO− 66 −NH_2-2 own the best photocatalytic performance, and pseudo-level kinetics also verified the order of the photodegradation rate (Fig. 14n), with Sr@TiO_2/UiO− 66 −NH_2-2 degrading ACE almost completely within 4 h. Noteworthily, photocatalytic degradation mechanism of Sr@TiO_2/UiO− 66 −NH_2 was explored. When TEA and p-BQ were utilized as h^+ and $\bullet O_2^-$ scavengers, respectively, degradation curve decreased significantly, explaining h^+ and $\bullet O_2^-$ were main reactive radicals with photodegradation ACE (Fig. 14o). Based on above theoretical basis, the author successfully explained photocatalytic degradation mechanism of ACE (Fig. 14p). Under simulated solar irradiation, Sr^{2+} serving as e^- trap to transfer photogenerated e^-, at the same time, h^+ flowed in the opposite direction, where it interacted with ACE directly. Thus, photogenerated e^- and h^+ were spatially separated. The formation of $\bullet O_2^-$ was permitted because of the greater E_{CB} of both semiconductors, which also verified results of free radical trapping tests. Nevertheless, The E_{VB} location of the photocatalyst was not suitable for the formation of •OH, which explained low correlation of •OH in mechanism. Similarly, Chong-Chen Wang's team successfully prepared S-TiO_2/UiO− 66 −NH_2 composites by a facile ball milling method [134]. Notably, S-TiO_2/ UiO− 66 −NH_2 exhibited excellent catalytic activity for the degradation of BPA and the reduction of Cr(VI) under low-power LED light conditions. A strong chemical interface exists

between the two components, which helps to accelerate carrier migration and improve the separation efficiency of electron and hole pairs. The degradation efficiency of S-TiO_2/UiO− 66 −NH_2 for BPA was as high as 97.4% under the optimal component conditions. Notably, we show the research progress of TiO_2/UiO-based heterojunction photocatalysts in the degradation of organic contaminants in recent years (Table S5).

4.2. TiO_2/MIL series

When stimulated by the outside world, MOFs of the MIL series appeared "breathing phenomenon". This was because water molecules were connected to the MOF's skeleton through hydrogen bonds. When the polar molecules contact with the skeleton, the skeleton will produce a strong electrostatic force, resulting in an enlarged pore size [135]. Preparation and catalytic performance of different TiO_2/MIL series composites were presented in the following section according to the different transition metals.

MIL− 100(Fe) was a rare Fe(III) carboxylate with permanent porosity and very large pore size. As well, MIL− 100(Fe) had unique characteristics as a support matrix, incorporating mesoporous structure and good thermal stability, which allowed easy and fast diffusion of reacting agents [136]. Divertingly, Liu et al. synthesized B−TiO_2/MIL− 100(Fe) using simple co-precipitation method [137].

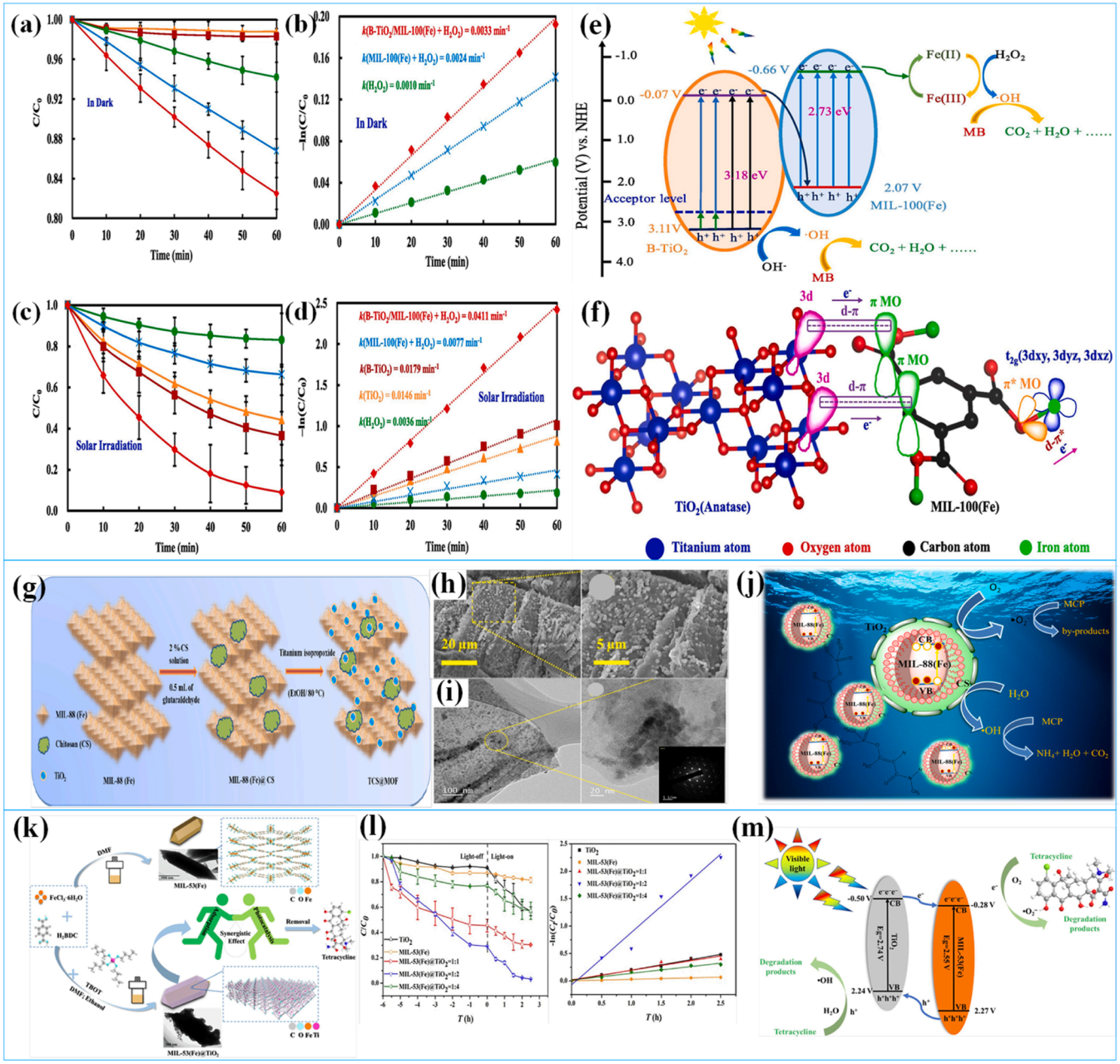

Fig. 15. (a) Degradation performance of under dark, (b) Pseudo-first-order kinetic fitting. (c) Photodegradation performance of MB, (d) Pseudo-first-order kinetic fitting. (e) Energy-band theory, (f) molecular orbital theory. (g) TCS@MOF preparation process. (h) SEM image of TCS@MOF, (i) TCS@MOF TEM images. (j) Mechanism of TCS@MOF. (k) Preparation process of MIL-53 (Fe)@TiO_2, (l) Study of the photocatalytic efficiency. (m) Photocatalytic mechanism of MIL-53(Fe) @TiO_2 is depicted.
(a-f) Reproduced with permission from Ref. [137]. (g-j) Reproduced with permission from Ref. [139]. Copyright 2021, Elsevier. (k-m) Reproduced with permission from Ref [46]. Copyright 2022, Elsevier.

Under dark, degradation of MB was not significant (Fig. 15a), and the removal rate was only 17.50% even with the assistance of H_2O_2. The fitted pseudo-primary kinetics also remained consistent with the above findings (Fig. 15b). At the same time, it was obvious that MB decomposition with B−TiO_2/MIL− 100(Fe) + H_2O_2 was greatly enhanced under the simulated solar radiation, with a degradation rate of 91.12% within 1 h (Fig. 15c-d). The mechanism of action of the catalyst was also discussed, and from molecular orbital theory, the orbitals of Ti in three dimensions formed a d-π conjugation with the π orbitals of melamine acid, thus the photogenerated e^- in B-TiO_2 were efficiently diverted to MIL− 100(Fe). An electron leap in MIL− 100(Fe) resulted in the generation of photogenerated electrons, Fe^{2+} participated in the Fenton degradation of MB as a reduction product, and e^- recombined with h^+, significantly reducing photogenerated carrier complexation probability in MIL− 100(Fe) (Fig. 15e-f). In conclusion, photocatalytic oxidation and the Fenton reaction worked together synergistically to effectively degrade MB.

Noticeably, Fe−MOFs have been extensively researched in

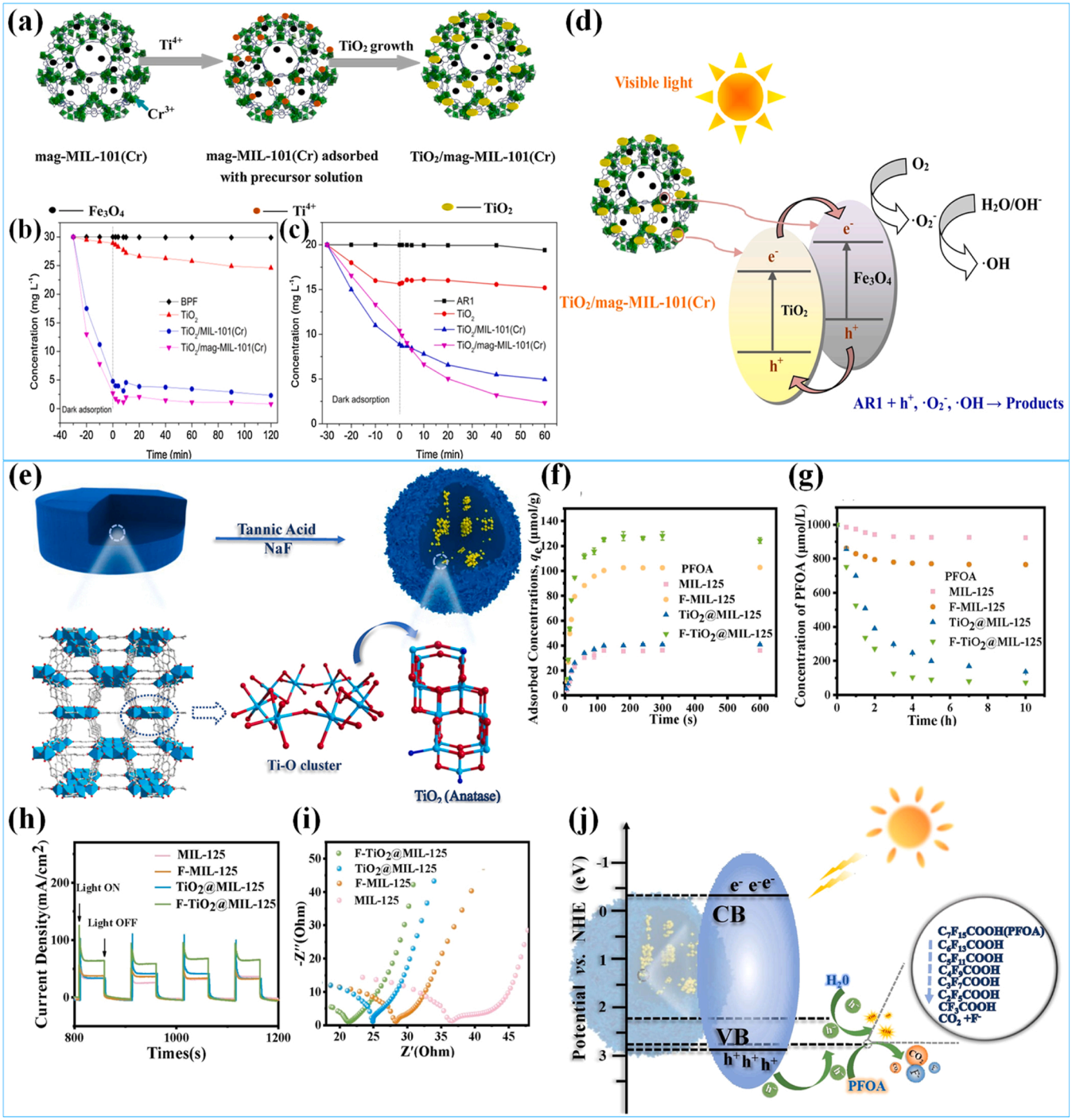

Fig. 16. (a) TiO_2/mag−MIL− 101(Cr) preparation route. (b) BPF and (c) AR1 removal effect by all samples. (d) Mechanism of AR1 photo-degradation. (e) Morphological illustration of the effects caused by Ti−F bonding. (f) Adsorption test including PFOA, (g) Photocatalytic degradation performance of PFOA. (h) Photocurrent density, (i) EIS Nyquist plots. (j) Schematic removal of PFOA.
(a-d) Reproduced with permission from Ref. [140]. Copyright 2020, Elsevier. (b) (e-j) Reproduced with permission from Ref [141]. Copyright 2022, Elsevier.

photodegradation owing to their weak toxicity, characteristic optical properties, chemical stability, etc.[138]. Vigneshwaran et al. [139]. prepared TCS@MOF by growing granular TiO_2 on MIL− 88(Fe) nanosheets surface via solvothermal method (Fig. 15g). In addition, the authors performed characterization of the morphological structure of the TCS@MOF nanocomposites (Fig. 15h-i). TiO_2 NPs loaded on MIL− 88 (Fe) nanosheets, and TEM further confirmed two-dimensional layered structure of MIL− 88(Fe). The catalytic activity of photocatalyst for MCP removal was as high as 99.79% within 0.5 h. To explore the photocatalytic degradation mechanism, the results of ESR spectroscopy and radical quenching assay showed both •OH, and $•O_2^-$ were active in light reaction process of MCP, then dominant one was •OH, which was shown in Fig. 15j. Among them, the MCP degradation mechanism of TCS @ MOF hybrid composites by • OH is as follows: (Eq. (9) − (14)).

$$TCS@MOF + hv \rightarrow (h^+ + e^-)\ TCS@MOF \quad (9)$$

$$O_2 + e^- \rightarrow •O_2^- \quad (10)$$

$$2\ •OH \rightarrow H_2O_2 \quad (11)$$

$$H_2O_2 + •OH \rightarrow •OOH + H_2O \quad (12)$$

$$TCS@MOF + MCP \rightarrow •OH + •O_2^- \quad (13)$$

$$MCP + (•OH, •O_2^-, \text{and } H_2O_2) \rightarrow H_2O + CO_2 + NH_4 \text{ (Intermediates)} \quad (14)$$

It is difficult to avoid that MOFs containing Fe generally had poor adsorption performance on organic pollutants, and the photogenerated e^- and h^+ complexation rate was still fast. To overcome the above-mentioned defects, Zhang et al. [46]. developed (MIL−53(Fe)@TiO_2) composite. The detailed formation process can be illustrated in Fig. 15k. An effective photocatalyst for TC elimination was MIL− 53(Fe)@TiO_2, Fig. 15l compared photocatalytic power of prepared MIL− 53 (Fe), TiO_2, and MIL− 53(Fe)@TiO_2 with different Fe: Ti molar ratios. MIL− 53(Fe) @TiO_2(1:2) had maximum degrading activity for TC when exposed to visible light. This may be due to formation of n-n heterojunction between TiO_2 and MIL53(Fe), which promoted its photocatalytic degradation ability. The action mechanism of MIL− 53(Fe)@TiO_2 under Vis light was discussed, and elucidating the reason for the enhanced catalytic performance (Fig. 15m). A possible reaction process is (Eq. (15) − (19)).

$$MIL{-}53(Fe)@TiO_2 + hv \rightarrow MIL{-}53(Fe)@TiO_2(h^+) + e^- \quad (15)$$

$$MIL{-}53(Fe)@TiO_2(h^+) + H_2O \rightarrow •OH + H^+ \quad (16)$$

$$•OH + \text{antibiotics} \rightarrow \text{degradation products} \quad (17)$$

$$e^- + O_2 \rightarrow •O_2^- \quad (18)$$

$$\text{antibiotics} + •O_2^- \rightarrow \text{degradation products} \quad (19)$$

MIL− 101(Cr) (M101), composed of chromium metal ions and terephthalic acid ligands, had a large aperture and fine thermal/chemical/water stability. It was gratifying to discover that (M101) as a TiO_2 NPs supporting material can effectively tackle the inherent flaws of TiO_2, and make them have adsorption ability and excellent photocatalytic performance. Zhang and his coworkers investigated a new adsorption photocatalyst was created, TiO_2/mag− (M101) [140]. Due to the metal bonding on surface of this MOF and chelating effect of −COOH, Ti^{4+} ions and Cr^{3+} ions combined to form TiO_2 uniformly on the mag− (M101) surface (Fig. 16a). The close contact between TiO_2 and mag−MOF was very favorable for charge separation and transfer. In Fig. 16b-c, the outcomes showed that the natural photolysis of BPF and AR1 was negligible. However, TiO_2/(M101) and TiO_2/mag− (M101) eliminated 75% and 90% of AR1, respectively. Thus, photocatalytic activity, it might be said MOF or mag−MOF combined with TiO_2 increased. Secondly, adsorption of pollutants on composite the surface was significantly enhanced, which increased the probability of photolytic reactions between the active radicals and the pollutants. In Fig. 16d, TiO_2 played main photocatalytic role, moreover, Fe_3O_4 and Cr−MOF were the promoters. Otherwise, magnetic MOF facilitated charge separation and reduced band-gap of TiO_2, rapid transfer of photogenerated e^- allowed a continuous flow of active substances (h^+, •OH, and $•O_2^-$) to engage in reaction. Ultimately, we can draw from this work that coupling of mag− (M101) with semiconductor photocatalysts provided stronger adsorption and charge separation effects.

MIL− 125 was an emerging Ti-MOF derived from Ti^{4+} and carboxylate organic ligands. However, MIL-125 catalytic power resulted in low activity owing to organic ligands blocking the active metal center [142]. Interestingly, Kong et al. [141]. utilized in-situ growth by MIL− 125(Ti) to fabricate F−TiO_2 @MIL− 125. The XPS study revealed the presence of additional Ti−F in composite materials, demonstrating provided more fluorine group attachment sites (Fig. 16e). In Fig. 16f, the adsorption occurred instantaneously, with a quick increase in adsorption during the first 100 s, reaching an equilibrium state at around 200 s. After the adsorption, all samples could reduce the concentration of PFOA in the first 2 h, but only composites continued to degrade PFOA after 2 h. F−TiO_2 @MIL− 125 composite achieved 91% degradation of PFOA within 7 h (Fig. 16g). Important aspect in determining the photocatalytic activity was carrier separation ability. In Fig. 16h, displaying a greater photocurrent density was F−TiO_2 @MIL− 125. EIS spectrum (Fig. 16i) exhibited smallest radius, which indicated the smallest transfer resistance of photoexcited carriers. Combined with the above analysis, F−TiO_2 @MIL− 125 had excellent catalytic performance. Significantly, the authors' team elucidated the specific process of PFOA degradation (Fig. 16j), starting with the ionization of POFA into the corresponding negative ion ($C7F15COO^-$), followed by reacting with h^+ to form C7F15COO• (Eq. (20)). The breakage of C−C bond occurs between carbon chains of carboxylate groups, which, together with the elimination of fluorine, produced the formation of intermediate short-chain PFCAs (Eq. (21)) [143]. Meanwhile, the photocatalytic ally generated •OH continues to attack the PFCAs to generate C7F15OH (Eq. (22)), which is a further process of cutting F. It was then progressively defluorinated to produce C6F13COF and C6F13COOH (Eqs. (23–24)). In this order, the cycle continues until POFA degrades to CO_2 and F^-. A sufficient amount of PFOA adsorbed on the fluorine group triggered the degradation and the increased photo availability of photocatalyst contributed to the effective attack on PFOA via h^+ and •OH. Lastly, PFOA degraded by gradually losing CF_2 units to F^- and CO_2, releasing occupied adsorption sites for use in the next cycle.

$$C7F15COO^- + h^+ \rightarrow C7F15COO• + OH^- \quad (20)$$

$$C7F15COO• \rightarrow C7F15• + CO2 \quad (21)$$

$$C7F15• + •OH \rightarrow C7F15OH \quad (22)$$

$$C7F15OH \rightarrow C6F13COF + F− + H+ \quad (23)$$

$$C6F13COF + H2O \rightarrow C6F13COOH + F− \quad (24)$$

Besides the typical examples mentioned above, recent studies on TiO_2/MIL series composites are listed in Table S6.

4.3. TiO_2/ZIF series

ZIFs were usually novel types of MOF materials created by self-assembly of Co (II) or Zn (II) with imidazole ligands. ZIFs possess many excellent characteristics, including low density, large SSA, high porosity, and reasonable structure[144]. To overcome the defects in the performance of single TiO_2 catalysts and combine the advantages of ZIF− 8, ZIF− 8/TiO_2 composites gradually became a focus of current photocatalysis research.

Jing and coworkers used PVP-modified TiO_2 −ZIF− 8 as the precursor and performed crystallization, adsorption, pyrolysis, and in situ generation ways to finally obtain Pt/TiO_2 −ZnO@ZIF− 8 (Fig. 17a) [45]. Both the two showed excellent degradation performance for

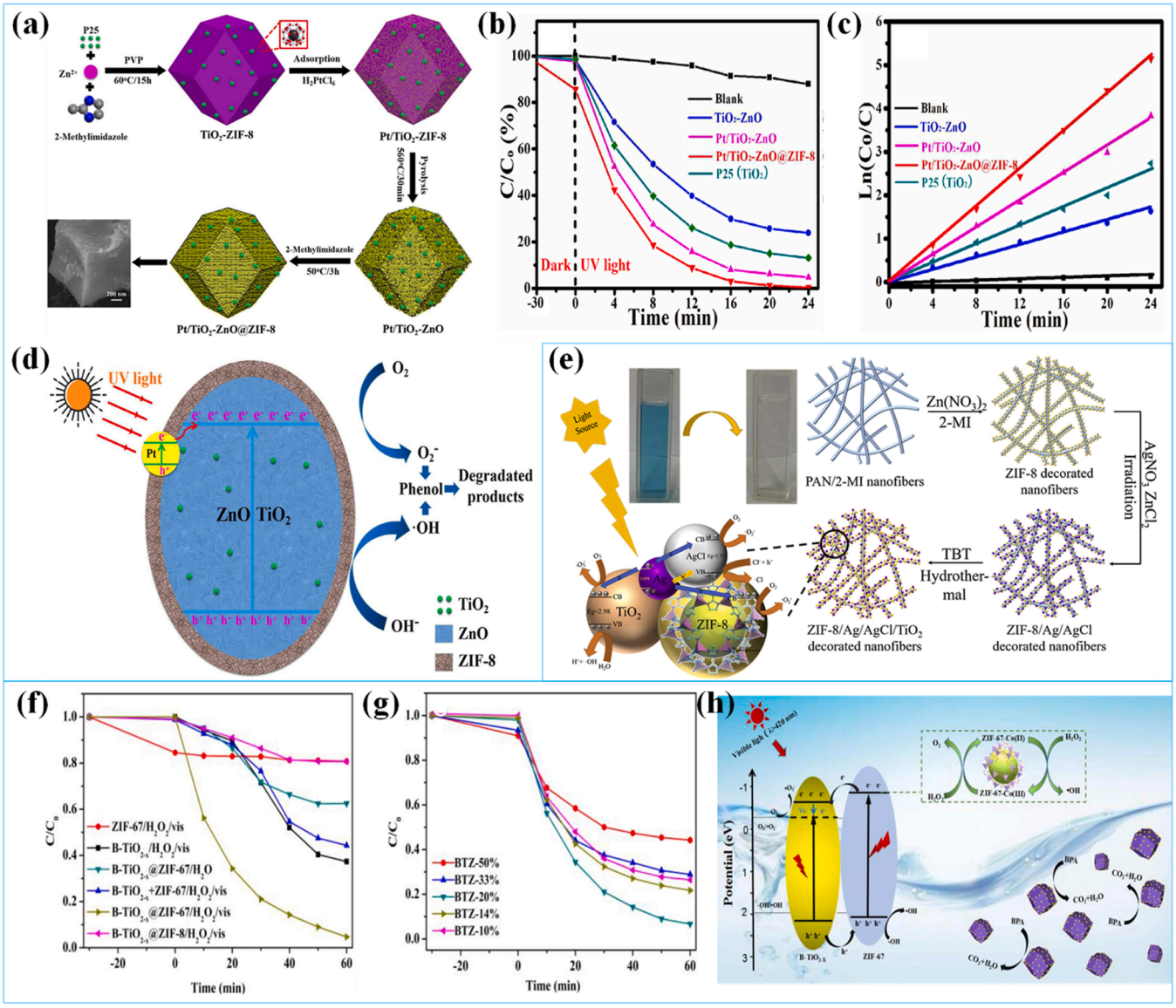

Fig. 17. (a) Synthesis demonstration of Pt/TiO_2 −ZnO@ZIF− 8. (b) Photocatalytic degradation and (c) kinetics were recorded for all samples. (d) Mechanism of phenol degradation. (e) Preparation route and mechanism of the ZIF− 8/Ag/AgCl/TiO_2/NF. (f) Photocatalytic activities of BPA degradation. (g) BPA degradation power with BTZ-y. (h) The Photo-Fenton synergistic mechanism of synthesis demonstration.
(a-d) Reproduced with permission from Ref. [45]. Copyright 2022, Elsevier. (e) Reproduced with permission from Ref. [145]. Copyright 2020, Elsevier. f-h) Reproduced with permission from Ref [75] Copyright 2020, Elsevier.

phenol in UV light, but Pt/TiO_2 −ZnO@ZIF− 8 was still slightly better, with 99.7% of phenol degraded within 24 min. The degradation kinetics of the samples were analyzed, and the k value of Pt/TiO_2 −ZnO@ZIF− 8 was the highest. Further demonstrating that Pt/TiO_2 −ZnO@ZIF− 8 had terrific catalytic activity (Fig. 17b-c). Under UV light conditions, TiO_2 −ZnO induced e^-−h^+ creation, Pt doping acts as a co-catalyst, which made e^-−h^+ easier to generate. The O_2 dissolved reacted with e^- in CB to form •O_2^-, and h^+ reacted with OH^- to form •OH. Critically, ZIF-8 coating adsorbed phenol in large amounts, and then •O_2^- and •OH oxidized phenol adsorbed on material face to smaller molecules (Fig. 17d). So, a synergistic effect of Pt, TiO_2 −ZnO, and ZIF− 8 enabled composites to exhibit excellent photocatalytic degradation activity of phenol. Zhan et al. [145]. synthesized ZIF− 8/Ag/AgCl/TiO_2/NF by electrostatic spinning technique and in situ growth process with excellent photocatalytic activity under visible light irradiation and fine recyclability (Fig. 17e). It showed good photocatalytic activity under both Vis and sunlight, and MB degradation efficiency was as high as 98.02% within 120 min. As expected, the photocatalytic removal efficiency of nanofiber mats remained at about 80% after 10 cycles.

The ZIF− 67 had lots of catalytic sites, and the compound with TiO_2 was expected to yield catalytic materials with excellent performance [146]. Tang et al. [75]. developed a novel visible-light-driven Photo--Fenton-like system based on the ability of ZIF− 67 to activate H_2O_2 to degrade organic pollutants. B−TiO_{2-x} with defects was clad on ZIF− 67 by a simple solvothermal, and the resulting B−TiO_{2-x} @ZIF− 67 composite. In Fig. 17f, the addition of H_2O_2 under simulated sunlight conditions led to •OH generation, acting as a bridge that made it possible to synergize photocatalytic reactions with Fenton-like reactions to promote the degradation of BPA. Experimental results showed removal rate of photocatalytic system was dramatically increased in the presence of a tiny amount of H_2O_2, and 95.3% of BPA was removed within 1 h. The synergistic effect of B−TiO_{2-x} with ZIF− 67 was further explored (Fig. 17g). When ZIF− 67 (10%), the removal rate reached 73.52%, and the catalytic activity was optimal when the ZIF− 67 content increased to 20%. Fig. 17h showed the probable catalytic degradation mechanism of the BTZ-20%/H_2O_2/vis system. Under visible light, B−TiO_{2-x} was

photoexcited to generate e^-–h^+, while photo-generated e^- are simultaneously excited to the LOMO of ZIF− 67 and h^+ are retained on the HOMO, and then e^- and h^+ are transferred according to charge transfer path of type II heterojunctions, with photo-generated e^- going to CB of B−TiO_{2-x} and h^+ going to HOMO of ZIF− 67. In particular, oxygen vacancies in photocatalysts were trapped by e^-, suppressing carrier complexation rate. Dominant •OH in the degradation process oxidized BPA to inorganic small molecules. This work provided ideas for subsequent efficient visible-light-driven photo-Fenton degradation systems for contaminants development. Interestingly, Zhang et al. successfully prepared ZIF− 67/F-TiO_2 composite photocatalysts using a facile hydrothermal method. The presence of special fluorine on the surface of the composite catalyst served as an electron trapping site to promote oxygen adsorption and accelerate the migration of holes to the TiO_2 surface, thus realizing a better electron-hole separation efficiency. In addition, the Z-scheme heterojunction structure extended the lifetime of photogenerated carriers. When the content of ZIF− 67 was 10%, the removal rate of tetracycline hydrochloride by ZIF− 67/F-TiO_2 reached 87%.

Table S7 summarizes the published applications of TiO_2/ZIF−based composite photocatalysts in the direction of organic pollution degradation in recent years.

Summary: This chapter systematically reviews and evaluates the application of heterojunction photocatalysts constructed by the popular coordination polymers MOFs and TiO_2 both in the field of environmental remediation. Due to the large specific surface area and tunable structural properties of MOFs, this opens up unlimited possibilities for the design of composite photocatalytic materials. Therefore, after summarization, TiO_2/coordinated polymer heterojunction has the following advantages over the classical TiO_2/metal oxide heterojunction:

1. Multiple catalytic activity centers: TiO_2/coordinated polymer heterojunctions can improve the rate and efficiency of photocatalytic reactions due to the presence of multiple catalytic activity centers.
2. Enhanced photoelectron transport capacity: TiO_2/coordinated polymer heterojunction has high photoelectron transport capacity, which helps to reduce the complexation of photogenerated electrons and holes, and thus improves the photocatalytic degradation efficiency.
3. Enhanced redox capacity: TiO_2/coordinated polymer heterojunction has stronger redox capacity, which can effectively reduce the activation energy and accelerate the degradation reaction.
4. Improvement of photostability: TiO_2/coordinated polymer heterojunction has better photostability, and can maintain high photocatalytic activity under prolonged illumination.
5. Structural diversity: TiO_2/coordinated polymer heterojunction has rich structural and compositional diversity, which can provide targeted photocatalysts for different application scenarios, whereas traditional metal oxide/TiO_2 heterojunction photocatalysts are relatively monolithic in structure and composition.
6. Environmental friendliness: TiO_2/coordinated polymer heterojunction usually has low toxicity, high degradation efficiency, and good environmental friendliness, which can reduce the negative impact on the environment in practical applications, and has a higher application value than traditional metal oxide/TiO_2 heterojunction photocatalysts.

5. Other polymers

Polymers, often defined as repetitive structures formed by monomer units linked by covalent bonds, constitute high molecular weight molecules that can be directly modified by strategies such as molecular design and controlled aggregation to improve the relevant properties of the material, which were unmatched by conventional inorganic semiconductor materials[30,147,148]. It is noteworthy that g-C_3N_4 mentioned in the previous section belongs to classic conjugated polymers, while MOFs are classic coordination polymers. Following the rapid development of TiO_2-based photocatalytic materials, TiO_2/polymer composite photocatalytic materials have made remarkable progress in the photocatalysis of organic pollutants field. This chapter aims to explore the research progress of other composites constructed of polymers and TiO_2 in organic pollutants degradation, adding new content to the field.

For conjugated polymers, polyaniline (PANI) possessed a conjugated large π-bond system from a linear structural point of view, which gave it excellent electrical conductivity and environmental stability. Researchers Kazi Hasibur Rahman et al. [149]. sensitized PANI using chemical oxidative polymerization to form PANIL-TiO_2 p-n heterojunctions. The absorption range of composites was enhanced by sensitization of PANI, encompassing light in the UV–VIS–NIR spectral region. Under this sensitization, the toxic dye MB degraded with 2.5 and 3.1 times the effectiveness of PANI and TiO_2, respectively. In addition, conjugated triazine skeletons were a class of porous polymeric materials with high nitrogen content and stable chemical structures. Hu et al. [150]. prepared a novel π-conjugated polymer, poly(diphenylbutadiene) (PDPB), using an in-situ synthesis strategy and doped it into TiO_2 to form a PDPB/TiO_2 heterojunction. This heterojunction resulted in a 2.72-fold improvement in degradation performance of RhB over pure TiO_2. Experimental and characterization analyses revealed that the Z-type heterojunction formed by these two was the main factor for enhancing catalytic performance, providing a new idea for conjugated polymers in TiO_2-based heterojunction photocatalysts development.

The "lock-in effect" has been used for molecular conformations in organic semiconductors. It promotes the delocalization of intramolecular π-electrons along the main chain, thus enhancing intramolecular charge transfer and reducing the band gap [151,152]. Interestingly, the "lock-in effect" between conjugated polymers and TiO_2 is a promising strategy in the field of photocatalytic degradation. Liu et al. utilized the "lock-in effect" to open the concept of a bridge between conjugated polymers and TiO_2 composites [153]. The research team designed and synthesized two new thiophene-based conjugated polymers with side-chain carboxyl groups: poly [(thiophene-ethylene-thiophene)-thiophene] (PTET-T) and poly[(thiophene-ethylene-thiophene)-thiophene-3-carboxylic acid] (PTET-T-COOH) with side-chain carboxyl groups. -COOH and TiO_2 through the interaction of carboxyl and hydroxyl groups, which greatly improved the interfacial charge transfer ability and inhibited the electron-hole combination in PTET-T-COOH/TiO_2. The photocatalytic degradation of 15% PTET-T--COOH/TiO_2 was the strongest, and the RhB was almost completely removed within 80 min, with the kinetic rate constant 41.7 times higher than that of TiO_2. The proposed "locking effect" opens up a brand new idea for the design and development of new organic-inorganic heterojunction photocatalysts.

In recent years, coordination polymers have seen an increase in interest in a particular type of material called extended networks of metal clusters and organic ligands. Other varieties of coordination polymers, besides MOFs, have shown promise for improving photocatalytic performance [154]. Shadpour et al. successfully synthesized PVC/TiO_2-BSA nanocomposites using ultrasound combined with mechanical stirring and demonstrated the success of this modification strategy by thermogravimetric analysis, which showed that thermal stability of material was enhanced by PVC addition [155]. Recently, Zhang et al. [156]. investigated the modification of MoS_2-TiO_2 onto polyacrylonitrile (PAN) to prepare highly efficient and recyclable 3D composite photocatalytic membrane materials. MoS_2-TiO_2 @PAN membrane showed the best efficiency in organic dye degradation, reaching 97.7%. This provided a new idea for the development of low-cost, recyclable, and efficient dye degradation membrane materials.

Despite some stage-by-stage breakthroughs in the field of TiO_2-conjugated/coordinated polymer heterojunction photocatalysts research, most of the studies have focused on improving the stability and recyclability of materials, with limited improvements in the performance of

the catalysts themselves, and the description of the mechanism of the photocatalysts is still ambiguous. In addition, the choice of reaction types and substrates available is relatively limited. Excitingly, due to the controllable structural properties of polymeric materials, this provides unlimited opportunities and challenges for the future development of efficient TiO_2/polymer photocatalytic systems.

6. Effect of operating parameters on photocatalytic degradation efficiency

There is a lack of discussions on optimizing operating parameters in relation to the conjugated/coordination polymer heterojunction. This is an important aspect to consider in order to maximize the efficiency and effectiveness of these heterojunctions in various applications, particularly in environmental remediation. Furthermore, the specific interactions between the conjugated/coordination polymers and the TiO_2 in the heterojunction also play a crucial role in determining its overall performance. Understanding and optimizing these interactions under different operating conditions is essential for harnessing the full potential of these materials in environmental remediation. Therefore, the Efficiency of photo-degradation of organic contaminants in wastewater using TiO_2-conjugated/coordination polymer heterojunction is influenced by a range of operating parameters. Various factors exempli gratia pH, light sources, catalyst dosage, initial concentration of pollutants, co-existing inorganic ions, and co-existing organic, critically impacted the photocatalytic degradation efficiency. Future research should focus on systematically investigating and optimizing these operating parameters to elucidate their impact on the catalytic activity and stability of the conjugated/coordination polymer heterojunction. This will ultimately lead to the development of more efficient and reliable photocatalytic materials for environmental remediation applications. A visual representation of the most significant factors affecting the photocatalytic degradation efficiency can be found in Fig. 18. Building on the above analysis, a thorough discussion of the typical operating parameters is provided.

6.1. pH

The pH of the solution had some impact on the photocatalytic removal of pollutants [157]. That was because the pH level changed the surface charge of the photocatalyst thus modifying electrostatic gravity between the surface of a material and tiny contaminating, which regulated the adsorption ability of organic pollutants at the interface [158]. Especially associated with zero charge point (PZC) of photocatalyst, when $pH = pH_{pzc}$, photocatalyst surface was neither nor negatively charged, the adsorption capacity was weakest; when $pH < pH_{pzc}$, photocatalyst surface was positively charged, adsorption of anionic organic pollutants was enhanced; when $pH > pH_{pzc}$, photocatalyst surface was negatively charged, which accelerated adsorption of cationic organic contaminants [79]. Table 2 showed that optimal pH of degrading pollutants was acidic, following the principle that basic pH contributes less than acidic pH to a breakdown of contaminants.

Table 2
The photodegradation of photocatalysts on organic pollutants at different pHs.

Photocatalyst	pH tested	Optimum pH	Pollutant	Degradation efficiency (%)	Ref.
2D/2D TiO_2/g−C_3N_4	1.98, 4.13, 7.96, 10.57	4.13	LVFX	94.7%	[159]
g−C_3N_4 −TiO_2 (GNT)	3, 5, 9, 11	3	BG	> 97%	[160]
TiO_2-P/g−C_3N_4	5.4, 6.3, 7.0, 7.7	7.7	TC	> 90%	[161]
C_3N_4 −TE@TiO_2/UiO− 66	2, 4, 5.5, 7, 9	4	TC	> 98%	[130]
BiOI/TiO_2/ZIF− 8	3.40, 5.97, 9.85, 12.07	5.97	NOR	85.3%	[162]
Ca/TiO_2/NH_2 −MIL− 125	3, 5, 7, 9, 11	5	MO	83.21%	[163]

Gan et al. [159]. studied the degradation performance of TiO_2/g-C_3N_4 on levofloxacin (LVFX) at different pH. When pH = 1.96, LVFX molecules were cationic molecules, at which time the photocatalyst molecules were also cationic, and the two generated electrostatic repulsion, which prevented the effective adsorption of LVFX. Nevertheless, the surface charge of the photocatalyst will be negative as the pH rises to 4.13, at which time the effective adsorption of LVFX was promoted due to the electrostatic adsorption effect, thus improving the photocatalytic degradation efficiency. Unfortunately, in an alkaline environment, LVFX will be anionic molecules, and the presence of electrostatic repulsion hindered the adsorption of LVFX. LVFX therefore showed the highest degradation performance in a weakly acidic environment (pH=4.13). Similarly, the degradation performance of C_3N_4-TE@TiO_2/UiO-66 photocatalyst for TC was discussed in the study of Safaralizadeh et al. The findings revealed that pH = 4 produced the best degrading performance [130].

6.2. Light sources

Activation of the photocatalyst depended on certain key parameters, such as specific energy and light intensity. The excitation state occurred only when photons of sufficient energy impacted the sample. Generally speaking, the higher energy of light, the more photons were available and the faster photocatalyst material can be excited and generate active

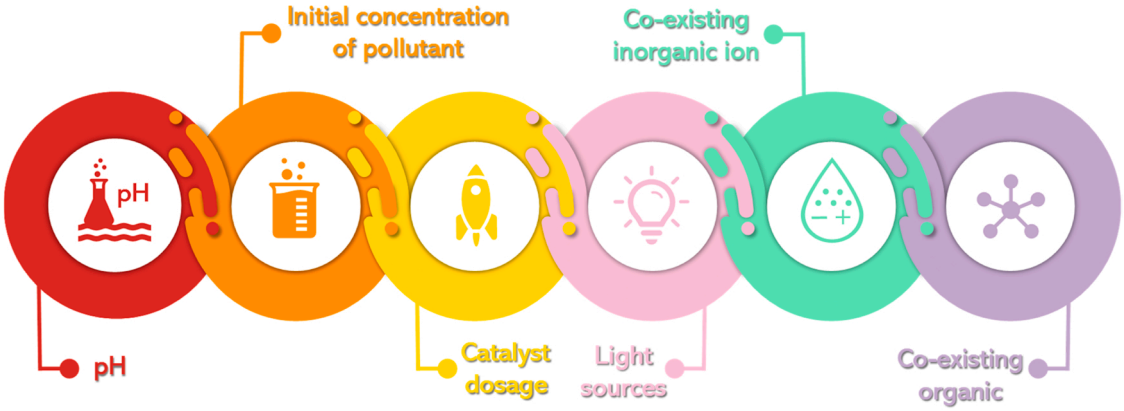

Fig. 18. The influence parameters of photocatalytic degradation process.

substances [2]. For wide band gap materials such as TiO_2, the band gap was between 3.0 ~ 3.8 eV, excitation wavelength was 300 ~ 400 nm. In contrast, the forbidden band of g-C_3N_4 was narrower with a wavelength of > 400 nm for an energy source. Therefore, different light sources must be employed based on the energy gap of the photocatalyst.

He et al. studied the effect of using various light sources (visible, solar, and UV) on the degradation of TC. The degradation rates were 65%, 90%, and 95% within 5 min of visible light, sunlight, and UV irradiation, respectively [164]. Hence, it was very necessary to use ultraviolet light from solar rays. Likewise, Narkbuakaew et al. [165]. investigated catalytic power of g−C_3N_4/Ag−TiO_2 photocatalysts with various proportions of g−C_3N_4 and Ag−TiO_2. Ag−TiO_2 can be well activated by UV light, which was consistent with Ag-TiO_2 (3.02 eV), and at the appropriate ratio, visible light's photocatalytic activity was higher than UV light's, which was beneficial to the practical application of the catalyst.

6.3. Catalyst dosage

The catalyst dosage was also one of the most significant parameters affecting the photocatalytic efficiency as well as cost control [166]. The effect of photocatalyst dosage on degradation performance had been reported statin the higher the photocatalyst dosage in the appropriate interval, a higher concentration of e^- and h^+ can generate more active radicals. So, the photocatalytic performance was proportional to the amount of photocatalyst. However, excessive catalyst dosage can lead to catalyst agglomeration, and the photocatalytic performance was inhibited [48].

According to Yang et al. [167], a series of (0.2, 0.5, 1.0, and 1.5 g/L) catalyst dosages were designed to test the effect on the degradation of BPA. BPA degradation efficiency and rate were increased with the increase of photocatalyst dosages. Tang and his colleagues [77] synthesized TiO_2 @MIL-101(Cr) to degrade BPA successfully and investigated the degradation efficiency of the catalyst at different dosages. Indicated photocatalytic degradation efficiency increased from 0.003 min^{-1} to 0.006 min^{-1} as photocatalyst dosage increased from 0.125 g/L to 0.75 g/L, while further increase in catalyst dosage showed little improvement in efficiency of degradation. It might be the result of adding too many catalysts, resulting in the light shielding phenomenon from the aggregation of catalysts. In addition to this, Cao et al. [96]. investigated catalyst effect dosage on TTZ removal in the range of 0.4 ~ 3.2 g/L. With an increase in catalyst dosage, the TTZ degradation rate showed a rising and then decreasing trend, and the highest TTZ removal rate was achieved at 0.8 g/L concentration. An appropriate increase in catalyst concentration provided additional active chemicals and reaction centers. On the contrary, too much catalyst will increase the turbidity of the reaction solution, thus reducing the effective light utilization and inhibiting the photocatalytic activity.

6.4. Initial concentration of pollutant

The initial concentration of pollutants and their effects were considered to be another determinant of the photo-degradation of organic contaminants. Generally, as the concentration of pollutants increased, the degradation rate gradually decreased under condition that the amount of photocatalyst remained constant.

For example, the degradation rates of endosulfan at concentrations of 5,10, and 15 ppm by the g-C_3N_4/Cu/TiO_2 photocatalyst were 60%, 48%, and 34%, respectively [168]. It was probably attributed to the fact that at high endosulfan concentrations, the emitted photons could not reach the photocatalyst due to scattering. In addition, the active site of the photocatalyst was occupied at higher concentrations of pollutant molecules, and therefore, increasing the endosulfan concentration resulted in photocatalytic activity declining. In research on UiO-66 @TiO_2 photocatalyst reported by Man et al., it was mentioned degradation efficiency decreased when DMS concentration increased [169]. Outcomes indicated that in low concentration range, the catalyst's active sites were not completely saturated, and increased concentration enhances effective contact of reactive radicals with DMS. However, in the higher concentration region, active spots on the face of the photocatalyst were in a saturated adsorption state, so that effective interaction between the reactants and the photocatalytic process was not further accelerated by the higher concentration.

6.5. Co-existing inorganic ion

The chemical composition of the actual wastewater was awful complex and often contained inorganic ions in addition to organic pollutants[170]. Based on available research, all indicated that inorganic anions inhibited the photocatalytic degradation progression. The possible reasons were, that active spots on the catalyst surface were occupied by inorganic anions; some reducing inorganic ions competed with pollutants for active oxygen, resulting in a reduced amount of active oxygen; some inorganic anions would increase the solution alkalinity and pH, which resulted in lower redox potential and inhibited photocatalyst catalytic ability [171]. This fact was reported by several authors.

For instance, Tang and his colleagues investigated the influence of CO_3^{2-}, HCO_3^-, SO_4^{2-}, NO_3^-, and Cl^- ions on the removal of CIP by the C−TiO_2/PCN regime [171]. Except for the coexistence with CO_3^{2-}, which caused a more obvious inhibition effect because CO_3^{2-} would react with •OH, the inorganic anions had a weaker inhibition effect, and the degradation rate of CIP all remained above 90%. In addition, Gan et al. examined the effect of common inorganic ions such as CO_3^{2-}, F^-, SO_4^{2-}, NO_3^-, and Cl^- on degradation of LVFX. Different concentrations of Cl^-, SO_4^{2-}, and NO_3^- showed an inhibitory effect on degradation efficiency. Because these ions can be used as reactants to convert reactive radicals or passivate active sites. The introduction of CO_3^{2-} raised the pH of the catalyst and hindered the adsorption of LVFX on the photocatalyst surface. In conclusion, inorganic ions hold a pivotal role in the photocatalytic degradation of organic pollutants, among which inorganic anions were studied more comprehensively and their role was more obvious.

6.6. Co-existing organic

Natural organic matter (NOM) is commonly found in natural water bodies. The common ones were humic acid (HA), fulvic acid (FA), and citric acid (CA) to achieve environmental simulation. Usually, organic substances play a role in hindering the photocatalytic process. For instance, Tang et al. [82]. investigated the effect of different concentrations of HA, FA, and CA on the removal of ATZ. Among them, CA inhibited the photocatalytic breakdown of ATZ and increased with increasing concentration, probably because active groups in CA can adsorb on reaction sites and prevent photoreaction from occurring. Interestingly, FA was increased to 100 mg/L, the promotion effect was obvious, and the degradation rate of ATZ was up to 95%, proving FA had a beneficial impact on the degradation of ATZ. In contrast, the degradation of ATZ by HA showed a stable positive effect, and the response continued to accelerate with increasing HA. As such, the promoting or inhibiting effect of NOM was essentially a competition between two opposite effects.

It was worth mentioning that Hu et al. examined the effect of different concentrations of HA on the removal efficiency of diclofenac (DCF) and carbamazepine (CBZ), respectively [172]. For DCF, the increased concentration of HA enhanced the photocatalytic performance. In the CBZ/30% BCCNT/vis system, the degradation of CBZ by h^+ was dominant and was partially depleted after the addition of HA, resulting in inhibition of activity. So, HA will attack reactive oxygen species ($•O_2^-$, •OH) at longer light reaction time, and e^- will react with the free radical intermediates generated during the degradation of CBZ, which was not conducive to the removal of CBZ. The specific expression

equation was as follows: (Eq. (25) – (28)).

$$HA-30\%BCCNT\ (h^{+}_{VB}) \rightarrow HA^{\bullet+} + 30\%BCCNT \quad (25)$$

$$HA^{*}-30\%BCCNT \rightarrow HA\bullet+ + 30\%BCCNT\ (eCB-) \quad (26)$$

$$O2 + 30\%BCCNT\ (eCB-) \rightarrow \bullet O2- \quad (27)$$

$$CBZ\bullet+ + 30\%BCCNT\ (eCB-) \rightarrow CBZ \quad (28)$$

7. Other photocatalytic applications

In summary, TiO_2-conjugated/coordination polymer heterojunction photocatalysts have been widely used for the efficient degradation of organic pollutants due to their efficient charge separation and strong redox capacity, which have made significant contributions to the field of environmental purification. In addition, such photocatalysts are potentially valuable in environmental remediation, energy shortage and organic synthesis. In this chapter, three different areas are presented: hydrogen evolution, CO_2 reduction, and organic synthesis. It is hoped that the study of the different properties of TiO_2-conjugated/coordination polymer heterojunction photocatalysts will provide readers with valuable insights and encourage them to further explore their potential applications in various fields.

7.1. Hydrogen evolution

Hydrogen energy (H_2) is a green and clean renewable energy source. Given its abundant reserves, high combustion value, zero pollution, and other advantages, hydrogen energy was regarded as a feasible solution to address energy shortage and environmental pollution issues [173–176]. It met the requirements of sustainable development, green and low-carbon, and was considered the secondary energy with significant development potential in the 21st century. Prior to now, photocatalytic water decomposition has been proven to be one of the main strategies for hydrogen production. To enhance the hydrogen production rate, researchers have been developing efficient new catalysts. TiO_2-conjugated/coordination polymer heterojunction photocatalysts might have been a good choice for photocatalytic hydrogen production. Nonetheless, there were few studies on photocatalytic hydrogen production.

As a typical example, Yang et al. designed a TiO_2/g-C_3N_4 (TCN) heterojunction material deposited by the monoatomic metal Ni [177]. During the photocatalytic process, the photogenerated electrons could be transferred to these single-atom metal Ni, which provided a better transport path and thus effectively prevented charge compounding. Meanwhile, the Ni atoms participated in the water decomposition reaction as the surface catalytic center, which greatly enhanced the reactivity of the photocatalyst. The hydrogen precipitation rate reached 134 μmol g^{-1} h^{-1}, which was five times higher than that of TCN. Similarly, Biswal and coworkers developed Ti_3C_2/N,S-TiO_2/g-C_3N_4 ternary heterojunctions with excellent hydrogen precipitation properties using a strategy of thermal annealing and ultrasound-assisted impregnation [178]. The heterojunction consisted of a cleverly designed n-n heterojunction and a noble metal-free Schottky junction. Optimization experiments showed that the 4-TC/NST/CN heterojunction nanocomposite had the highest hydrogen production rate of 495.06 μmol g^{-1} h^{-1}, which was 3.1 and 4.1 times higher than that of N, S-TiO_2 and g-C_3N_4, respectively. This remarkable result was attributed to the formation of dual heterojunctions (n-n heterojunction and Schottky junction), which generated strong photogenerated carrier separation and dual charge transfer channels, conferring a powerful performance to the photocatalyst. Despite the fact that TiO_2/MOFs heterojunction composites had been less studied in the field of photocatalytic hydrogen production, the existing related studies had demonstrated notable catalytic hydrogen production performance, which was worthy for researchers to further explore their applications in photocatalytic hydrogen production. Typically, inspired by the charge transfer chain in natural photosynthesis, Chen et al. proposed a novel multi-step charge transfer strategy by depositing TiO_2 nanoparticles on the surface of core-shell MOF@MOF heterostructure to construct a MOF@MOF/TiO_2 double heterojunction photocatalyst (NM@OM/TiO_2) [179]. The energy band potentials of the three groups in NM@OM/TiO_2 had multi-step characteristics, with small differences in energy band gradients, charges dispersed in multiple energy bands, small interfacial resistances, and high charge transfer efficiencies. The photocatalytic hydrogen production rate reached 7.108 mmol g^{-1} h^{-1} under full-spectrum irradiation.

7.2. CO_2 reduction

The greenhouse effect is becoming increasingly serious with the large amount of CO_2 emissions caused by the burning of fossil fuels. In order to solve the energy crisis and improve the environmental problems, utilizing renewable energy to convert CO_2 into fuels and high-value chemicals is an ideal strategy [180]. However, existing photocatalysts have some drawbacks, such as high activation barriers, fast photogenerated e^{-}-h^{+} complexation, and poor stability. Therefore, scientists are trying to develop more efficient photocatalysts [181]. TiO_2-conjugated/coordination polymer heterojunction photocatalysts can significantly improve the efficiency of CO_2 photoreduction and provide important technical support to alleviate the global energy demand.

Bao et al. successfully prepared boron-doped g-C_3N_4/TiO_{2-x} composites (BCT) by one-step thermal reduction using a “kill two birds with one stone” strategy [182]. The composite catalyst exhibited extended full-spectrum absorption and excellent CO_2 photoreduction performance (265.2 μmol g^{-1} h^{-1}), which were 7.5 and 9.2 times higher than those of pure TiO_2 and g-C_3N_4, respectively. Moreover, its CO_2 photoreduction performance could be further enhanced to 345.1 μmol g^{-1} h^{-1} due to its excellent photothermal effect. This photothermal synergy helped to lower the conversion energy barrier by adsorption and activation of CO_2 molecules, which was a key factor for the dramatic improvement in catalytic performance. Jiang and colleagues attempted to create “molecular compartments” within MOF crystals by growing TiO_2 within different pores of chromate-based MOF (MIL-101) and its derivatives [183]. Due to the synergistic interaction between the TiO_2 units and the catalytic metal clusters in the main chain of the MOF, the photocatalytic CO_2 reduction was facilitated with the simultaneous generation of O_2. An apparent quantum efficiency of 11.3% for the CO_2 photoreduction was observed in the composite composed of 42% TiO_2-in-MIL-101-Cr-NO_2. This strong catalytic activity was closely related to the role of TiO_2 in the precise localization of the system.

7.3. Organic synthesis

The synthesis of organic compounds using TiO_2-conjugated/coordination polymer heterojunction photocatalysts opens a green and efficient pathway in organic synthesis. Since these processes are usually carried out at ambient temperature and pressure, the photocatalytic process is very compatible with the requirements of green chemistry and has attracted the attention of many research teams.

2D nanosheet-based composites were very promising in promoting photocatalytic organic synthesis due to their unique electronic and optical properties and the synergistic effect of heterojunctions. According to Zhang et al., in situ growth of ultrathin 2D TiO_2 on 2D g-C_3N_4 nanosheets formed a ^{2}D–^{2}D TiO_2/g-C_3N_4 heterojunction with strong interfacial coupling [184]. Under visible light irradiation, the yield of the benzylamine coupling reaction reached 80%, which was much larger than the yield of ~30% for 2D TiO_2 or g-C_3N_4. Taheri et al. successfully synthesized a well-performing TiO_2-HPA@Fe_3O_4/EN-MIL-101 (HPA = Heteropoly acid) hollow magnetic catalyst with some spacers using a

four-step hydrothermal method [185]. Magnetic core-shell nanoparticles were used as multiphase catalysts to obtain good multicomponent green synthesis of benzo[*a*]furo[2,3-*c*]phenazine derivatives with easy separation and good recyclability.

8. Conclusion and outlook

In our commitment to achieving a sustainable future, it is crucial to prioritize the preservation of an eco-friendly environment. The presence of organic pollutants in wastewater, such as pesticides, dyes, and antibiotics, has had a significant negative impact on aquatic ecosystems. Researchers have made progress in improving water quality, but challenges remain. One promising solution is the use of advanced oxidation processes (AOPs), with photocatalysis standing out as a cost-effective and environmentally friendly technology. However, the effectiveness of this approach is largely dependent on the performance of the photocatalyst. Standalone photocatalysts often struggle with limited visible light absorption and low quantum yield, limiting their widespread use. The conjugated/coordination polymers show promise due to their universal significance and unique structural attributes, making them suitable for use in photocatalysis. As such, we present the TiO_2-conjugated/coordination polymer heterojunction photocatalyst systems, wherein both systems were innovatively developed using TiO_2 as the research substrate and a heterojunction construction strategy, showcasing the promise of these materials in future environmental applications.

This review provides a comprehensive examination of key areas, including:

(1) An introduction to photocatalytic processes and the heterojunction structure of two distinct systems, with a summary of degradation pathways for common organic pollutants and methods for preparing composite materials.
(2) A classification of TiO_2/g−C_3N_4 −based heterojunction photocatalyst system according to carrier transfer pathway is depicted. This system is segmented into three types: type II, Z-scheme, and S-scheme heterojunction. This includes an overview of their synthesis strategies, photocatalytic performance, and degradation mechanisms.
(3) TiO_2/MOFs−based heterojunction photocatalyst system is broken down into TiO_2/UiO, TiO_2/MIL, and TiO_2/ZIF series, according to the specific MOFs materials. Among them, an overview of their synthesis strategies, photocatalytic performances, and degradation mechanisms is also provided.
(4) Discussion of crucial parameters affecting the photocatalytic degradation efficiency of these systems, including pH, light source, catalyst dosage, initial concentration of pollutants, co-existing inorganic ions, and co-existing organic matter.

Overall, the prospects of further research on photocatalytic degradation of organic pollutants using the two systems are expansive, however, there remain some challenges and breakthroughs that need to be addressed, as illustrated in Fig. 19.

(i) In-depth analysis of the reaction mechanism of photocatalysts for organic pollutants removal.

Admittedly, the study of reaction mechanisms is often encumbered by ambiguity due to the complex nature of the reaction system's structure. Furthermore, the commonly used methods for characterizing heterojunctions rely heavily on reasoning based on characterization and experimental data, lacking individual verification. To address these challenges, a more direct and accurate characterization technique should be explored. This should be complemented by DFT calculations to conduct comprehensive studies on critical aspects such as charge dynamics, optical absorption capacity, and electronic energy band structure. By adopting this approach, a more profound understanding of photocatalysts can be attained.

(ii) Full utilization of sunlight by photocatalysts.

The composites reported so far about the two TiO_2-based systems respond mainly to the visible region of the solar spectrum, while few kinds of research have been conducted

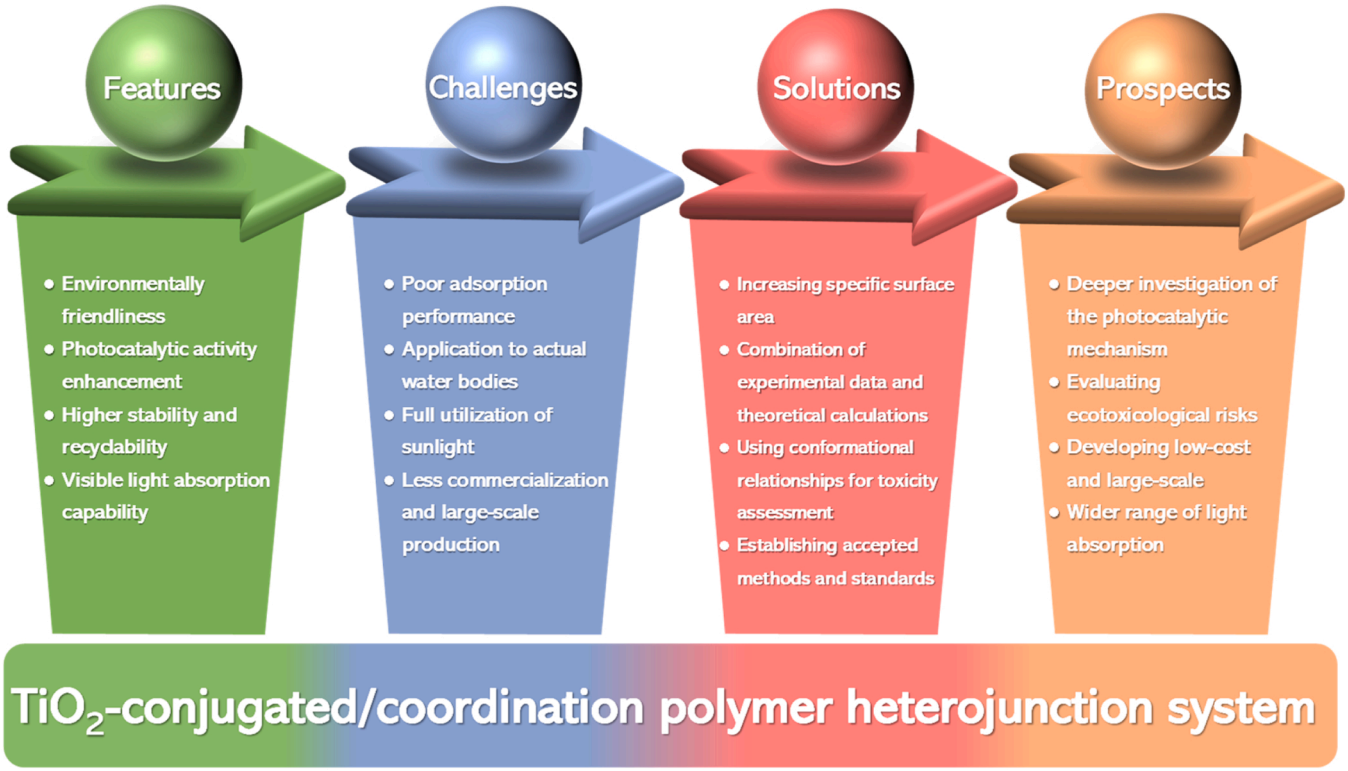

Fig. 19. Some prospects for further research.

on a near-infrared region which accounts for 43% of the entire solar spectrum. Therefore, it is imperative to broaden the absorption range of these composites to explore longer wavelengths beyond the visible region and even into the near-infrared region. To address this challenge, future research should focus on the design of composite photocatalysts with suitable energy band structures to effectively utilize and reuse solar energy. By tuning the bandgap and energy levels of the photocatalysts, we can enhance their absorptive capacity over a wider range of wavelengths, thereby improving the overall utilization of sunlight. This can be achieved by strategies such as incorporating suitable co-catalysts, designing multi or ternary systems, and adjusting the crystal structure or particle size of the photocatalysts.

With increased research efforts in these directions, we can expect to develop more efficient photocatalysts that maximize the use of sunlight and contribute to sustainable energy solutions.

(iii) Stability and recyclability of heterojunction photocatalyst.

Although the effectiveness of photocatalysis can be considerably enhanced by heterojunction structures, accompanying decreased stability to a certain extent will depict. During periodic usage, interaction will gradually dwindle, which will affect the interfacial charge migration rate, leading to a decrease in photocatalytic performance. The as-developed heterojunction composites are usually nanopowders, which not only pose difficulties for the recycling of photocatalysts but also may cause environmental pollution. How to improve photocatalytic efficiency while maintaining good material stability and recyclability is also a challenge for photocatalysts in practical applications.

(iv) Handling of complicated components in actual water bodies.

Currently, the application of the two system composites is focused on the removal of single organic pollutants in laboratory simulations rather than in real wastewater containing organic pollutants. The actual water bodies often contain a variety of different types of organic pollutants, with a wide pH scale, simultaneously involving suspended matter and heavy metal ions. Hence, more research focusing on new organic pollutants such as POP pollutants as well as heavy metal ions should be investigated in the future. Moreover, the use of genuine wastewater bodies of water to evaluate the effectiveness of composites is also encouraged.

(v) Determination of photoreaction intermediates and toxicological inquiry.

The majority of earlier research centered on the effectiveness and mechanism of pollutants' degradation, while toxicological studies on degradation pathways and intermediates of contaminants are scarce. Furthermore, despite the high degradation efficiency, the research on their mineralization degree is still in its initial stage. During photodegradation, toxic and even more toxic by-products may be generated because of incomplete mineralization. Therefore, it is essential to conduct relevant studies to elucidate the composite degradation pathways and identification of intermediates. Toxicity tests should also be considered after the degradation process to assess the ecological risk of treated wastewater.

(vi) Optimization of the adsorption performance of two systems of heterojunction photocatalysts.

While current research on photocatalysts is largely focused on expanding the light absorption range and enhancing effective charge carrier migration at the interface to optimize photocatalytic efficiency, it is evident that further improvement is required to enhance the photocatalytic activity. This arises from the inadequate adsorption affinity of most composites for organic pollutants. Maximizing the number of adsorption sites on the exteriors of photocatalysts can lead to enhanced contact with organic pollutants, thereby accelerating the photocatalytic reaction process. To address this challenge, it is imperative to enhance the adsorption capacity of composite materials. Potential solutions include exploring the utilization of carbon materials with strong adsorption capabilities as carriers, or designing optimized photoreactors that can maintain exceptional catalytic performance while simultaneously increasing adsorption capacity. Additionally, innovative strategies for improving SSA should be developed to effectively enhance the adsorption capacity of composite materials.

By implementing these solutions, we can anticipate the development of more efficient photocatalysts with heightened organic pollutant adsorption capacity, ultimately advancing the overall performance of photocatalytic processes for sustainable energy solutions.

(vii) Control and consideration of secondary experimental conditions such as photoreactor, light source, and pH value.

The consideration of the above-mentioned sub-experimental condition factors in relevant studies is very lacking, and some necessary attempts are very meaningful. Therefore, it is not easy to ensure that the optimal experimental conditions are consistent by being applied in the amplified experimental conditions even to industrial production, which needs further exploration. For example, the relationship between a light source and reactor on the yield effect has not been systematically studied; the pH size affects the zeta site of the photocatalyst that will determine the photocatalytic performance. As such, the control and consideration of sub-experimental conditions in future studies should be of concern.

(viii) Economic preparation of heterojunction photocatalysts for industrial production.

Until now, the vast majority of photocatalysts of both systems remain in the laboratory preparation stage, wherein some methods should be carried out under harsh conditions with complicated processes. The crystal yield of MOF materials is low, and the price of mass production is high., so the industrial production principle of pursuing economic efficiency and high utilization of atoms is desirable. Accordingly, the development of simpler and more economical synthesis routes under mild reaction conditions to be put into large-scale industrial production is an urgent and important orientation that deserves to be developed. Overall, the transition from laboratory to industrial scale is the hurdle that must be overcome to make this the next generation of practical photocatalytic systems.

CRediT authorship contribution statement

Ma Tianyi: Formal analysis, Supervision, Writing – review & editing. **Yang Song:** Formal analysis. **Zhang Heng:** Conceptualization, Funding acquisition, Supervision, Writing – review & editing. **Li Hui:** Software. **He Lijuan:** Formal analysis. **Yue Caiyan:** Writing – review & editing. **Wang Hao:** Investigation, Writing – original draft. **Zhou Heng:** Formal analysis, Investigation, Writing – original draft.

Declaration of Competing Interest

The authors declare that they have no known competing financial

interests or personal relationships that could have appeared to influence the work reported in this paper.

Data Availability

Data will be made available on request.

Acknowledgments

This work was supported by the National Natural Science Foundation of China (32302418), Guizhou Provincial Key Technology R&D Program (ZC[2023]330), Guizhou Provincial Basic Research Program (Natural Science, ZK[2022]141), Guizhou Provincial Education Project (KY (2022)162), Australian Research Council (ARC) through Future Fellowship (FT210100298, FT210100806), Discovery Project (DP220100603), Linkage Project (LP210100467, LP210200504, LP210200345, LP220100088), and Industrial Transformation Training Centre (IC180100005) schemes, and the Australian Government through the Cooperative Research Centres Projects (CRCPXIII000077).

Appendix A. Supporting information

Supplementary data associated with this article can be found in the online version at doi:10.1016/j.apcatb.2023.123605.

References

[1] F. Yang, M. Du, K. Yin, Z. Qiu, J. Zhao, C. Liu, G. Zhang, Y. Gao, H. Pang, Applications of metal-organic frameworks in water treatment: a review, Small 18 (2022), 2105715.
[2] C. Yue, L. Chen, H. Zhang, J. Huang, H. Jiang, H. Li, S. Yang, Metal–organic framework-based materials: emerging high-efficiency catalysts for the heterogeneous photocatalytic degradation of pollutants in water, Environ. Sci. Water Res. Technol. 9 (2023) 669–695.
[3] Y. He, Z. Wang, H. Wang, E. Almatrafi, H. Qin, D. Huang, Y. Zhu, C. Zhou, Q. Tian, P. Xu, G. Zeng, Confinement of ZIF-derived copper-cobalt-zinc oxides in carbon framework for degradation of organic pollutants, J. Hazard. Mater. 440 (2022), 129811.
[4] S. Nayak, K.M. Parida, Deciphering Z-scheme charge transfer dynamics in heterostructure NiFe-LDH/N-rGO/g-C_3N_4 nanocomposite for photocatalytic pollutant removal and water splitting reactions, Sci. Rep. 9 (2019) 2458.
[5] N. Lin, Y. Gong, R. Wang, Y. Wang, X. Zhang, Critical review of perovskite-based materials in advanced oxidation system for wastewater treatment: Design, applications and mechanisms, J. Hazard. Mater. 424 (2022), 127637.
[6] A. Yadav, N. Bagotia, A.K. Sharma, S. Kumar, Advances in decontamination of wastewater using biomass-basedcomposites: A critical review, Sci. Total Environ. 784 (2021), 147108.
[7] Z.H. Xie, H.Y. Zhou, C.S. He, Z.C. Pan, G. Yao, B. Lai, Synthesis, application and catalytic performance of layered double hydroxide based catalysts in advanced oxidation processes for wastewater decontamination: a review, Chem. Eng. J. 414 (2021), 128713.
[8] F. Mahmoudi, K. Saravanakumar, V. Maheskumar, L.K. Njaramba, Y. Yoon, C. M. Park, Application of perovskite oxides and their composites for degrading organic pollutants from wastewater using advanced oxidation processes: review of the recent progress, J. Hazard. Mater. 436 (2022), 129074.
[9] X. Li, L. Zhang, S. Niu, Z. Dong, C. Lyu, Quantitatively regulating the ketone structure of triazine-based covalent organic frameworks for efficient visible-light photocatalytic degradation of organic pollutants: tunable performance and mechanisms, J. Hazard. Mater. 444 (2023), 130366.
[10] X. Hu, X. Hu, Q. Peng, L. Zhou, X. Tan, L. Jiang, C. Tang, H. Wang, S. Liu, Y. Wang, Z. Ning, Mechanisms underlying the photocatalytic degradation pathway of ciprofloxacin with heterogeneous TiO_2, Chem. Eng. J. 380 (2020), 122366.
[11] K.M. Lee, C.W. Lai, K.S. Ngai, J.C. Juan, Recent developments of zinc oxide based photocatalyst in water treatment technology: A review, Water Res 88 (2016) 428–448.
[12] L. Cheng, Q. Xiang, Y. Liao, H. Zhang, CdS-based photocatalysts, Energy Environ. Sci. 11 (2018) 1362–1391.
[13] S.M. Alluqmani, M. Loulou, J. Ouerfelli, A. Alshahrie, N. Salah, Elaboration of TiO_2/carbon of oil fly ash nanocomposite as an eco-friendly photocatalytic thin-film material, Ceram. Int. 47 (2021) 13544–13551.
[14] N.T. Padmanabhan, N. Thomas, J. Louis, D.T. Mathew, P. Ganguly, H. John, S. C. Pillai, Graphene coupled TiO_2 photocatalysts for environmental applications: a review, Chemosphere 271 (2021), 129506.
[15] Y. Lin, Q. Wang, M. Ma, P. Li, V. Maheskumar, Z. Jiang, R. Zhang, Enhanced optical absorption and photocatalytic water splitting of g-C_3N_4/TiO_2 heterostructure through C&B codoping: a hybrid DFT study, Int. J. Hydrog. Energy 46 (2021) 9417–9432.
[16] H. Qian, Q. Hou, E. Duan, J. Niu, Y. Nie, C. Bai, X. Bai, M. Ju, Honeycombed Au@C-TiO_2-Xcatalysts for enhanced photocatalytic mineralization of Acid red 3R under visible light, J. Hazard. Mater. 391 (2020), 122246.
[17] H. Tada, T. Kiyonaga, S.I. Naya, Rational design and applications of highly efficient reaction systems photocatalyzed by noble metal nanoparticle-loaded titanium(iv) dioxide, Chem. Soc. Rev. 38 (2009) 1849–1858.
[18] J. Kim, D. Monllor-Satoca, W. Choi, Simultaneous production of hydrogen with the degradation of organic pollutants using TiO_2 photocatalyst modified with dual surface components, Energy Environ. Sci. 5 (2012) 7647–7656.
[19] J. Schneider, M. Matsuoka, M. Takeuchi, J. Zhang, Y. Horiuchi, M. Anpo, D. W. Bahnemann, Understanding TiO_2 photocatalysis: Mechanisms and materials, Chem. Rev. 114 (2014) 9919–9986.
[20] M. Nolan, A. Iwaszuk, A.K. Lucid, J.J. Carey, M. Fronzi, Design of novel visible light active photocatalyst materials: surface modified TiO_2, Adv. Mater. 28 (2016) 5425–5446.
[21] J. Low, B. Dai, T. Tong, C. Jiang, J. Yu, In situ irradiated X-ray photoelectron spectroscopy investigation on a direct Z-scheme TiO_2/CdS composite film photocatalyst, Adv. Mater. 31 (2019) 1802981.
[22] S. Kreft, D. Wei, H. Junge, M. Beller, Recent advances on TiO_2-based photocatalytic CO_2 reduction, EnergyChem 2 (2020), 100044.
[23] H. Zeng, Z. Li, G. Li, X. Cui, M. Jin, T. Xie, L. Liu, M. Jiang, X. Zhong, Y. Zhang, H. Zhang, K. Ba, Z. Yan, Y. Wang, S. Song, K. Huang, S. Feng, Interfacial engineering of TiO_2/Ti_3C_2 MXene/carbon nitride hybrids boosting charge transfer for efficient photocatalytic hydrogen evolution, Adv. Energy Mater. 12 (2022) 2102765.
[24] L. Liccardo, M. Bordin, P.M. Sheverdyaeva, M. Belli, P. Moras, A. Vomiero, E. Moretti, Surface defect engineering in colored TiO_2 hollow spheres toward efficient photocatalysis, Adv. Funct. Mater. 33 (2023) 2212486.
[25] C. Zhang, H. Hua, J. Liu, X. Han, Q. Liu, Z. Wei, C. Shao, C. Hu, Enhanced photocatalytic activity of nanoparticle-aggregated Ag–AgX(X = Cl, Br)@TiO_2 microspheres under visible light, Nano-Micro Lett. 9 (2017) 49.
[26] E. Wahlström, E.K. Vestergaard, R. Schaub, A. Rønnau, M. Vestergaard, E. Lægsgaard, I. Stensgaard, F. Besenbacher, Electron transfer-induced dynamics of oxygen molecules on the TiO_2(110) surface, Science 303 (2004) 511–513.
[27] Z. Wang, Z. Lin, S. Shen, W. Zhong, S. Cao, Advances in designing heterojunction photocatalytic materials, Chin. J. Catal. 42 (2021) 710–730.
[28] J. Low, J. Yu, M. Jaroniec, S. Wageh, A.A. Al-Ghamdi, Heterojunction photocatalysts, Adv. Mater. 29 (2017) 1601694.
[29] X. Zhang, S.P. Jiang, Layered g-C_3N_4/TiO_2 nanocomposites for efficient photocatalytic water splitting and CO_2 reduction: a review, Mater. Today Energy 23 (2022), 100904.
[30] S. Qiao, M. Di, J.X. Jiang, B.H. Han, Conjugated porous polymers for photocatalysis: the road from catalytic mechanism, molecular structure to advanced applications, EnergyChem 4 (2022), 100094.
[31] M. Liras, M. Barawi, V.A. de la Peña O'Shea, Hybrid materials based on conjugated polymers and inorganic semiconductors as photocatalysts: from environmental to energy applications, Chem. Soc. Rev. 48 (2019) 5454–5487.
[32] K. Oka, H. Nishide, B. Winther-Jensen, Copolymer of phenylene and thiophene toward a visible-light-driven photocatalytic oxygen reduction to hydrogen peroxide, Adv. Sci. 8 (2021) 2003077.
[33] C.C. Li, M.Y. Gao, X.J. Sun, H.L. Tang, H. Dong, F.M. Zhang, Rational combination of covalent-organic framework and nano TiO_2 by covalent bonds to realize dramatically enhanced photocatalytic activity, Appl. Catal., B 266 (2020), 118586.
[34] R. Zhang, Y. Yu, H. Wang, J. Du, Mesoporous TiO_2/g-C_3N_4 composites with O-Ti-N bridge for improved visible-light photodegradation of enrofloxacin, Sci. Total Environ. 724 (2020), 138280.
[35] J. Zhu, P. Xiao, H. Li, S.A.C. Carabineiro, Graphitic carbon nitride: synthesis, properties, and applications in catalysis, ACS Appl. Mater. Interfaces 6 (2014) 16449–16465.
[36] S. Moradi, A.A. Isari, F. Hayati, R. Rezaei Kalantary, B. Kakavandi, Co-implanting of TiO_2 and liquid-phase-delaminated g-C_3N_4 on multi-functional graphene nanobridges for enhancing photocatalytic degradation of acetaminophen, Chem. Eng. J. 414 (2021), 128618.
[37] R. Acharya, K. Parida, A review on TiO_2/g-C_3N_4 visible-light- responsive photocatalysts for sustainable energy generation and environmental remediation, J. Environ. Chem. Eng. 8 (2020), 103896.
[38] W.X. Zhang, P.Q. Liao, R.B. Lin, Y.S. Wei, M.H. Zeng, X.M. Chen, Metal cluster-based functional porous coordination polymers, Coord. Chem. Rev. 293-294 (2015) 263–278.
[39] S. Kitagawa, R. Kitaura, S.I. Noro, Functional porous coordination polymers, Angew. Chem. Int. Ed. 43 (2004) 2334–2375.
[40] Q. Wang, Q. Gao, A.M. Al-Enizi, A. Nafady, S. Ma, Recent advances in MOF-based photocatalysis: environmental remediation under visible light, Inorg. Chem. Front. 7 (2020) 300–339.
[41] K. Zhang, H. Hu, L. Shi, B. Jia, H. Huang, X. Han, X. Sun, T. Ma, Strategies for optimizing the photocatalytic water-splitting performance of metal–organic framework-based materials, Small Sci. 1 (2021) 2100060.
[42] J.Y. Zeng, X.S. Wang, B.R. Xie, Q.R. Li, X.Z. Zhang, Large π-conjugated metal–organic frameworks for infrared-light-driven CO_2 reduction, J. Am. Chem. Soc. 144 (2022) 1218–1231.
[43] C. Zhao, X. Pan, Z. Wang, C.C. Wang, 1 + 1 > 2: A critical review of MOF/bismuth-based semiconductor composites for boosted photocatalysis, Chem. Eng. J. 417 (2021), 128022.

[44] C.C. Wang, X. Wang, W. Liu, The synthesis strategies and photocatalytic performances of TiO_2/MOFs composites: a state-of-the-art review, Chem. Eng. J. 391 (2020), 123601.

[45] Y. Jing, H. Yin, C. Li, J. Chen, S. Wu, H. Liu, L. Xie, Q. Lei, M. Sun, S. Yu, Fabrication of Pt doped TiO_2–ZnO@ZIF-8 core@shell photocatalyst with enhanced activity for phenol degradation, Environ. Res. 203 (2022), 111819.

[46] X. Zhang, N. Yuan, Y. Li, L. Han, Q. Wang, Fabrication of new MIL-53(Fe)@TiO_2 visible-light responsive adsorptive photocatalysts for efficient elimination of tetracycline, Chem. Eng. J. 428 (2022), 131077.

[47] D. Kanakaraju, A. Chandrasekaran, Recent advances in TiO_2/ZnS-based binary and ternary photocatalysts for the degradation of organic pollutants, Sci. Total Environ. 868 (2023), 161525.

[48] R.B. Rajput, S.N. Jamble, R.B. Kale, A review on TiO_2/SnO_2 heterostructures as a photocatalyst for the degradation of dyes and organic pollutants, J. Environ. Manag. 307 (2022), 114533.

[49] A. Sewnet, M. Abebe, P. Asaithambi, E. Alemayehu, Visible-light-driven g-C_3N_4/TiO_2 based heterojunction nanocomposites for photocatalytic degradation of organic dyes in wastewater: a review, Air Soil Water Res 15 (2022), 11786221221117266.

[50] S. Sharma, S. Basu, Highly reusable visible light active hierarchical porous WO_3/SiO_2 monolith in centimeter length scale for enhanced photocatalytic degradation of toxic pollutants, Sep. Purif. Technol. 231 (2020), 115916.

[51] A. Kumar, M. Khan, J. He, I.M.C. Lo, Visible–light–driven magnetically recyclable terephthalic acid functionalized g−C_3N_4/TiO_2 heterojunction nanophotocatalyst for enhanced degradation of PPCPs, Appl. Catal., B 270 (2020), 118898.

[52] Q. Xu, L. Zhang, B. Cheng, J. Fan, J. Yu, S-scheme heterojunction photocatalyst, Chem 6 (2020) 1543–1559.

[53] H. Wang, L. Zhang, Z. Chen, J. Hu, S. Li, Z. Wang, J. Liu, X. Wang, Semiconductor heterojunction photocatalysts: design, construction, and photocatalytic performances, Chem. Soc. Rev. 43 (2014) 5234–5244.

[54] G. Di Liberto, S. Tosoni, G. Pacchioni, Z-scheme versus type-II junction in g-C_3N_4/TiO_2 and g-C_3N_4/$SrTiO_3$/TiO_2 heterostructures, Catal. Sci. Technol. 11 (2021) 3589–3598.

[55] T.Q. Zi, X.R. Zhao, C. Liu, Y.Q. Cao, A.D. Li, A facile route to prepare TiO_2/g-C_3N_4 nanocomposite photocatalysts by atomic layer deposition, J. Alloy. Compd. 855 (2021), 157446.

[56] A.S. Belousov, D.G. Fukina, A.V. Koryagin, Metal–organic framework-based heterojunction photocatalysts for organic pollutant degradation: design, construction, and performances, J. Chem. Technol. Biotechnol. 97 (2022) 2675–2693.

[57] R. Li, W. Zhang, K. Zhou, Metal–organic-framework-based catalysts for photoreduction of CO_2, Adv. Mater. 30 (2018) 1705512.

[58] L. Xie, T. Du, J. Wang, Y. Ma, Y. Ni, Z. Liu, L. Zhang, C. Yang, J. Wang, Recent advances on heterojunction-based photocatalysts for the degradation of persistent organic pollutants, Chem. Eng. J. 426 (2021), 130617.

[59] K. Xie, S. Xu, K. Xu, W. Hao, J. Wang, Z. Wei, BiOCl Heterojunction photocatalyst: construction, photocatalytic performance, and applications, Chemosphere 317 (2023), 137823.

[60] T.U. Tran, D.A. Nguyen, N.T. Duong, D.Y. Park, D.H. Nguyen, P.H. Nguyen, C. Park, J. Lee, B.W. Ahn, H. Im, Gate tunable photoresponse of a two-dimensional pn junction for high performance broadband photodetector, Appl, Mater. Today 26 (2022), 101285.

[61] M. Jourshabani, Z. Shariatinia, G. Achari, C.H. Langford, A. Badiei, Facile synthesis of NiS_2 nanoparticles ingrained in a sulfur-doped carbon nitride framework with enhanced visible light photocatalytic activity: Two functional roles of thiourea, J. Mater. Chem. A 6 (2018) 13448–13466.

[62] Y. Ren, D. Zeng, W.J. Ong, Interfacial engineering of graphitic carbon nitride (g-C_3N_4)-based metal sulfide heterojunction photocatalysts for energy conversion: A review, Chin. J. Catal. 40 (2019) 289–319.

[63] H. Guo, H.Y. Niu, C. Liang, C.G. Niu, D.W. Huang, L. Zhang, N. Tang, Y. Yang, C. Y. Feng, G.M. Zeng, Insight into the energy band alignment of magnetically separable Ag_2O/$ZnFe_2O_4$ p-n heterostructure with rapid charge transfer assisted visible light photocatalysis, J. Catal. 370 (2019) 289–303.

[64] F. Guo, W. Shi, H. Wang, M. Han, W. Guan, H. Huang, Y. Liu, Z. Kang, Study on highly enhanced photocatalytic tetracycline degradation of type II AgI/CuBi2O_4 and Z-scheme AgBr/$CuBi_2O_4$ heterojunction photocatalysts, J. Hazard. Mater. 349 (2018) 111–118.

[65] J. Wang, Q. Zhang, F. Deng, X. Luo, D.D. Dionysiou, Rapid toxicity elimination of organic pollutants by the photocatalysis of environment-friendly and magnetically recoverable step-scheme $SnFe_2O_4$/$ZnFe_2O_4$ nano-heterojunctions, Chem. Eng. J. 379 (2020), 122264.

[66] B. Wang, Q. Cao, M. Cheng, G. Li, J. Zhang, H. Jiang, Photocatalytic degradation of antibiotics in water by pollution-free photocatalytic films with a three-dimensional layered structure and the reaction mechanism study, J. Water Process Eng. 52 (2023), 103550.

[67] Z. Li, J. He, H. Ma, L. Zang, D. Li, S. Guo, Y. Ci, Preparation of heterogeneous TiO_2/g-C_3N_4 with a layered mosaic stack structure by use of montmorillonite as a hard template approach: TC degradation, kinetic, mechanism, pathway and DFT investigation, Appl. Clay Sci. 207 (2021), 106107.

[68] P. Chen, S. Di, X. Qiu, S. Zhu, One-step synthesis of F-TiO_2/g-C_3N_4 heterojunction as highly efficient visible-light-active catalysts for tetrabromobisphenol A and sulfamethazine degradation, Appl. Surf. Sci. 587 (2022), 152889.

[69] D. Chen, Y. Cheng, N. Zhou, P. Chen, Y. Wang, K. Li, S. Huo, P. Cheng, P. Peng, R. Zhang, L. Wang, H. Liu, Y. Liu, R. Ruan, Photocatalytic degradation of organic pollutants using TiO_2-based photocatalysts: a review, J. Clean. Prod. 268 (2020), 121725.

[70] S. Iqbal, J. Liu, H. Ma, W. Liu, S. Zuo, Y. Yu, Fabrication of TiO_2/Fe_2O_3/g-C_3N_4 ternary photocatalyst via a low-temperature calcination and solvothermal route and its visible light assisted photocatalytic properties, J. Mol. Struct. 1282 (2023), 135166.

[71] Y.R. Girish, Udayabhanu, G. Alnaggar, A. Hezam, M.B. Nayan, G. Nagaraju, K. Byrappa, Facile and rapid synthesis of solar-driven TiO_2/g-C_3N_4 heterostructure photocatalysts for enhanced photocatalytic activity, J. Sci.: Adv. Mater. Devices 7 (2022), 100419.

[72] B. Zhang, Q. Wang, J. Zhuang, S. Guan, B. Li, Molten salt assisted in-situ synthesis of TiO_2/g-C_3N_4 composites with enhanced visible-light-driven photocatalytic activity and adsorption ability, J. Photochem. Photobiol., A 362 (2018) 1–13.

[73] X. Zhang, G. Yang, C. Han, J. Yang, Z. Zeng, Z. Xiong, J. Jia, K. Sa, H. Ye, Y. Liang, Construction of 0D/2D CdZnS quantum dots/$SnIn_4S_8$ nanosheets heterojunction photocatalysts for boosting photocatalytic performance, Colloids Surf., A 664 (2023), 131184.

[74] Y.L. Wang, M. Peñas-Garzón, J.J. Rodriguez, J. Bedia, C. Belver, Enhanced photodegradation of acetaminophen over Sr@TiO_2/UiO-66-NH_2 heterostructures under solar light irradiation, Chem. Eng. J. 446 (2022), 137229.

[75] Y. Tang, X. Li, H. Zhang, T. Ouyang, Y. Jiang, M. Mu, X. Yin, Cobalt-based ZIF coordinated hybrids with defective TiO_{2-x} for boosting visible light-driven photo-Fenton-like degradation of bisphenol A, Chemosphere 259 (2020), 127431.

[76] P. Wu, Z. Zhang, Y. Luo, Y. Bai, J. Fan, Bioremediation of phenolic pollutants by algae-current status and challenges, Bioresour. Technol. 350 (2022), 126930.

[77] Y. Tang, X. Yin, M. Mu, Y. Jiang, X. Li, H. Zhang, T. Ouyang, Anatase TiO_2@MIL-101(Cr) nanocomposite for photocatalytic degradation of bisphenol A, Colloids Surf., A 596 (2020), 124745.

[78] L. Xu, L. Meng, X. Zhang, X. Mei, X. Guo, W. Li, P. Wang, L. Gan, Promoting Fe^{3+}/Fe^{2+} cycling under visible light by synergistic interactions between P25 and small amount of Fenton reagents, J. Hazard. Mater. 379 (2019), 120795.

[79] D. Vaya, P.K. Surolia, Semiconductor based photocatalytic degradation of pesticides: An overview, Environ. Technol. Innov. 20 (2020), 101128.

[80] A. Saljooqi, T. Shamspur, A. Mostafavi, Synthesis and photocatalytic activity of porous ZnO stabilized by TiO_2 and Fe_3O_4 nanoparticles: investigation of pesticide degradation reaction in water treatment, Environ. Sci. Pollut. Res. 28 (2021) 9146–9156.

[81] A.H.C. Khavar, G. Moussavi, A.R. Mahjoub, M. Satari, P. Abdolmaleki, Synthesis and visible-light photocatalytic activity of In,S-TiO_2@rGO nanocomposite for degradation and detoxification of pesticide atrazine in water, Chem. Eng. J. 345 (2018) 300–311.

[82] R. Tang, D. Gong, Y. Deng, S. Xiong, J. Deng, L. Li, Z. Zhou, J. Zheng, L. Su, L. Yang, π-π Stacked step-scheme PDI/g-C_3N_4/TiO_2@Ti_3C_2 photocatalyst with enhanced visible photocatalytic degradation towards atrazine via peroxymonosulfate activation, Chem. Eng. J. 427 (2022), 131809.

[83] J.S. Wang, X.H. Yi, X. Xu, H. Ji, A.M. Alanazi, C.C. Wang, C. Zhao, Y.V. Kaneti, P. Wang, W. Liu, Y. Yamauchi, Eliminating tetracycline antibiotics matrix via photoactivated sulfate radical-based advanced oxidation process over the immobilized MIL-88A: Batch and continuous experiments, Chem. Eng. J. 431 (2022), 133213.

[84] W. Gan, J. Guo, X. Fu, J. Jin, M. Zhang, R. Chen, C. Ding, Y. Lu, J. Li, Z. Sun, Introducing oxygen-doped g-C_3N_4 onto g-C_3N_4/TiO_2 heterojunction for efficient catalytic gatifloxacin degradation and H_2O_2 production, Sep. Purif. Technol. 317 (2023), 123791.

[85] F. Wang, S.S. Liu, Z. Feng, H. Fu, M. Wang, P. Wang, W. Liu, C.C. Wang, High-efficient peroxymonosulfate activation for rapid atrazine degradation by FeSx@MoS_2 derived from MIL-88A(Fe), J. Hazard. Mater. 440 (2022), 129723.

[86] Y.C. Chou, Y.Y. Lin, C.S. Lu, F.Y. Liu, J.H. Lin, F.H. Chen, C.C. Chen, W.T. Wu, Controlled hydrothermal synthesis of BiO_xCl_y/BiO_mBr_n/g-C_3N_4 composites exhibiting visible-light photocatalytic activity, J. Environ. Manag. 297 (2021), 113256.

[87] M. Shandilya, R. Rai, J. Singh, Review: Hydrothermal technology for smart materials, Adv. Appl. Ceram. 115 (2016) 354–376.

[88] A.M. Nasir, N. Awang, J. Jaafar, A.F. Ismail, M.H.D. Othman, M.A. Rahman, F. Aziz, M.A. Mat Yajid, Recent progress on fabrication and application of electrospun nanofibrous photocatalytic membranes for wastewater treatment: a review, J. Water Process Eng. 40 (2021), 101878.

[89] M. Parashar, V.K. Shukla, R. Singh, Metal oxides nanoparticles via sol–gel method: a review on synthesis, characterization and applications, J. Mater. Sci.: Mater. Electron 31 (2020) 3729–3749.

[90] A. Goktas, F. Aslan, A. Tumbul, S.H. Gunduz, Tuning of structural, optical and dielectric constants by various transition metal doping in ZnO:TM (TM=Mn, Co, Fe) nanostructured thin films: A comparative study, Ceram. Int. 43 (2017) 704–713.

[91] Y. Zhang, J. Liu, X. Chu, S. Liang, L. Kong, Preparation of g–C_3N_4–SnO_2 composites for application as acetic acid sensor, J. Alloy. Compd. 832 (2020), 153355.

[92] P. Chen, X. Dai, P. Xing, X. Zhao, Q. Zhang, S. Ge, J. Si, L. Zhao, Y. He, Microwave heating assisted synthesis of novel SnSe/g-C_3N_4 composites for effective photocatalytic H_2 production, J. Ind. Eng. Chem. 80 (2019) 74–82.

[93] T. Lv, L. Pan, X. Liu, T. Lu, G. Zhu, Z. Sun, C.Q. Sun, One-step synthesis of CdS–TiO_2–chemically reduced graphene oxide composites via microwave-assisted reaction for visible-light photocatalytic degradation of methyl orange, Catal. Sci. Technol. 2 (2012) 754–758.

[94] J. Low, C. Jiang, B. Cheng, S. Wageh, A.A. Al-Ghamdi, J. Yu, A review of direct Z-scheme photocatalysts, Small Methods 1 (2017) 1700080.

[95] M. Zhang, N. Han, Y. Fei, J. Liu, L. Xing, A. Núñez-Delgado, M. Jiang, S. Liu, TiO_2/g-C_3N_4 photocatalyst for the purification of potassium butyl xanthate in mineral processing wastewater, J. Environ. Manag. 297 (2021), 113311.
[96] Y. Cao, G. Yuan, Y. Guo, X. Hu, G. Fang, S. Wang, Facile synthesis of TiO_2/g-C_3N_4 nanosheet heterojunctions for efficient photocatalytic degradation of tartrazine under simulated sunlight, Appl. Surf. Sci. 600 (2022), 154169.
[97] X. Qu, C. Chen, J. Lin, W. Qiang, L. Zhang, D. Sun, Engineered defect-rich TiO_2/g-C_3N_4 heterojunction: a visible light-driven photocatalyst for efficient degradation of phenolic wastewater, Chemosphere 286 (2022), 131696.
[98] S. Tan, Z. Xing, J. Zhang, Z. Li, X. Wu, J. Cui, J. Kuang, Q. Zhu, W. Zhou, Ti^{3+}-TiO_2/g-C_3N_4 mesostructured nanosheets heterojunctions as efficient visible-light-driven photocatalysts, J. Catal. 357 (2018) 90–99.
[99] R. Wu, J. Yi, R. Bao, P. Liu, The excellent photocatalytic capability of TiO_2@C/O-doped g-C_3N_4 heterojunction photocatalyst, Colloids Surf., A 648 (2022), 129351.
[100] Y. Sheng, Z. Wei, H. Miao, W. Yao, H. Li, Y. Zhu, Enhanced organic pollutant photodegradation via adsorption/photocatalysis synergy using a 3D g-C_3N_4/TiO_2 free-separation photocatalyst, Chem. Eng. J. 370 (2019) 287–294.
[101] S. Faryad, U. Azhar, M.B. Tahir, W. Ali, M. Arif, M. Sagir, Spinach-derived boron-doped g-C_3N_4/TiO_2 composites for efficient photo-degradation of methylene blue dye, Chemosphere 320 (2023), 138002.
[102] W.J. Ong, L.L. Tan, Y.H. Ng, S.T. Yong, S.P. Chai, Graphitic carbon nitride (g-C_3N_4)-based photocatalysts for artificial photosynthesis and environmental remediation: Are we a step closer to achieving sustainability? Chem. Rev. 116 (2016) 7159–7329.
[103] J. Li, H. Yuan, W. Zhang, B. Jin, Q. Feng, J. Huang, Z. Jiao, Advances in Z-scheme semiconductor photocatalysts for the photoelectrochemical applications: a review, Carbon Energy 4 (2022) 294–331.
[104] T. Wei, J. Xu, C. Kan, L. Zhang, X. Zhu, Au tailored on g-C_3N_4/TiO_2 heterostructure for enhanced photocatalytic performance, J. Alloy. Compd. 894 (2022), 162338.
[105] W. Gao, C. Kan, S. Ke, Q. Yun, X. Zhu, X. Zhu, Au nanobipyramids with Pt decoration enveloped in TiO_2 nanoboxes for photocatalytic reactions, Nanoscale Adv. 3 (2021) 4226–4234.
[106] B. Guo, C. Zhao, L. Zhou, Z. Yu, X. Liu, Z. Zhao, H. Yuan, Constructing a novel multi-hierarchical TiO_2/g-C_3N_4/Ag-AgBr photocatalyst with dual Z-scheme heterojunction utilizing Ag as the charge transfer mediator, J. Alloy. Compd. 900 (2022), 163514.
[107] Z. Wu, Y. Liang, X. Yuan, D. Zou, J. Fang, L. Jiang, J. zhang, H. Yang, Z. Xiao, MXene Ti_3C_2 derived Z–scheme photocatalyst of graphene layers anchored TiO_2/g–C_3N_4 for visible light photocatalytic degradation of refractory organic pollutants, Chem. Eng. J. 394 (2020), 124921.
[108] K. Rabé, L. Liu, N.A. Nahyoon, Y. Zhang, A.M. Idris, J. Sun, L. Yuan, Fabrication of high efficiency visible light Z-scheme heterostructure photocatalyst g-C_3N_4/Fe^0(1%)/TiO_2 and degradation of rhodamine B and antibiotics, J. Taiwan Inst. Chem. Eng. 96 (2019) 463–472.
[109] S. Kai, B. Xi, H. Li, S. Xiong, Z-scheme CdS/Co_9S_8-RGO for photocatalytic hydrogen production, Inorg. Chem. Front. 7 (2020) 2692–2701.
[110] F. Wu, X. Li, W. Liu, S. Zhang, Highly enhanced photocatalytic degradation of methylene blue over the indirect all-solid-state Z-scheme g-C_3N_4-RGO-TiO_2 nanoheterojunctions, Appl. Surf. Sci. 405 (2017) 60–70.
[111] T.D. Nguyen-Phan, V.H. Pham, E.W. Shin, H.D. Pham, S. Kim, J.S. Chung, E. J. Kim, S.H. Hur, The role of graphene oxide content on the adsorption-enhanced photocatalysis of titanium dioxide/graphene oxide composites, Chem. Eng. J. 170 (2011) 226–232.
[112] S. Xue, H. Li, F. Cao, Y. Cao, X. Yue, Preparation of g-C_3N_4(Ag)/Gr/TiO_2 Z-scheme photocatalyst with enhanced reduction property and the efficient degradation of rhodamine B, J. Alloy. Compd. 898 (2022), 162759.
[113] R. Liu, X. Han, R. Liu, Z. Qi, B. Ren, Y. Sun, Molecularly imprinted Fe_3O_4/g-C_3N_4/TiO_2 catalyst for selective photodegradation of chlorotetracycline, Colloids Surf., A 680 (2024), 132691.
[114] K. Qi, B. Cheng, J. Yu, W. Ho, A review on TiO_2-based Z-scheme photocatalysts, Chin. J. Catal. 38 (2017) 1936–1955.
[115] M. Vijayan, V. Manikandan, C. Rajkumar, A.A. Hatamleh, B.K. Alnafisi, G. Easwaran, X. Liu, K. Sivakumar, H. Kim, Constructing Z-scheme g-C_3N_4/TiO_2 heterostructure for promoting degradation of the hazardous dye pollutants, Chemosphere 311 (2023), 136928.
[116] B. Zhang, X. He, X. Ma, Q. Chen, G. Liu, Y. Zhou, D. Ma, C. Cui, J. Ma, Y. Xin, In situ synthesis of ultrafine TiO_2 nanoparticles modified g-C_3N_4 heterojunction photocatalyst with enhanced photocatalytic activity, Sep. Purif. Technol. 247 (2020), 116932.
[117] Y. Liu, X. Zheng, Y. Yang, J. Li, W. Liu, Y. Shen, X. Tian, Photocatalytic hydrogen evolution using ternary-metal-sulfide/TiO_2 heterojunction photocatalysts, ChemCatChem 14 (2022), e202101439.
[118] X. Li, J. Xiong, Y. Xu, Z. Feng, J. Huang, Defect-assisted surface modification enhances the visible light photocatalytic performance of g-C_3N_4@C-TiO_2 direct Z-scheme heterojunctions, Chin. J. Catal. 40 (2019) 424–433.
[119] H. Yu, S. Xu, S. Zhang, S. Wang, Z. He, In-situ construction of core–shell structured TiB_2-TiO_2@g-C_3N_4 for efficient photocatalytic degradation, Appl. Surf. Sci. 579 (2022), 152201.
[120] S. Sun, H. Ding, L. Mei, Y. Chen, Q. Hao, W. Chen, Z. Xu, D. Chen, Construction of SiO_2-TiO_2/g-C_3N_4 composite photocatalyst for hydrogen production and pollutant degradation: Insight into the effect of SiO2, Chin. Chem. Lett. 31 (2020) 2287–2294.
[121] R. Rajendran, S. Vignesh, V. Raj, B. Palanivel, A.M. Ali, M.A. Sayed, M. Shkir, Designing of TiO_2/α-Fe_2O_3 coupled g-C_3N_4 magnetic heterostructure composite for efficient Z-scheme photo-degradation process under visible light exposures, J. Alloy. Compd. 894 (2022), 162498.
[122] J. Fu, Q. Xu, J. Low, C. Jiang, J. Yu, Ultrathin 2D/2D WO_3/g-C_3N_4 step-scheme H_2-production photocatalyst, Appl. Catal., B 243 (2019) 556–565.
[123] X. He, M. Wu, Z. Ao, B. Lai, Y. Zhou, T. An, S. Wang, Metal–organic frameworks derived C/TiO_2 for visible light photocatalysis: Simple synthesis and contribution of carbon species, J. Hazard. Mater. 403 (2021), 124048.
[124] C. Yang, X. Zhang, Y. Zhou, S. Hao, Well-designed MOF-derived hollow octahedral structure TiO_2 coupled with ultra-thin porous g-C_3N_4 to enhance the degradation of real liquor brewing wastewater, Appl. Surf. Sci. 616 (2023), 156471.
[125] H. Su, W. Wang, H. Jiang, L. Sun, T. Kong, Z. Lu, H. Tang, L. Wang, Q. Liu, Boosting interfacial charge transfer with a giant internal electric field in a TiO_2 hollow-sphere-based S-scheme heterojunction for efficient CO_2 photoreduction, Inorg. Chem. 61 (2022) 13608–13617.
[126] J. Wang, G. Wang, B. Cheng, J. Yu, J. Fan, Sulfur-doped g-C_3N_4/TiO_2 S-scheme heterojunction photocatalyst for Congo Red photodegradation, Chin. J. Catal. 42 (2021) 56–68.
[127] S. Dong, S. Chen, F. He, J. Li, H. Li, K. Xu, Construction of a novel N-doped oxygen vacancy-rich TiO_2 N-TiO_{2-x}/g-C_3N_4 S-scheme heterostructure for visible light driven photocatalytic degradation of 2,4-dinitrophenylhydrazine, J. Alloy. Compd. 908 (2022), 164586.
[128] S. Riaz, S.J. Park, An overview of TiO_2-based photocatalytic membrane reactors for water and wastewater treatments, J. Ind. Eng. Chem. 84 (2020) 23–41.
[129] P. Parnicka, W. Lisowski, T. Klimczuk, A. Mikolajczyk, A. Zaleska-Medynska, A novel (Ti/Ce)UiO-X MOFs@TiO_2 heterojunction for enhanced photocatalytic performance: Boosting via Ce^{4+}/Ce^{3+} and Ti^{4+}/Ti^{3+} redox mediators, Appl. Catal., B 310 (2022), 121349.
[130] E. Safaralizadeh, A.R. Mahjoub, F. Fazlali, H. Bagheri, Facile construction of C_3N_4-TE@TiO_2/UiO-66 with double Z-scheme structure as high performance photocatalyst for degradation of tetracycline, Ceram. Int. 47 (2021) 2374–2387.
[131] J. Ding, Z. Yang, C. He, X. Tong, Y. Li, X. Niu, H. Zhang, UiO-66(Zr) coupled with Bi_2MoO_6 as photocatalyst for visible-light promoted dye degradation, J. Colloid Interface Sci. 497 (2017) 126–133.
[132] J. Gascon, M.D. Hernández-Alonso, A.R. Almeida, G.P.M. van Klink, F. Kapteijn, G. Mul, Isoreticular MOFs as efficient photocatalysts with tunable band gap: An operando FTIR study of the photoinduced oxidation of propylene, ChemSusChem 1 (2008) 981–983.
[133] S. Li, X. Wang, Q. He, Q. Chen, Y. Xu, H. Yang, M. Lü, F. Wei, X. Liu, Synergistic effects in N-$K_2Ti_4O_9$/UiO-66-NH_2 composites and their photocatalysis degradation of cationic dyes, Chin. J. Catal. 37 (2016) 367–377.
[134] Y.X. Li, X. Wang, C.C. Wang, H. Fu, Y. Liu, P. Wang, C. Zhao, S-TiO_2/UiO-66-NH_2 composite for boosted photocatalytic Cr(VI) reduction and bisphenol A degradation under LED visible light, J. Hazard. Mater. 399 (2020), 123085.
[135] J. Qiu, X. Zhang, Y. Feng, X. Zhang, H. Wang, J. Yao, Modified metal-organic frameworks as photocatalysts, Appl. Catal., B 231 (2018) 317–342.
[136] F. Zhang, Y. Jin, J. Shi, Y. Zhong, W. Zhu, M.S. El-Shall, Polyoxometalates confined in the mesoporous cages of metal–organic framework MIL-100(Fe): Efficient heterogeneous catalysts for esterification and acetalization reactions, Chem. Eng. J. 269 (2015) 236–244.
[137] L. Liu, Y. Liu, X. Wang, N. Hu, Y. Li, C. Li, Y. Meng, Y. An, Synergistic effect of B-TiO_2 and MIL-100(Fe) for high-efficiency photocatalysis in methylene blue degradation, Appl. Surf. Sci. 561 (2021), 149969.
[138] F. Zhao, Y. Liu, S.B. Hammouda, B. Doshi, N. Guijarro, X. Min, C.J. Tang, M. Sillanpää, K. Sivula, S. Wang, MIL-101(Fe)/g-C_3N_4 for enhanced visible-light-driven photocatalysis toward simultaneous reduction of Cr(VI) and oxidation of bisphenol A in aqueous media, Appl. Catal., B 272 (2020), 119033.
[139] S. Vigneshwaran, P. Sirajudheen, P. Karthikeyan, M. Nikitha, K. Ramkumar, S. Meenakshi, Immobilization of MIL-88(Fe) anchored TiO_2-chitosan(2D/2D) hybrid nanocomposite for the degradation of organophosphate pesticide: characterization, mechanism and degradation intermediates, J. Hazard. Mater. 406 (2021), 124728.
[140] C. Zhang, D. Guo, T. Shen, X. Hou, M. Zhu, S. Liu, Q. Hu, Titanium dioxide/magnetic metal-organic framework preparation for organic pollutants removal from water under visible light, Colloids Surf., A 589 (2020), 124484.
[141] Z. Kong, L. Lu, C. Zhu, J. Xu, Q. Fang, R. Liu, Y. Shen, Enhanced adsorption and photocatalytic removal of PFOA from water by F-functionalized MOF with in-situ-growth TiO_2: regulation of electron density and bandgap, Sep. Purif. Technol. 297 (2022), 121449.
[142] H. Assi, G. Mouchaham, N. Steunou, T. Devic, C. Serre, Titanium coordination compounds: from discrete metal complexes to metal–organic frameworks, Chem. Soc. Rev. 46 (2017) 3431–3452.
[143] H. Hori, A. Yamamoto, K. Koike, S. Kutsuna, M. Murayama, A. Yoshimoto, R. Arakawa, Photocatalytic decomposition of a perfluoroether carboxylic acid by tungstic heteropolyacids in water, Appl. Catal., B 82 (2008) 58–66.
[144] S. Kouser, A. Hezam, M.J.N. Khadri, S.A. Khanum, A review on zeolite imidazole frameworks: Synthesis, properties, and applications, J. Porous Mater. 29 (2022) 663–681.
[145] Y. Zhan, J. Lan, J. Shang, L. Yang, X. Guan, W. Li, S. Chen, Y. Qi, S. Lin, Durable ZIF-8/Ag/AgCl/TiO_2 decorated PAN nanofibers with high visible light photocatalytic and antibacterial activities for degradation of dyes, J. Alloy. Compd. 822 (2020), 153579.
[146] S. Bibi, E. Pervaiz, M. Ali, Synthesis and applications of metal oxide derivatives of ZIF-67: a mini-review, Chem. Pap. 75 (2021) 2253–2275.

[147] Y. Wang, Y. Yang, Q. Deng, W. Chen, Y. Zhang, Y. Zhou, Z. Zou, Recent progress of amorphous porous organic polymers as heterogeneous photocatalysts for organic synthesis, Adv. Funct. Mater., N./a (2023), 2307179.
[148] H. Chu, C.C. Wang, Metal-organic frameworks meet synthetic polymers for water decontamination: a critical review, Chem. Eng. J. 476 (2023), 146684.
[149] K.H. Rahman, A.K. Kar, Effect of band gap variation and sensitization process of polyaniline (PANI)-TiO_2 p-n heterojunction photocatalysts on the enhancement of photocatalytic degradation of toxic methylene blue with UV irradiation, J. Environ. Chem. Eng. 8 (2020), 104181.
[150] Y. Hu, X. Zhang, X. Zhang, H. Feng, L. Xu, In situ strategy to construct Z-scheme poly(diphenylbutadiene)/TiO_2 heterojunctions with enhanced visible light photocatalytic performance, J. Solid State Chem. 311 (2022), 123085.
[151] H. Huang, L. Yang, A. Facchetti, T.J. Marks, Organic and polymeric semiconductors enhanced by noncovalent conformational Locks, Chem. Rev. 117 (2017) 10291–10318.
[152] S. Yu, A. Peng, S. Zhang, H. Huang, Noncovalent conformational locks in organic semiconductors, Sci. China Chem. 61 (2018) 1359–1367.
[153] L. Liu, W. Jiang, X. Song, Q. Duan, E. Zhu, A novel strategy of lock-in effect between conjugated polymer and TiO_2 towards dramatic enhancement of photocatalytic activity under visible light, Sci. Rep. 10 (2020) 6513.
[154] H. Zhang, G. Liu, L. Shi, H. Liu, T. Wang, J. Ye, Engineering coordination polymers for photocatalysis, Nano Energy 22 (2016) 149–168.
[155] S. Mallakpour, S. Shamsaddinimotlagh, Ultrasonic-promoted rapid preparation of PVC/TiO_2-BSA nanocomposites: Characterization and photocatalytic degradation of methylene blue, Ultrason. Sonochem. 41 (2018) 361–374.
[156] X. Zhang, K. Fu, Z. Su, Fabrication of 3D MoS_2-TiO_2@PAN electro-spun membrane for efficient and recyclable photocatalytic degradation of organic dyes, Mater. Sci. Eng., B 269 (2021), 115179.
[157] L. Chen, L. He, B. Zheng, G. Wei, H. Li, H. Zhang, S. Yang, Bifunctional acid-activated montmorillonite catalyzed biodiesel production from non-food oil: Characterization, optimization, kinetic and thermodynamic studies, Fuel Process. Technol. 250 (2023), 107903.
[158] O. Fawzi Suleiman Khasawneh, P. Palaniandy, Removal of organic pollutants from water by Fe_2O_3/TiO_2 based photocatalytic degradation: A review, Environ. Technol. Innov. 21 (2021), 101230.
[159] W. Gan, J. Guo, X. Fu, M. Zhang, C. Ding, Y. Hai, Y. Lu, J. Li, Z. Li, Z. Sun, Dual-defects modified ultrathin 2D/2D TiO_2/g-C_3N_4 heterojunction for efficient removal of levofloxacin: Performance, degradation pathway, and mechanism, Sep. Purif. Technol. 306 (2023), 122578.
[160] R.S. Sutar, R.P. Barkul, S.D. Delekar, M.K. Patil, Sunlight assisted photocatalytic degradation of organic pollutants using g-C_3N_4-TiO_2 nanocomposites, Arab. J. Chem. 13 (2020) 4966–4977.
[161] Y. Li, Q. Zhang, Y. Lu, Z. Song, C. Wang, D. Li, X. Tang, X. Zhou, Surface hydroxylation of TiO_2/g-C_3N_4 photocatalyst for photo-Fenton degradation of tetracycline, Ceram. Int. 48 (2022) 1306–1313.
[162] Y. Zhu, Q. Xv, D. Wang, B. Sun, Y. Wang, Z. Han, Y. Gou, J. Liu, B. Li, Construction of a hollow BiOI/TiO_2/ZIF-8 heterojunction: Enhanced photocatalytic performance for norfloxacin degradation and mechanistic insight, J. Alloy. Compd. 914 (2022), 165326.
[163] N. Ahmadpour, M.H. Sayadi, S. Homaeigohar, A hierarchical Ca/TiO_2/NH_2-MIL-125 nanocomposite photocatalyst for solar visible light induced photodegradation of organic dye pollutants in water, RSC Adv. 10 (2020) 29808–29820.
[164] L. He, Y. Dong, Y. Zheng, Q. Jia, S. Shan, Y. Zhang, A novel magnetic MIL-101 (Fe)/TiO_2 composite for photo degradation of tetracycline under solar light, J. Hazard. Mater. 361 (2019) 85–94.
[165] T. Narkbuakaew, S. Sattayaporn, N. Saito, P. Sujaridworakun, Investigation of the Ag species and synergy of Ag-TiO_2 and g-C_3N_4 for the enhancement of photocatalytic activity under UV–Visible light irradiation, Appl. Surf. Sci. 573 (2022), 151617.
[166] L. He, L. Chen, B. Zheng, H. Zhou, H. Wang, H. Li, H. Zhang, C.C. Xu, S. Yang, Deep eutectic solvents for catalytic biodiesel production from liquid biomass and upgrading of solid biomass into 5-hydroxymethylfurfural, Green. Chem. 25 (2023) 7410–7440.
[167] L. Yang, X. Bai, J. Shi, X. Du, L. Xu, P. Jin, Quasi-full-visible-light absorption by D35-TiO_2/g-C_3N_4 for synergistic persulfate activation towards efficient photodegradation of micropollutants, Appl. Catal., B 256 (2019), 117759.
[168] R. Nekooie, J.B. Ghasemi, A. Badiei, T. Shamspur, A. Mostafavi, S. Moradian, Design and synthesis of g-C_3N_4/(Cu/TiO_2) nanocomposite for the visible light photocatalytic degradation of endosulfan in aqueous solutions, J. Mol. Struct. 1258 (2022), 132650.
[169] Z. Man, Y. Meng, X. Lin, X. Dai, L. Wang, D. Liu, Assembling UiO-66@TiO_2 nanocomposites for efficient photocatalytic degradation of dimethyl sulfide, Chem. Eng. J. 431 (2022), 133952.
[170] Y. Vasseghian, M. Berkani, F. Almomani, E.N. Dragoi, Data mining for pesticide decontamination using heterogeneous photocatalytic processes, Chemosphere 270 (2021), 129449.
[171] R. Tang, H. Zeng, C. Feng, S. Xiong, L. Li, Z. Zhou, D. Gong, L. Tang, Y. Deng, Twisty C-TiO_2/PCN S-scheme heterojunction with enhanced n→π * electronic excitation for promoted piezo-photocatalytic effect, Small 19 (2023) 2207636.
[172] Z. Hu, X. Cai, Z. Wang, S. Li, Z. Wang, X. Xie, Construction of carbon-doped supramolecule-based g-C_3N_4/TiO_2 composites for removal of diclofenac and carbamazepine: A comparative study of operating parameters, mechanisms, degradation pathways, J. Hazard. Mater. 380 (2019), 120812.
[173] H. Shi, Y. Li, X. Wang, H. Yu, J. Yu, Selective modification of ultra-thin g-C_3N_4 nanosheets on the (110) facet of Au/$BiVO_4$ for boosting photocatalytic H_2O_2 production, Appl. Catal., B 297 (2021), 120414.
[174] H. Wang, Y. Sun, Y. Wu, W. Tu, S. Wu, X. Yuan, G. Zeng, Z.J. Xu, S. Li, J.W. Chew, Electrical promotion of spatially photoinduced charge separation via interfacial-built-in quasi-alloying effect in hierarchical $Zn_2In_2S_5$/Ti_3C_2(O, OH)x hybrids toward efficient photocatalytic hydrogen evolution and environmental remediation, Appl. Catal., B 245 (2019) 290–301.
[175] G.H. Zhang, H.R. Zhang, J.G. He, Y.C. Jiang, H.L. Zhang, Q.B. Zhou, J.L. Cao, Facile construction Z-scheme anatase/rutile TiO_2/g-C_3N_4 hybrid for efficient photocatalytic H_2 evolution under visible-light irradiation, Ceram. Int. 48 (2022) 36644–36654.
[176] H. Wang, H. Zhou, Q. Yan, X. Wu, H. Zhang, Superparamagnetic nanospheres with efficient bifunctional acidic sites enable sustainable production of biodiesel from budget non-edible oils, Energy Convers. Manag. 297 (2023), 117758.
[177] S. Yang, K. Wang, Q. Chen, Y. Wu, Enhanced photocatalytic hydrogen production of S-scheme TiO_2/g-C_3N_4 heterojunction loaded with single-atom Ni, J. Mater. Sci. Technol. 175 (2024) 104–114.
[178] L. Biswal, S. Nayak, K. Parida, Rationally designed Ti_3C_2/N, S-TiO_2/g-C_3N_4 ternary heterostructure with spatial charge separation for enhanced photocatalytic hydrogen evolution, J. Colloid Interface Sci. 621 (2022) 254–266.
[179] Y. Chen, D. Yang, X. Xin, Z. Yang, Y. Gao, Y. Shi, Z. Zhao, K. An, W. Wang, J. Tan, Z. Jiang, Multi-stepwise charge transfer via MOF@MOF/TiO_2 dual-heterojunction photocatalysts towards hydrogen evolution, J. Mater. Chem. A 10 (2022) 9717–9725.
[180] X. Deng, Q. Liang, J. Fan, X. Yan, H. Si, H. Huang, Z. Li, Z. Kang, Interface engineering of hollow $CsPbBr_3$/Co_3O_4 p-n heterojunction with rich oxygen vacancy for highly enhanced photocatalytic CO_2 reduction, Chem. Eng. J. 475 (2023), 146385.
[181] T. Zhang, C. Hu, J. Wu, B. Shen, S. Peng, Y. Qi, M. Tao, X. Mao, Y. Tao, Y. Wang, Fabrication, structure, and application of sulfur-and sulfide-modified bismuth based photocatalysts: A review, Sep. Purif. Technol. 323 (2023), 124352.
[182] X. Bao, D. Lu, Z. Wang, H. Yin, B. Zhu, B. Chen, M. Shi, Y. Zhang, Q. Xu, Y. Qin, X. C. Shen, K. Wu, Significantly enhanced photothermal catalytic CO_2 reduction over TiO_2/g-C_3N_4 composite with full spectrum solar light, J. Colloid Interface Sci. 638 (2023) 63–75.
[183] Z. Jiang, X. Xu, Y. Ma, H.S. Cho, D. Ding, C. Wang, J. Wu, P. Oleynikov, M. Jia, J. Cheng, Y. Zhou, O. Terasaki, T. Peng, L. Zan, H. Deng, Filling metal–organic framework mesopores with TiO_2 for CO_2 photoreduction, Nature 586 (2020) 549–554.
[184] Y. Zhang, J. Xu, J. Mei, S. Sarina, Z. Wu, T. Liao, C. Yan, Z. Sun, Strongly interfacial-coupled ^2D–^2D TiO_2/g-C_3N_4 heterostructure for enhanced visible-light induced synthesis and conversion, J. Hazard. Mater. 394 (2020), 122529.
[185] M. Taheri, R. Mohebat, A magnetically separable TiO_2–$H_3PW_{12}O_{40}$@Fe_3O_4/EN as magnetic core–shell nanoparticles on metal–organic framework MIL-101(Cr), J. Mater. Sci.: Mater. Electron. 32 (2021) 3104–3115.